

AD-A099 037

ARMY MILITARY PERSONNEL CENTER ALEXANDRIA VA  
THE EFFECT OF PARTICLE SIZE ON RADIATIVE HEAT TRANSFER IN HIGH --ETC(U)  
MAY 81 T R FRANKENFIELD

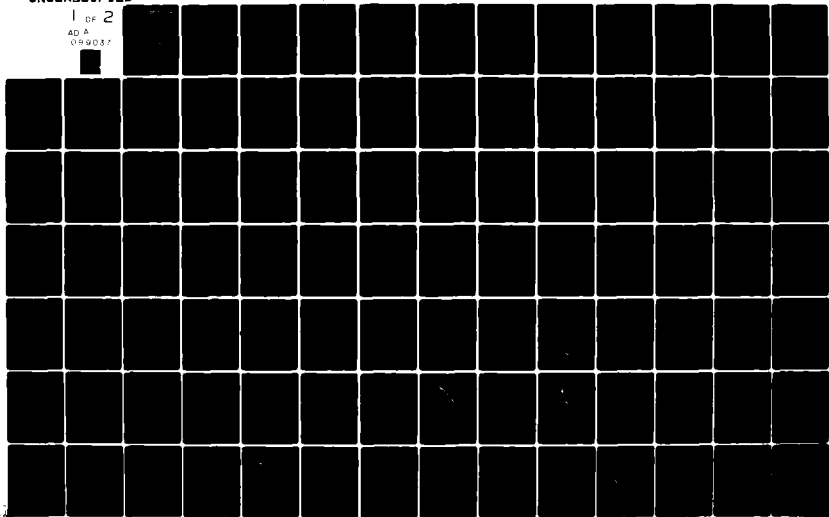
F/6 20/13

UNCLASSIFIED

NL

1 OF 2

AD A  
099037



**LEVEL II**

②

**REPORT DOCUMENTATION PAGE**

READ INSTRUCTIONS BEFORE COMPLETING FORM

1. REPORT NUMBER		2. GOVT. AGENCY USE ONLY (Do not enter)		3. AUTHOR'S CATALOG NUMBER	
4. TITLE (and Subtitle) The Effect of Particle Size on Radiative Heat Transfer in High Temperature Fluidized Beds		5. TYPE OF REPORT & PERIOD COVERED Final Report, 1 May '61			
7. AUTHOR(s) CPT Thomas R. Frankenfield		8. CONTRACT OR GRANT NUMBER(s)			
9. PERFORMING ORGANIZATION NAME AND ADDRESS Student, HQDA, MILPERCEN (DAFC-OFF-E), 200 Stovall Street, Alexandria, VA 22332		10. PROGRAM ELEMENT, PROJECT, TASK AREA & WORK UNIT NUMBERS			
11. CONTROLLING OFFICE NAME AND ADDRESS HQDA, MILPERCEN, ATTN: DAFC-OFF-E, 200 Stovall Street, Alexandria, VA 22332		12. REPORT DATE 1 May 1981		13. NUMBER OF PAGES 121	
4. MONITORING AGENCY NAME & ADDRESS (if different from Controlling Office)		15. SECURITY CLASS. (of this report) Unclassified		15a. DECLASSIFICATION/DOWNGRADING SCHEDULE	

6. DISTRIBUTION STATEMENT (of this Report)  
Approved for public release; distribution unlimited.

17. DISTRIBUTION STATEMENT (of the abstract entered in Block 20, if different from Report)

**DTIC ELECTRIC**  
MAY 18 1981

18. SUPPLEMENTARY NOTES  
A thesis submitted to Lehigh University, Bethlehem, PA 18015 in partial fulfillment of the requirements for the degree of Master of Science in Mechanical Engineering

19. KEY WORDS (Continue on reverse side if necessary and identify by block number)  
radiative component of heat transfer  
fluidized beds

20. ABSTRACT (Continue on reverse side if necessary and identify by block number)  
The effect of particle size on the radiative component of heat transfer in high temperature fluidized beds is examined. One radiometer probe is used to measure both the total and radiative components of heat flux. Two sizes of silica sand particles are tested at bed temperatures of 200 to 750 C. The radiation heat flux, percentage of total heat flux due to radiation, total heat transfer coefficient, radiative heat transfer

OTIC FILE COPY AD A 099 037

coefficient, and bed emissivity are the parameters considered.

The radiative heat flux does not vary with particle size, and the values obtained agree with those of previous studies. The percentage of total heat transfer due to radiation is found to be significant for bed temperatures greater than 400 C and increases with increasing particle size. At 750 C, the radiative component is 20 percent of the total heat flux for the small particles and 30 percent for the larger particles.

The smaller particles have a larger total heat transfer coefficient than the large particles at all bed temperatures. When the fluidizing velocity is increased, the total heat transfer coefficient decreases for both particle sizes. The radiative heat transfer coefficient has the same values for both particle types at all bed temperatures.

The emissivity of the bed is larger for the large particles at all temperatures but always remains less than one. The small particles reach a maximum emissivity of 0.90 at 400 C while the maximum emissivity of the larger particles is 0.98 at 500 C. At 750 C the emissivities of the small and large particles are 0.75 and 0.80, respectively.

THE EFFECT OF PARTICLE SIZE ON RADIATIVE HEAT TRANSFER  
IN HIGH TEMPERATURE FLUIDIZED BEDS

BY THOMAS R. FRANKENFIELD  
NSDA, WILPERSEN (DAFC-011-E)  
200 Stovall Street  
Alexandria, VA 22334

Final report 1 May 1961

Approved for public release; distribution unlimited.

A thesis submitted to Lehigh University, Bethlehem, PA 18015  
in partial fulfillment of the requirements for the degree  
of Master of Science in Mechanical Engineering

81 5 18 080

THE EFFECT OF PARTICLE SIZE ON RADIATIVE  
HEAT TRANSFER IN HIGH TEMPERATURE  
FLUIDIZED BEDS.

by

Thomas Robert/Frankenfield

9 Final P. 115

A Thesis

Presented to the Graduate Committee

of Lehigh University

in Candidacy for the Degree of

Master of Science

in

Mechanical Engineering

11, 1 11, 1

12, 1 11, 1

Lehigh University

1981

Approved For	
GRABER	X
DATE	
BY	
REVISION	

A

39 11 11 11

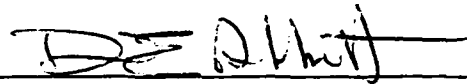
This thesis is accepted and approved in partial fulfillment of the requirements for the degree of Master of Science in Mechanical Engineering.

---

(date)

---

Professor in Charge



---

Chairman of Department

### ACKNOWLEDGMENTS

I would like to express my sincere thanks and deepest gratitude to Dr. Taner F. Özkaynak for his assistance, guidance, and support throughout the course of this study. His technical expertise in the field of fluidization engineering provided me invaluable assistance and allowed this work to be brought to a successful conclusion. I would also like to thank Dr. John C. Chen for his constructive suggestions and encouragement.

## TABLE OF CONTENTS

	<u>Page</u>
Title Page.....	i
Certificate of Approval.....	ii
Acknowledgments.....	iii
Table of Contents.....	iv
List of Tables.....	vi
List of Figures.....	vii
Notation.....	x
1. Abstract.....	1
2. Introduction.....	3
3. Background.....	5
4. Experimental Method.....	17
A. Experimental Analysis.....	17
B. Description of the Probe.....	19
C. Description of the Hot Bed Facility.....	24
D. Calibration of the Probe.....	27
E. Heat Balance on the Probe.....	30
F. Properties of the Sand Particles.....	32
G. Collection of Data.....	34
5. Results and Discussion.....	36
A. Radiation Heat Flux $q_r$ .....	36
B. Percentage of Total Heat Flux Due to Radiation.....	37
C. Total Heat Transfer Coefficient $h_t$ .....	39
D. Radiative Heat Transfer Coefficient $h_r$ .....	42
E. Bed Emissivity.....	43
F. Error Analysis.....	44
6. Conclusions.....	45
Figures.....	48
Tables of Experimental Data.....	89

TABLE OF CONTENTS (Continued)

	<u>Page</u>
References.....	108
Vita.....	110

## LIST OF TABLES

	<u>Page</u>
Table 1 Summary of Results from Previous Studies	16
Table 2 Materials Considered for the Window	22
Table 3 Test Data, SP-1 Particles, Probe with ZnSe Window	89
Table 4 Test Data, SP-2 Particles, Probe with ZnSe Window	100
Table 5 Test Data, SP-1 Particles, Probe with Solid Copper Face	104
Table 6 Test Data, SP-2 Particles, Probe with Solid Copper Face	107

## LIST OF FIGURES

		<u>Page</u>
Figure 1	Percentage of radiation transmitted by a quartz window	48
Figure 2	Configuration of the probe with the zinc selenide window	49
Figure 3	Monochromatic emissive power of a black body as a function of wavelength and temperature	50
Figure 4	Wavelength range required for the window transmittance	51
Figure 5	Normal spectral transmittance of zinc selenide	52
Figure 6	Diagram of the hot bed facility	53
Figure 7	Schematic diagram of the control panel and air and fuel lines of the hot bed facility	54
Figure 8	The black cavity used for calibration of the probe	55
Figure 9	Calibration curve for the probe	56
Figure 10	Configuration of the probe with the solid copper face	57
Figure 11	Dimensions and conductivities of probe materials	58
Figure 12	Size distribution of the SP-1 particles	59
Figure 13	Size distribution of the SP-2 particles	60
Figure 14	Probe in the test section	61
Figure 15	Radiation heat flux, SP-1 particles	62
Figure 16	Radiation heat flux, SP-2 particles	63
Figure 17	Percentage of total heat flux due to radiation, SP-1 particles	64

LIST OF FIGURES (Continued)

	<u>Page</u>
Figure 18 Percentage of total heat flux due to radiation, SP-2 particles	65
Figure 19 Percent radiation, SP-1 particles, at constant fluidizing velocity, $V = 1.26$ m/sec	66
Figure 20 Percent radiation, SP-1 particles, at constant fluidizing velocity, $V = 1.92$ m/sec	67
Figure 21 Percent radiation, SP-2 particles, at constant fluidizing velocity, $V = 2.5$ m/sec	68
Figure 22 Percent radiation, SP-2 particles, at constant fluidizing velocity, $V = 3.88$ m/sec	69
Figure 23 Percent radiation, SP-1 particles, at constant bed temperature, $T_b = 697^\circ\text{C}$	70
Figure 24 Percent radiation, SP-1 particles, at constant bed temperature, $T_b = 751^\circ\text{C}$	71
Figure 25 Percent radiation, SP-2 particles, at constant bed temperature, $T_b = 600^\circ\text{C}$	72
Figure 26 Total heat transfer coefficient as a function of bed temperature, SP-1 particles	73
Figure 27 Total heat transfer coefficient as a function of bed temperature, SP-2 particles	74
Figure 28 Total heat transfer coefficient, SP-1 particles, at constant fluidizing velocity, $V = 1.26$ m/sec	75
Figure 29 Total heat transfer coefficient, SP-1 particles, at constant fluidizing velocity, $V = 2.0$ m/sec	76

LIST OF FIGURES (Continued)

	<u>Page</u>
Figure 30 Total heat transfer coefficient, SP-2 particles, at constant fluidizing velocity, $V = 2.5$ m/sec	77
Figure 31 Total heat transfer coefficient, SP-2 particles, at constant fluidizing velocity, $V = 3.9$ m/sec	78
Figure 32 Total heat transfer coefficient as a function of fluidizing velocity, SP-1 particles	79
Figure 33 Total heat transfer coefficient as a function of fluidizing velocity, SP-2 particles	80
Figure 34 Total heat transfer coefficient, SP-1 particles, at constant bed temperature, $T_b = 610^\circ\text{C}$	81
Figure 35 Total heat transfer coefficient, SP-1 particles, at constant bed temperature, $T_b = 751^\circ\text{C}$	82
Figure 36 Total heat transfer coefficient, SP-2 particles, at constant bed temperature, $T_b = 600^\circ\text{C}$	83
Figure 37 Total heat transfer coefficient, SP-2 particles, at constant bed temperature, $T_b = 755^\circ\text{C}$	84
Figure 38 Radiative heat transfer coefficient, SP-1 particles	85
Figure 39 Radiative heat transfer coefficient, SP-2 particles	86
Figure 40 Bed emissivity, SP-1 particles	87
Figure 41 Bed emissivity, SP-2 particles	88

## NOTATION

A	surface area of the whole probe face = 28.581 cm <sup>2</sup>
A <sub>s</sub>	side surface area of the copper face = 6.02 cm <sup>2</sup>
C	constant used in determining the radiation heat flux
C <sub>p<sub>a</sub></sub>	specific heat of air
C <sub>p<sub>w</sub></sub>	specific heat of water
d <sub>p</sub>	particle diameter
E	electromotive force in millivolts
E <sub>bλ</sub>	monochromatic emissive power of an ideal black body
h <sub>i</sub>	heat transfer coefficient for the interior surface of the probe
h <sub>o</sub>	heat transfer coefficient for the outside surface of the probe
h <sub>r</sub>	radiative heat transfer coefficient
h <sub>t</sub>	total heat transfer coefficient
k	thermal conductivity
L	length of the probe = 34.9 mm
$\dot{m}_a$	mass flow rate of air
$\dot{m}_w$	mass flow rate of water
Nu	Nusselt number
q <sub>a</sub>	heat transferred to the coolant air
q <sub>g</sub>	heat gained through the side of the probe
q <sub>r</sub>	radiation heat flux
q <sub>t</sub>	total heat gained by the probe face
q <sub>w</sub>	heat transferred to the coolant water

NOTATION (Continued)

SP	silica sand particle size designation
	SP-1: $\bar{d}_p = 733 \mu\text{m}$
	SP-2: $\bar{d}_p = 1030 \mu\text{m}$
$T_{a_i}$	inlet temperature of the coolant air
$T_{a_o}$	outlet temperature of the coolant air
$T_b$	bed temperature
$T_w$	temperature of the copper face of the probe
$T_{wd}$	temperature of the zinc selenide window
$T_{w_i}$	inlet temperature of the coolant water
$T_{w_o}$	outlet temperature of the coolant water
$U$	overall heat transfer coefficient of the side of the probe
$V$	fluidizing velocity of the hot bed
$V_{mf}$	minimum fluidization velocity
$\epsilon_{bed}$	bed emissivity
$\lambda$	wavelength
$\sigma$	Stefan-Boltzmann constant

## 1. ABSTRACT

The effect of particle size on the radiative component of heat transfer in high temperature fluidized beds is examined. One radiometer probe is used to measure both the total and radiative components of heat flux. Two sizes of silica sand particles are tested at bed temperatures of 200 to 750°C. The radiation heat flux, percentage of total heat flux due to radiation, total heat transfer coefficient, radiative heat transfer coefficient, and bed emissivity are the parameters considered.

The radiative heat flux does not vary with particle size, and the values obtained agree with those of previous studies. The percentage of total heat transfer due to radiation is found to be significant for bed temperatures greater than 400°C and increases with increasing particle size. At 750°C, the radiative component is 20 percent of the total heat flux for the small particles and 30 percent for the larger particles.

The smaller particles have a larger total heat transfer coefficient than the large particles at all bed temperatures. When the fluidizing velocity is increased, the total heat transfer coefficient decreases for both particle sizes. The radiative heat transfer coefficient has the same values for both particle types at all bed temperatures.

The emissivity of the bed is larger for the large particles at all temperatures but always remains less than one. The small

particles reach a maximum emissivity of 0.98 at 460°C while the maximum emissivity of the larger particles is 0.98 at 500°C. At 750°C the emissivities of the small and large particles are 0.75 and 0.80, respectively.

## 2. INTRODUCTION

Fluidized beds have been used in a wide range of industrial applications to include power generation, thermal cracking of heavy hydrocarbons, gasification of oil shale and coal, drying of granular materials, heat treatment of metals, heating and cooling of gases and granular solids, and the coating of metal surfaces with plastics.

The particular application for which this research work was conducted is the combustion of coal for power production. The use of fluidized beds is particularly important in the combustion of bituminous coal having a high sulfur content. Combustion of bituminous coal using a fluidized bed allows the use of an abundant resource which was previously restricted due to the atmospheric pollution it causes when burned. By using an additive such as limestone or dolomite in the fluidized bed, the sulfur dioxide produced during combustion can be retained in the combustor, greatly reducing the amount of sulfur dioxide released to the atmosphere. The reaction of the sulfur dioxide with the limestone also helps minimize corrosion of the boiler system within the bed. The steam generated in the boiler is then used to drive turbines for electrical power generation [13].

In addition to the advantages mentioned above, fluidized beds are highly desirable for power generation because of their high rate of heat transfer and their extremely high thermal conductivity

(up to one hundred times that of silver) [12]. They also produce a uniform temperature which can be easily controlled.

Many variables affect the heat transfer rate in a fluidized bed. These include the velocity and thermal conductivity of the gas, the size and density of the solid particles and the geometric properties of the bed and the heat exchanger [12]. Further, many of these properties are interrelated thus making analysis of the heat transfer more complicated. However, the physical means by which the heat transfer takes place at the heat exchanger surface can be described by the operation of four mechanisms:

1. Heat transfer through a thin film of gas. The thickness of the film can vary depending on whether a gas bubble is near the surface or the emulsion is uniform and close to the surface.
2. Heat transfer through direct contact of the solid particles with the exchanger surface accompanied by frequent replacement of the particles at the surface.
3. Unsteady-state absorption of heat by fresh emulsion which is swept up to and then away from the surface.
4. Steady-state conduction through an emulsion layer which is only replaced occasionally by fresh emulsion from the core of the bed or by bubbles rising along the surface.

Mechanisms 1 and 2 operate in parallel, followed by either mechanism 3 or 4 or a combination of the two [12]. Throughout the interactions

of these mechanisms, heat transfer takes place by conduction, convection, and radiation. The significance of the radiation mode in the total heat transfer process within fluidized beds has been the subject of much discussion.

The purpose of this study is to examine the significance of the radiation mode within the entire heat transfer process and to determine the effect of particle size on radiation. This is accomplished by measuring both the radiative and total heat fluxes transmitted to a radiometer probe immersed in a fluidized bed of silica sand.

### 3. BACKGROUND

L. J. Jolley performed one of the first high temperature heat transfer experiments in 1949. He assumed that for temperatures greater than 100°C, the total heat flux was composed of both a radiative and non-radiative part.

$$q_{\text{tot}} = q_{\text{rad}} + q_{\text{non-rad}}$$

He measured the total heat transfer by lowering a cylindrical metal block of either copper or aluminum into a fluidized bed. He removed the block from the bed after 20-30 seconds and immediately immersed it in water in a calorimeter. He maintained the bed temperature in a range of 800 to 1000°C by the combustion of coke. The radiative component of heat transfer was determined by assuming black body radiation from the bed to the metal block which was maintained at

an average temperature of 100°C.

$$q_{\text{rad}} = \sigma \left[ T_{\text{bed}}^4 - (100 + 273)^4 \right]$$

The non-radiative component was estimated by recording the cooling rate of a metal block at 100°C in a fluidized bed at room temperature. Jolley then linearly extrapolated his results for high temperatures. The sum of these radiative and non-radiative components seemed to agree with the total heat transfer measurements [9].

In 1964, Kharchenko and Makhorin conducted heat transfer experiments using a fluidized bed of clay or sand and a spherical copper probe, six centimeters in diameter. The bed temperature ranged up to 1050°C and was controlled by burning natural gas. Their results yielded a linear relationship between the bed temperature and the maximum heat transfer coefficient. For radiation to contribute significantly to the total heat transfer, they believed that it should have caused the total heat transfer coefficient to vary as the third power of the bed temperature. Since it did not, they concluded that radiative heat transfer between the bed and the submerged probe was not significant, even at high temperatures [10].

In 1968, Il'chenko et al. used two radiometer probes to determine the radiative component of heat transfer in fluidized beds with temperatures up to 1700°K. One probe measured the total heat flux while the other measured only the radiant flux. Sand, chamotte, fused magnesite, corundum, and zirconium dioxide particles were used for the experiments. They found that the total heat flux was

linearly dependent on bed temperature for all the particle sizes tested except for corundum at temperatures greater than 1500°K. The radiant heat flux was found to be less than that calculated for an ideal black body at the same temperature. They concluded that this difference between the experimental and calculated values of radiant heat flux was due to two simultaneously acting factors: the bed emissivity was less than one and the particles were being cooled at the probe surface [8].

Also in 1968, Szekely and Fisher performed experiments in which they tried to attain purely radiant heat transfer for source temperatures as low as 600°K. In these experiments, they transmitted heat through a transparent wall while maintaining the wall at the bulk bed temperature. They used particles of iron shot, silicon carbide, and porous alumina with bed temperatures to 650°K. By comparing the radiant heat transfer coefficients determined from their experiments with the bed to wall heat transfer coefficients reported in literature, they concluded that the radiation contribution to total heat transfer was negligible for wall temperatures on the order of 600 to 700°K. They used an analytical analysis to estimate the relative importance of radiative heat transfer for temperatures greater than those used in their experimental work. In addition to radiation, they considered conduction through the gas into the solid particles. They found that radiant heat transfer increases with increasing source temperature and particle residence time. In analyzing the effects of particle size, they

determined that the ratio of radiant to convective heat flux tends to increase with decreasing particle size for particle diameters less than 200 microns. However, for larger particle diameters, the ratio increased with increasing particle size. This was explained by the fact that small particles attain thermal equilibrium rapidly, and the final approach to equilibrium is faster for the radiant transfer mechanism. Finally, they concluded it was an oversimplification to consider the radiative and convective heat transfer modes independently [15].

In 1970, Botterill and Sealey further analyzed the results of Il'chenko et al. They determined that when the radiation component is neglected, the limiting factor for heat transfer is the thermal conductivity of the gas. The convective component of heat transfer was found to remain fairly constant and showed no increase at higher bed temperatures even though the conductivity of the air increased with increasing air temperature. Since the overall heat transfer coefficient also continued to increase, they concluded that at higher temperatures some heat is transferred by radiation "at the expense" of convection, and the two mechanisms are not simply additive [6].

Baskakov and Goldobin also investigated the experimental results of Il'chenko in 1970. They calculated the temperature of the glass surface of the radiant heat flux probe inside the fluidized bed and found that the temperature at the center of the glass surface was virtually the same as the bed temperature. They concluded

that Il'chenko's experiment had not determined the radiant component of heat transfer from the bed to the body which it heats, but instead had determined the total radiation of the bed without considering the temperature reduction in the particles pressed to the body's surface as compared to the actual temperature of the bed [1].

Baskakov and Goldobin also conducted their own experiments to determine the radiative component of the total heat transfer coefficient. These experiments involved the determination of heat transfer coefficients,  $\alpha_{bl}$  for a "black" stainless steel ball with an emissivity of 0.8 and  $\alpha_{wh}$  for a "white" sphere of the same size and material but coated with silver and having an emissivity of 0.02 to 0.07. They assumed that radiation had little effect on the conductive-convective component of heat transfer. Then considering the fact that the radiation on the "white" sphere is almost totally reflected, they concluded that the difference  $\alpha_{bl} - \alpha_{wh}$  yields the radiative component of the heat transfer coefficient. They also developed a "packet" model which considered the total heat transfer from the bed to the wall to be composed of both conductive-convective and radiative heat transfer when the wall is in contact with the particles of the packet but to be composed of only radiative heat transfer when the wall is in contact with a bubble. In comparing the calculations based on their packet model to the radiative component determined experimentally using the "black" and "white" spheres, they found that, although not in exact agreement, their results did show better agreement than the other models [1].

In 1972, Yoshida et al. extended their previous model of heat transfer to high temperature conditions. In their packet model, when bubbles cover the surface of the heat exchanger, heat is transferred by radiation from the inner surface of the bubbles to the surface of the heat exchanger. When the heat exchanger surface is covered by the emulsion, heat is transferred by conduction. The radiant heat transfer inside an emulsion element is taken into account by the effective thermal conductivity of the emulsion. They found that the contribution of radiant heat transfer was negligible when compared with that due to conduction for operating temperatures less than 1200°C and concluded that the radiant heat transfer was not significant [19].

Vedamurthy and Sastri performed a similar analysis in 1973, based upon a gas film emulsion packet model. Their results contradicted those of Yoshida et al. For a bed temperature of 900°C, they found radiation to comprise 13 to 30 percent of the total heat flux. The radiative heat transfer coefficient increased with increasing fluidizing velocity while the conductive coefficient decreased. The combined effect decreased the total heat transfer coefficient. The increase in the radiative component was attributed to an increase in the area of gas film exposed to bubbles with increasing bed velocity. The conductive coefficient varied linearly with bed temperature while the radiative and total heat transfer coefficients were nonlinear especially at higher temperatures [18].

Based on their previous experiments with steel spheres of different emissivities, Baskakov et al. stated in 1973 that the fluidized particles close to the heat transfer surface were cooled by the heat exchange with the surface so that the radiant heat flux from these particles to the surface was less than if they were at bed temperature. By taking measurements from a flat quartz glass immersed within a fluidized bed, they found that the effective emissivity of the fluidized bed in contact with the glass surface area was dependent upon both the surface temperature of the glass and the bed temperature. It was also noted that the larger the particle size, the greater the percentage of total heat transferred by radiation, although the absolute quantity of heat transferred by radiation was not dependent on particle size or fluidizing velocity for the range of bed temperatures examined [2].

In 1976, Bhattacharya and Harrison performed a theoretical analysis using a packet model similar to that of Vedamurthy and Sastri. The only difference was that they treated the emulsion phase as both an absorbing and emitting medium. In comparing their calculated ratio of the average radiative to overall heat transfer coefficient as a function of surface temperature with Baskakov's experimental results, they found that their values were significantly higher than his. This discrepancy was attributed to the different emissivities used in the two studies ( $\epsilon = 0.8$  Baskakov,  $\epsilon = 1.0$  this study). They stated that the surface temperatures of the probes used in the experiments and the emissivities of the heat

transfer surfaces were very important. Furthermore, the radiative and conductive heat fluxes could not be evaluated separately. They found that increasing either the conductive or radiative components of heat transfer had the effect of suppressing the other [5].

Also in 1976, Thring developed three models of heat transfer, similar to those of Bhattacharya and Harrison and Vedamurthy and Sastri. In all three models, the convective heat transfer coefficient decreased with increasing wall temperature while the radiative coefficient increased with temperature. Thring noted differences between the predictions of his models and those of Bhattacharya and Harrison and Vedamurthy and Sastri. In order to explain these differences, he conducted an experimental analysis using all of these models. After comparing the results, he concluded that the model used makes a significant difference (on the order of a factor of two) in the predicted value of the radiative coefficient obtained between a fluidized bed and a heat transfer surface. However, all models predicted the total heat transfer coefficient within a reasonable range [16].

In 1976, Baskakov et al. conducted an experimental analysis to determine the radiative component of heat transfer using the Stefan-Boltzmann equation. Their analysis studied the cooling effect which a surface such as a radiometer probe had on the particles which came into contact with it. This emissivity was lower than the actual emissivity of the bed, and to account for this, they used the temperature of the core of the bed to represent the temperature of the

radiating particles. They concluded that total heat transfer could be determined by addition of the conduction-convection and radiation components. Their results further showed that the cooling of particles at the radiometer surface did have a significant effect on the radiative heat transfer component [3].

In 1978, Basu studied the effect of the combustion of coal on heat transfer to a surface immersed in a fluidized bed and the contribution made by radiation to the overall heat transfer. He used a theoretical method based on the single particle model to predict the effect of combustion. This model concentrates on single particles which are swept to the heat transfer surface and return back to the bed after a brief period of heat exchange with the wall. To determine the radiative component and the total heat transfer, Basu used two identical copper tubes positioned at identical locations within a fluidized bed of sand and pulverized coal. The tube used to measure the radiative heat transfer was covered with a coaxial transparent silica tube to minimize conduction and make radiation the primary mode of heat transfer. The other plain tube measured the total heat transfer. The total heat transfer coefficient was found to increase with increasing carbon content in the bed except when the carbon particles were much larger than the inert bed material. Also, the radiation heat flux was found to be 5 to 10 percent of the total heat flux for bed temperatures of 800 to 900°C [4].

Kolar et al., in 1979, used the alternate slab method of Gabor to examine the radiative component of heat transfer in a high

temperature fluidized bed. The alternate slab method assumes that the bed is composed of alternate vertical slabs of gas and solids. The bed and heat transfer surfaces are assumed to be gray bodies, and the gas is radiatively transparent. The temperatures of successive slabs are then calculated starting at the heat transfer surface. Calculations at an individual time step continue through successive slabs until the temperature differs from the core bed temperature by a very small amount. The radiative and total heat transfer coefficients can then be determined. After comparing the results of this model with previous studies and experimental results, Kolar et al. concluded that the alternate slab method generally overestimated the radiation component and the average heat transfer coefficients but within reasonable limits and agreed very well at high bed and heat transfer surface temperatures. They further concluded that the radiative percentage of total heat transfer was significant for large particle diameters and high heat transfer surface and bed temperatures. The radiative component varied directly with these values but was found to be more sensitive to the surface temperature than the bed temperature [11].

In summary, it is apparent that the uncertainty about the relative importance of radiation in high temperature fluidized beds still exists, although most of the later studies indicate that the contribution of the radiative component is significant. The value of the radiative component of the total heat flux does vary appreciably for different studies. Table 1 summarizes the results

of some of these studies. The major differences are the result of the experimental method or theoretical model used in the analysis. There are three basic categories of theoretical models used in calculating the radiative heat transfer component. The first assumes black body radiation from the bed. The second category calculates the radiation between the phases (emulsion-void) and the heat exchanger surface, while the third considers the radiation exchange between a single particle and the heat exchanger surface. Since in the first category, radiation is treated separately from conduction, it is difficult to determine the relative importance of radiation. For the two other categories, solutions are difficult to obtain unless critical assumptions are made and, of course, the final results are dependent upon the validity of the assumption. Experimental studies also have difficult problems to resolve, such as the degree to which the surface temperature of the probe or the emissivity of the heat transfer surface affects the radiation component of total heat flux. Also the nonadditive nature of the radiative and conductive components of heat transfer has not been treated consistently. The mechanism of heat transfer in high temperature fluidized beds requires much additional experimental and theoretical work before it can be fully understood.

This study will investigate only one aspect of this heat transfer mechanism. It will attempt to determine the effect of particle size on the radiative component of heat transfer in fluidized beds.

TABLE 1: Summary of Results from Previous Studies

Author	Method	$T_w$ (°C)	$T_b$ (°C)	$d_p$ ( $\mu\text{m}$ )	Percent Radiation
Jolley [9]	cylindrical blocks	15-251	775-980	up to 1600	33-43
Kharchenko et al. [10]	spherical calorimeter	30	160-1050	340-1600	negligible
Il'chenko et al. [8]	radiometer probe	100-200	427-1427	570-1750	18-50
Szekely [15]	transparent bed wall	40-100	315-377	100-150	insignificant
Botterill et al. [6]	radiometer probe	water cooled	500-1400	200-3000	5-60
Baskakov et al. [1]	emissivity difference	150-800	850	350-1250	6-32
Yoshida et al. [19]	emissivity difference	30-150	500-1500	180	1-6
Basu [4]	transparent wall	20-30	800-900	280	5-10

#### 4. EXPERIMENTAL METHOD

##### A. Experimental Analysis

There are basically two methods used to determine the radiative component of heat transfer in high temperature fluidized beds. One of these methods employs small spherical metal probes with different surface emissivities. Essentially, the difference in heat transfer between a black surface and a white one is considered to be the radiative component. The major disadvantages of this method can be summarized as follows:

1. Emissivity of a surface is difficult to determine and is usually a function of temperature. Even if it is determined accurately, the scouring action of the particles changes the emissivity, usually causing it to increase.
2. The surface temperatures of the small spherical probes submerged in the bed continuously rise during the experiment, thus reducing the net radiation by increasing re-radiation. Due to this phenomenon, the conductivity of the gas increases simultaneously with the probe temperature, and hence the total heat transfer coefficient also increases. As a result, experiments which use these types of probes obtain low percentages of radiation, as shown in Table 1.

The other method used to measure the radiation component employs

a transparent surface and a sensor to detect the radiation. The major disadvantages of this radiometer method are:

1. Most of the probes used previously have not been cooled properly. Baskakov and Goldobin investigated the experimental results of Il'chenko et al. who had used a probe of this kind. Calculations for the conditions of the experiments showed that the temperature at the center of the glass virtually did not differ from the bed temperature. They concluded that what had been determined in these experiments was not the radiant component of heat transfer but the total radiation of the bed since no reduction in the temperature of the particles had occurred at the glass surface. Experiments using this type of probe such as those of Il'chenko et al. and Botterill et al. predict high percentages of radiation as shown in Table 1.
2. In radiometer probes, quartz windows have been used to transmit the radiation onto the sensor. The transmittance band for quartz is approximately 0.15 to 3.5  $\mu\text{m}$ . In this band range only a small portion of the radiation is transmitted. The percentage of transmission through a quartz window for radiation from a black body source is shown in Figure 1 as a function of source temperature. Less than 50 percent of the radiation will

be transmitted for a bed temperature of 1100°K, assuming a transmittance of one for the window. As a result, the sensitivity and accuracy of the probe are limited.

3. Another disadvantage of the quartz window is its low thermal conductivity. Due to this lower conductivity and the thinness of the windows used in previous experiments, the center temperatures of the windows were high because of poor cooling from the sides.

The radiometer probe method is selected for use in this study. The disadvantages of this method are eliminated by proper cooling of the window and choosing a window material with a long range of transmittance and a high thermal conductivity. Also by designing a probe with a special geometry, both the radiation component and the total heat transfer are measured simultaneously at the same location in the bed.

#### B. Description of the Probe

A radiometer probe is designed to measure the radiative and total heat flux inside a fluidized bed. A detailed drawing of the probe used in this study is shown in Figure 2. The face of the probe is made of a copper ring with a radiatively transparent window at the center. The rest of the probe is made of brass.

Selection of the window material is dependent upon the temperature it will be exposed to and also on its transmittance in the

temperature range of the experiments. The monochromatic emissivity of a black body as a function of wavelength and temperature is given by Planck as:

$$E_{b\lambda} = \frac{C_1 \lambda^{-5}}{e^{\frac{C_2}{\lambda T}} - 1} \quad (1)$$

where

$\lambda$  = wavelength,  $\mu\text{m}$

$T$  = temperature,  $^{\circ}\text{K}$

$C_1 = 3.743 \times 10^8 \text{ W}\mu\text{m}^4/\text{m}^2$

$C_2 = 1.4387 \times 10^4 \mu\text{m}^{\circ}\text{K}$

A plot of  $E_{b\lambda}$  as a function of wavelength and temperature is given in Figure 3. It can be seen that at high temperatures most of the radiation is concentrated in the short wavelength band and at low temperatures in the long wavelength band.

Total emittance for each temperature range can be found by integrating the corresponding distribution curve. If we want a material for the window which can transmit 90 percent of the total emittance, assuming that it does not transmit the 5 percent at both the long and the short wavelengths, we can define the range of wavelengths required for transmittance from the window. This is shown in Figure 4. A window which transmits radiation from 1.71 to 11.34  $\mu\text{m}$  is good for 1100 $^{\circ}\text{K}$ , but it won't transmit all the radiation at 700 $^{\circ}\text{K}$  since the required transmittance there is 2.69-17.85  $\mu\text{m}$ .

A list of the materials considered for the window is given in Table 2. Some materials are hygroscopic, some toxic, and for some the wavelength range is not appropriate. The best suitable window materials are Irtran 4 and 6. Irtran 4 (ZnSe) is chosen for this study since it is commercially available.

The normal spectral transmittance of Irtran 4 is shown in Figure 5 for various thicknesses and temperatures. It is seen that Irtran 4 transmits radiation between 0.5 and 20  $\mu\text{m}$  which is good for the entire range of the hot bed experiments. This is a major advantage of the zinc selenide window over the quartz window which only transmits a small part of the radiation.

Another advantage of the zinc selenide window is its high thermal conductivity ( $k = 13 \text{ W/m}^\circ\text{K}$  at  $54^\circ\text{C}$ ) which is approximately nine times that of quartz ( $k = 1.4 \text{ W/m}^\circ\text{K}$ ). Thus the cooling of the window will be more effective, and a more uniform temperature distribution will be obtained. This in turn, eliminates the problems associated with poorly cooled windows as discussed previously.

Two zinc selenide windows are used in the probe as shown in Figure 2. They have a diameter of 25.4 mm and a thickness of 3.0 mm. The window inside the probe is used as a cover for the cavity which includes the heat flow transducer. Coolant air comes from one side of the probe in a 6.35 mm O.D. tube, passes between the zinc selenide windows, and exits on the other side in another 6.35 mm tube.

The heat flow transducer is 19 mm in diameter and 2 mm thick. It functions according to the theory and principle of a simple

TABLE 2: Materials Considered for the Window

Name	Melting Point (°C)	Wavelength Range (μm)
1-KBr	730	0.3<λ<30 (H)
2-KCl	790	0.2<λ<20 (H)
3-CsBr	636	0.3<λ<55 (H)
4-CsI	621	0.25<λ<80 (H)
5-LiF	870	0.12<λ<9.0 (OR)
6-NaCl	800	0.2<λ<26 (H)
7-Sapphire		0.2<λ<6 (OR)
8-Quartz	1700	0.2<λ<4 (OR)
9-CaF <sub>2</sub>	1418	0.1<λ<8 (OR)
10-BaF <sub>2</sub>	1320	0.15<λ<13 (OR)
11-KRS-5		0.5<λ<40 (T)
12-Irtran 2 (ZnS)	1850	1.0<λ<13 (OR)
13-Irtran 4 (ZnSe)	1500	0.5<λ<20 A
14-Irtran 6 (CdTe)	1098	0.9<λ<30 NA

H - Hygroscopic  
 OR - Out of Range  
 T - Toxic  
 NA - Not Available  
 A - Available

thermopile. An instrument operating on these principles provides a direct readout in millivolts proportional to the heat flux. The transducer consists of an insulating wafer with a series of thermocouples consisting of thermoelement combinations such that consecutive thermoelectric junctions fall on opposite sides of the wafer. This assembly is bonded to a heat sink to assure heat flow through the sensor. Heat is received on the exposed surface of the wafer and conducted through to the heat sink. Thus a temperature drop is developed across the wafer and is measured directly by each junction combination embodied along the wafer. Since the differential thermocouples are connected electrically in series, the voltages produced by each set of junctions are additive, thereby amplifying the signal in direct proportion to the number of junctions. The temperature drop across the wafer, and thus the output signal, is directly proportional to the heat flux. With the proper choice of materials, behavior of the sensor is such that a linear relationship is obtained between the heat flux and the thermopile output over the normal operating temperature range of the thermopile (-45°C to 200°C). A thermocouple is attached to the thermopile to assure that the temperature does not exceed the operating limits.

Coolant water enters the radiometer probe through a 6.35 mm copper tube, fills a small cylindrical hole, then goes through four 2.38 mm channels to a cylindrical annulus, and then leaves the probe through another copper tube. The thermopile sits on a 3.175 mm thick brass wafer which is cooled by the circulating water. The coolant

water acts as a heat sink for the thermopile, and a heat balance on the coolant water and air gives the total heat flux from the bed to the probe. The radiation heat flux is measured from the output of the thermopile after it has been properly calibrated.

### C. Description of the Hot Bed Facility

A detailed drawing of the hot bed facility is shown in Figure 6. The high bed temperatures required for this experiment are achieved by burning Number 2 fuel oil in a combustion chamber before the bed. The hot gases coming from the combustion chamber (3), go through the distributor plate (5), through the bed (6), and then are either sent directly to the atmosphere (11) or go to a quench box (8), cyclone (9), and through a fan (10) to the atmosphere (12) depending upon the amount of particles present in the gases.

The major components of the hot bed facility are described below:

#### No. on Fig. 6

- 1     Air Supply: Compressed air is supplied from two compressors, each with a capacity of  $850 \text{ m}^3/\text{hr}$  at 6 bars of pressure.
- 2     Fuel Supply: Number 2 fuel oil is pumped to the facility from a storage tank outside the building. The pump which delivers the fuel oil to the combustion chamber has a capacity of 35  $\text{t}/\text{hr}$ .

- 3        Combustion Chamber: The combustion chamber has an outside diameter of 50.8 cm and a 10.16 cm Lite-wate-35 refractory lining. It is equipped with an excess air burner, ignition transformer, and flame detector to provide safe combustion.
- 4        Hot Gas Plenum: The outside diameter of the plenum is 76.2 cm with 5.08 cm of mineral fibre block insulation and 10.16 cm of Lite-wate 35 refractory lining.
- 5        Distributor Plate: The distributor plate is made of sixty 1.27 cm stainless steel bolts bolted on a 1.90 cm thick stainless steel plate in a hexagonal pattern. The hot gases coming from the combustion chamber pass through a 6.35 mm concentric blind hole in the stem of the bolt and then go to the bed through three 4.76 mm horizontal radial holes, 120 degrees apart in the head of the bolt.
- 6        Test Section: The outside diameter of the test section is 76.2 cm and the inside diameter is 45.7 cm. The test section has the same type refractory as the gas plenum. It has two doors and five 7.62 cm diameter pipes which provide access for instrumentation and maintenance. The

test section is 304.8 cm in height measured from the distributor plate to the inlet of the quench box.

7 Discharge Section: The discharge section has the same diameter as the test section. There is a cap on top of the section for discharging the hot gases to the atmosphere if the temperature inside the quench box should exceed 315°C.

8 Quench Box: Two nozzles inside the quench box spray cooling water on the hot gases. The quench box is lined with refractory and can handle temperatures up to 315°C.

9 Cyclone: The cyclone is used to remove any particles contained in the hot gases before the gases are discharged to the atmosphere.

10 Fan: A special fan is installed for high temperature operation to induce forced draft. It is designed to operate at temperatures up to 315°C.

A control panel provides instrumentation and adjustment devices to monitor and control the gas temperatures and pressure in the plenum and the temperature in the quench box. A schematic diagram of the control panel and the air and fuel lines is shown in Figure 7.

The total air flow rate is measured by a hotwire probe mounted on a venturimeter. The linear output which is proportional to the flow rate is fed to a datalogger along with the rest of the thermocouples.

#### D. Calibration of the Probe

The radiometer probe is calibrated using an ideal black body so that when it is placed in the fluidized bed, the amount of radiant heat flux incident on the probe face at the various bed temperatures can be measured.

First, a flat copper plate covered with candleblack is used as the ideal black surface. A thermocouple attached to the surface of the plate measures its temperature. Results using this method prove to be inconsistent. The higher temperatures used in the calibration (500 to 800°C) cause the copper plate to oxidize, removing the candleblack surface and thus reducing both the emissivity of the plate and the radiation heat flux.

A cavity made from copper (Figure 8) is used to correct the problem caused by oxidation and to provide a thermal emittance closer to one. The actual emissivity of the cavity is calculated to be 0.991. The cavity is fastened together using brass screws and has a thermocouple mounted at the center of each interior face.

During calibration, the cavity is placed inside an oven and is heated to a temperature of 800°C. The probe is placed as close to the front of the cavity as possible without touching it, and the

probe window is centered on the cavity opening. The temperature variation of the interior faces is on the order of 10 to 15°C from the average temperature of all faces at a given data point. The coolant water and coolant air for the probe are turned on for the calibration so that conditions are similar to those which occur when the probe is placed in the hot fluidized bed.

The electromotive force (emf) readings of the thermopile and the corresponding temperature of the cavity are recorded for temperatures from 100°C to 800°C. Using the temperature of the back face, the ideal black body radiation heat flux of the cavity is calculated from the Stefan-Boltzmann equation. Then a best curve fit of the emf readings versus black body radiation heat flux is determined. This best curve fit is linear, as shown in Figure 9, and the calibration is of the form:

$$q_r = C \cdot E_f \quad (2)$$

When the probe is placed in the fluidized bed and the radiation heat flux is determined using this relationship, the radiation flux measured is greater than that anticipated for low temperatures and, in some cases, is greater than that for an ideal black body at the same temperature. For corresponding bed and black body temperature readings, the emf readings of the probe in the bed are consistently larger than those obtained during calibration. The temperatures of the window and the copper face during calibration are significantly cooler than when the probe is placed in the hot bed. Therefore, to

calibrate the probe for use in the hot bed, the additional radiant heat flux incident on the thermopile due to the higher window and copper face temperatures and the higher brass body temperature must be accounted for. Test runs using the probe with the solid copper face (Figure 10) are utilized to determine the effect of these higher temperatures on the thermopile reading. Since there is no window, the copper face and the brass body surrounding the thermopile are the only sources of radiation. When these are considered, the emf readings should be approximately zero for calibration of the thermopile to no-radiation conditions.

For different bed and copper surface temperatures, the additional emf output due to the higher temperatures of the copper face and the brass body of the probe is found to be:

$$\Delta E_{\text{add}} = \frac{\sigma T_w}{C} + 2.0 \quad (3)$$

where C is defined by equation (2)

The first term in equation (3) is the emf increase due to the increase in the temperature of the copper face and the second term accounts for the emf increase due to the increase in temperature of the probe body.

The final calibration for the probe with the zinc selenide window is:

$$E_f = E - \Delta E$$

$$E_f = E - \frac{\sigma T_{swd}^4}{C} - 2.0 \quad (4)$$

where  $T_{swd}$  is the surface temperature of the window,  $E$  is the emf output of the thermopile and  $E_f$  is the corrected emf output which will be used in equation (2) to calculate the radiative heat flux.

In the test runs with the solid copper face, resulting values of  $E_f$  are in the range of -0.9 to +0.9 millivolts for bed temperatures of 530 to 770°C and copper face temperatures of 100 to 140°C. This produces an error of zero to four percent in values of  $q_r$  for both particle types tested.

#### E. Heat Balance on the Probe

A heat balance is made on the probe to determine the total heat transferred to it. The inlet and outlet temperatures of the coolant air and coolant water for the probe are measured by thermocouples and the volumetric flow rates of each are measured by flowmeters. The specific heats, densities, and mass flow rates of the air and water for these conditions are then determined, and the heat transferred to each is calculated as follows:

$$\text{for air: } q_a = \dot{m}_a C_{p_a} (T_{a_o} - T_{a_i}) \quad (5)$$

$$\text{for water: } q_w = \dot{m}_w C_{p_w} (T_{w_o} - T_{w_i}) \quad (6)$$

The side of the probe is insulated with fiberfrax insulation and is enclosed within a stainless steel cylinder. Possible heat

gain through the side of the probe must be determined. The overall heat transfer coefficient for the side of the probe is:

$$U = \frac{1}{\frac{A_o}{A_i} \left(\frac{1}{h_i}\right) + \frac{A_o}{2\pi L} \left[ \frac{\ln\left(\frac{r_o}{r_i}\right)_{ss}}{k_{ss}} + \frac{\ln\left(\frac{r_o}{r_i}\right)_{ins}}{k_{ins}} + \frac{\ln\left(\frac{r_o}{r_i}\right)_{br}}{k_{br}} \right] + \frac{1}{h_o}} \quad (7)$$

with the dimensions and material properties given in Figure 11.

The heat transfer coefficient for the outside surface  $h_o$  is assumed to be approximately equal to that for the copper surface of the probe face:

$$h_o = \frac{q_a + q_w}{A(T_b - T_w)} \quad (8)$$

where  $A = 28.581 \text{ cm}^2$  is the surface area of the whole probe face.

Calculation of the heat transfer coefficient for the interior surface  $h_i$  is based upon the laminar flow of the coolant water within the water outlet tube:

$$Nu = \frac{h_i d_h}{k_w} = 4.364 \quad [7]$$

and

$$h_i = \frac{4.364 k_w}{d_h} \quad (9)$$

where  $k_w$  is the conductivity of the coolant water determined at its average temperature  $(T_{wi} + T_{wo})/2$ , and  $d_h = 9.6 \text{ mm}$  is the hydraulic

diameter of the tube. The total heat gained through the side of the probe due to conduction and convection is:

$$q_g = A_o U (T_b - T_w) \quad (10)$$

where  $q_g$  is on the order of 6-8 percent of the total heat gained by the probe for the SP-1 particles and 7.5-9 percent for the SP-2 particles.

Now the total heat gained only from the probe face can be found:

$$q_t = q_a + q_w - q_g \quad (11)$$

The total heat flux incident of the probe face is equal to  $q_t/A$ . When the probe is placed inside the hot fluidized bed, approximately 3.175 mm of the insulation is blown away, exposing the side edge of the copper face. The total heat flux is adjusted to account for heat gained through this additional surface area  $A_s$ . Therefore, the total heat flux becomes  $q_t/(A+A_s)$ .

#### F. Properties of the Sand Particles

##### *Size Analysis*

Two sizes of silica sand particles are used in this study. A sieve analysis is conducted on a 2000 gram sample of each particle type both prior to firing in the fluidized bed and upon completion of the test. The weight mean particle diameter is determined using the relation:

$$\bar{d}_p = \frac{1}{\sum \left(\frac{x}{d_{p_i}}\right)} \quad (12)$$

where  $x$  is the weight fraction of the particles in each size interval within the sample, and  $d_{p_i}$  is the average particle diameter for each size interval [12].

Figure 12 shows the size distribution and average particle diameter of the small particles (SP-1) prior to firing. The size distribution after firing has a similar profile with a mean particle diameter of 733  $\mu\text{m}$ . The SP-1 particles are spherical in shape and are processed such that the majority of particles lie in a narrow size range as shown in Figure 12.

The size distribution and average particle diameter of the larger particles (SP-2) prior to firing are shown in Figure 13. On completion of testing, a similar size distribution exists with a mean particle diameter of 1030  $\mu\text{m}$ . The SP-2 particles are sub-angular in shape. Spherical silica sand particles are not available in this large size range. These particles are well-graded having a wide distribution of sizes within the range shown in Figure 13.

#### *Other Properties*

The minimum fluidization velocities of both particle types measured in a cold fluidized bed with a cross sectional area of 62.1  $\text{cm}^2$  are:

Type SP-1:  $V_{mf} = 0.365$  m/sec

Type SP-2:  $V_{mf} = 0.682$  m/sec

The other physical properties are the same for both types of silica sand. These include:

density:  $\rho = 2650$  kg/m<sup>3</sup>

conductivity:  $k = 1.87$  W/m<sup>°K</sup>

specific heat:  $C_p = 845$  J/kg<sup>°K</sup>

#### G. Collection of Data

Six sets of test data are recorded for use in the analysis and determination of final results. Four are compiled using the probe with the zinc selenide window; three with the SP-1 particles and one with the SP-2 particles. The two final sets, one for each particle type, are made using the probe with the solid copper face as shown in Figure 10.

The probe is placed in the test section as shown in Figure 14 with its face 12.7 cm from the side of the bed. The particles are then put into the test section, and the static bed height is measured. The static bed height for all test runs in this study is 47.5 cm. The coolant air and coolant water to the probe are turned on before igniting the bed, and their flow rates are recorded. The bed is then fluidized and combustion initiated. The temperature of

the bed and the rate at which the bed temperature increases are controlled by the fuel-air mixture supplied to the combustion chamber. The total air flow rate is now recorded along with the pressure drop within the combustion chamber and the pressure drops at three locations within the fluidized bed; 2.5, 29.0, and 59.0 cm above the distributor plate. Additional pressure drop readings are taken anytime the total air flow into the combustion chamber and fluidized bed is varied.

The datalogger is used to record temperature and emf readings at critical locations in the test setup. These include: the bed temperatures 18.6 and 20.3 cm above the distributor plate, the inlet temperature of air supplied to the combustion chamber, the temperature inside the combustion chamber; and inside the probe: the temperature of the copper face, the window temperature, the inlet and outlet temperatures of both the coolant air and the coolant water, and the thermopile emf output. These readings are recorded at regular two or four minute intervals throughout the test run. Additional readings are also taken at critical points by activating the manual record mechanism of the datalogger.

The bed temperature is normally allowed to increase at a steady rate, but is held constant at selected temperatures (normally 500 to 700°C at 50 degree intervals) to record steady state readings. While holding the bed temperature constant, the air flow to the bed is varied to determine its effect on probe readings. The maximum bed temperature reading is 760°C.

Detailed results of the experiments for the SP-1 and SP-2 particles are recorded in Tables 3 and 4 for the probe with the zinc selenide window and in Tables 5 and 6 for the probe with the solid copper face.

## 5. RESULTS AND DISCUSSION

The SP-1 and SP-2 particles are both analyzed under similar conditions. The data from six separate test runs which is used in the following analysis is compiled as discussed in Section 4.G, Collection of Data. The data is taken for bed temperatures  $T_b$  of 200 to 760°C with values of 35 to 155°C for  $T_w$  and 30 to 220°C for  $T_{wd}$ . The range of fluidizing velocities used is 0.57 to 3.11 m/sec for the SP-1 particles and 1.50 to 4.83 m/sec for the SP-2 particles. The detailed data for all test runs is recorded in Tables 3 through 6.

The effects of particle size on radiation heat flux  $q_r$ , percentage of total heat flux due to radiation, total heat transfer coefficient  $h_t$ , radiative heat transfer coefficient  $h_r$ , and bed emissivity are now studied.

### A. Radiation Heat Flux

The radiation heat flux is calculated using equation (2) with  $E_f$  determined from equation (4). Figures 15 and 16 show the radiation heat flux at all bed temperatures and fluidizing velocities for the SP-1 and SP-2 particles, respectively. The radiation heat

flux increases with bed temperature. For temperatures below 400°C, the radiation heat flux is the same for both particle sizes, but at temperatures greater than 400°C, the 44- $\mu$  particles have a significantly greater radiation heat flux than the smaller 14- $\mu$  particles. The values of  $q_{rad}$  found here are equal to those found by [15] for bed temperatures of 400 to 750°C which is the temperature range common to both studies.

### 3. Percentage of Total Heat Flux due to Radiation

The percentage of the total heat flux due to radiation at all bed temperatures and fluidizing velocities is shown in Figure 10 and 18 for the SP-1 and SP-2 particles, respectively. The 44- $\mu$  particles have a significantly larger percentage of the total flux due to radiation. Thus for the larger particles, the radiation component of the total heat flux becomes significant at lower bed temperatures. For example, the radiation component does not become 15 percent of the total heat flux until the bed temperature reaches 560°C for the SP-1 particles, while for the larger SP-2 particles, this percentage is reached at a temperature of 440°C. The percentage of the total heat flux due to radiation for bed temperatures of 300 to 750°C are: 6-20 percent for the SP-1 particles and 4-17 percent for the SP-2 particles.

These findings compare favorably with the theoretical predictions of Szekely and Fisher [15] who noted that the percentage of total heat flux due to radiation increases with increasing particle

of the particles larger than  $100 \mu$ . This has also been verified by the findings of many later studies. One such study was that of Barkow et al. [11] who also noted that the absolute amount of heat transferred by radiation is independent of particle size. The findings of this study support these earlier results, while Figures 17 and 18 show an increase in the percentage of total heat flux due to radiation with increasing particle size. Figures 17 and 18 indicate that the absolute amount of heat transferred by radiation is approximately the same for both particle sizes tested.

The percent radiation is now analyzed for all bed temperatures but at a constant fluidizing velocity. Figures 19 and 20 at fluidizing velocities of  $V_f = 1.26$  and  $1.92$  msec, respectively, for the 19- $\mu$  particles show that the percent radiation increases with increasing bed temperature at a constant fluidizing velocity. In both cases, the percent radiation is approximately 20 percent of the total heat flux at a bed temperature of  $750^\circ\text{C}$ . This percentage increases very slightly as the fluidizing velocity is increased. The same trend can also be seen with the 49- $\mu$  particles where the radiation heat flux becomes 3 percent of the total at  $750^\circ\text{C}$  as shown in Figures 21 and 22 for the fluidizing velocities of  $V_f = 2.5$  and  $3.5$  msec.

When analyzing the data for all fluidizing velocities but at a constant bed temperature, it is observed that for the 19- $\mu$  particles, the percent radiation increases very slightly as the fluidizing

velocity is increased. Figures 23 and 24 at constant bed temperatures of 697°C and 751°C illustrate this. This phenomenon can be explained by the packet model of heat transfer in fluidized beds. When the bed velocity is increased, the probe face is exposed to more bubbles. While the total heat transferred to the probe face decreases, the amount transferred by radiation through the bubbles increases, accounting for the increase in percent radiation. This trend was not apparent in the larger SP-2 particles where at a constant bed temperature for all fluidizing velocities, the percent radiation appears to remain constant. This is shown in Figure 25 at a bed temperature of 600°C.

It is not very meaningful to compare the percentages of total heat flux due to radiation found in this study with the results of other reports due to the differing methods used to determine the radiative component and the different sizes and types of particles used. This study, as discussed in Section 4.A, Experimental Analysis, attempted to correct procedural and analytical shortcomings noted in previous investigations. In general, the values of 20 to 30 percent for percentage of total heat flux due to radiation found in this study are midway between the extremes found by previous analyses (see Table 1).

#### C. Total Heat Transfer Coefficient $h_t$

The total heat transfer coefficient is determined from the relation:

$$h_t = \frac{q_t}{T_b - T_w} \quad (13)$$

It increases gradually with increasing bed temperatures for both particle types. The total heat transfer coefficient for the smaller SP-1 particles (Figure 26) is larger than that for the SP-2 particles (Figure 27) for all bed temperatures. The sand particles have a large heat capacity and the heat transfer takes place primarily at the contact points of the particles with the probe surface. Since the smaller particles have a larger number of contact points per unit of surface area, they produce a larger total heat flux and thus have a larger  $h_t$ .

The increase of  $h_t$  with bed temperature is more clearly illustrated with data taken at a constant fluidizing velocity. Figure 28 at  $V = 1.26$  m/sec and Figure 29 at  $V = 2.0$  m/sec for the SP-1 particles show that at constant fluidizing velocity  $h_t$  increases with increasing bed temperature. The same result is shown in Figures 30 and 31 at  $V = 2.5$  and  $3.9$  m/sec for the SP-2 particles.

The total heat transfer coefficient decreases very slightly as the excess velocity ( $V - V_{mf}$ ) is increased for the SP-1 particles. Figure 32 which contains data taken at all bed temperatures for varying fluidizing velocities illustrates this. This can be explained using the packet model. Increasing the fluidizing velocity also increases the number of bubbles. When the probe face is exposed to more bubbles, the radiative heat flux increases while the amount of time that the probe face is exposed to the emulsion phase

decreases. However, most of the total heat transfer occurs through the conductive-convective mechanism during contact with the emulsion phase. Therefore the conductive-convective component decreases with increasing fluidizing velocity, and, in turn, the total heat transfer coefficient also decreases. This same trend is not as readily apparent in the data taken for the SP-2 particles (Figure 33) where the total heat transfer coefficient seems to remain relatively constant for all velocities used in this study.

The relationship discussed in the preceding paragraph is more readily visible when comparing  $h_t$  to the fluidizing velocity at a constant bed temperature. Figures 34 and 35 for bed temperatures of 610 and 751°C for the SP-1 particles show the decrease in  $h_t$  with increasing fluidizing velocity. At constant bed temperatures, it becomes apparent that  $h_t$  also decreases with increasing fluidizing velocity for the SP-2 particles, which was not apparent in Figure 33 for all data. Figures 36 and 37 for bed temperatures of 600 and 755°C illustrate a gradual decrease in  $h_t$  for the SP-2 particles.

The total heat transfer coefficient at a bed temperature of 750°C is approximately 350 W/m<sup>2</sup>°C for the SP-1 particles (733 μm) and 260 W/m<sup>2</sup>°C for the SP-2 particles (1030 μm). The decrease in  $h_t$  with increasing particle size and the linear variation with bed temperature noted in this study agree with the findings of Kharchenko and Makhorin [10]. The same trend for  $h_t$  noted by Vedamurthy and Sastri [18] is seen in this study, even though their

analysis was conducted with a particle size of 500  $\mu\text{m}$  and a bed temperature range of 800 to 1100°C. The total heat transfer coefficient varies linearly in both cases and increases gradually with bed temperature. Vedamurthy and Sastri's results yield values of  $h_t$  (225  $\text{W}/\text{m}^2\text{°C}$  at 800°C) which are smaller than those measured by this study. Kharchenko and Makhorin [10] found  $h_t = 300 \text{ W}/\text{m}^2\text{°C}$  for a particle size of 710  $\mu\text{m}$  and a bed temperature of 500°C. This is equal to the value found for  $h_t$  for the SP-1 particles in this study (Figure 26). Thring's [16] packet and spherical particle models predict  $h_t = 400 \text{ W}/\text{m}^2\text{°C}$  for a particle size of 780  $\mu\text{m}$  and  $T_b = 750\text{°C}$  as compared to the value of 350  $\text{W}/\text{m}^2\text{°C}$  for the SP-1 particles in this study. Kolar et al. [11] predicted  $h_t = 210 \text{ W}/\text{m}^2\text{°C}$  for 1000  $\mu\text{m}$  diameter particles at  $T_b = 750\text{°C}$  which compares well with the value found for the SP-2 particles in this study (Figure 27).

The variation of the total heat transfer coefficient with fluidizing velocity as shown in Figures 34 through 37 follows the same trend as found by Vedamurthy and Sastri and by Kolar. Both of these studies also found that the total heat transfer coefficient, after initially increasing with fluidizing velocity, reached a maximum value and then gradually decreased as the velocity continued to increase.

#### D. Radiative Heat Transfer Coefficient

The radiative heat transfer coefficient is found using the

relation:

$$h_r = \frac{q_r}{T_b - T_w} \quad (14)$$

It increases linearly with increasing bed temperature and has the same values at all bed temperatures for both particle types tested as shown in Figures 38 and 39. This trend is to be expected since the radiative heat flux for both particle types is also approximately the same for all bed temperatures, as was noted in Section 5.A.

Vedamurthy and Sastri [18] noted the same trend for the radiative heat transfer coefficient in their study. Extrapolating the results of this study into their temperature range yields values of  $h_r$  on the same order as their findings. In their study,  $h_r$  also varies linearly for bed temperatures less than 900°C and has a value of 75 to 80 W/m<sup>2</sup>°C for  $T_b = 800^\circ\text{C}$ .

#### E. Bed Emissivity

An apparent bed emissivity is calculated using the Stefan-Boltzmann equation and assuming that the emissivity of the probe face is one:

$$\epsilon_{\text{bed}} = \frac{q_r}{\sigma(T_b^4 - T_{wd}^4)} \quad (15)$$

Figures 40 and 41 show the variation of bed emissivity with bed temperature for the SP-1 and SP-2 particles, respectively. The

bed emissivity reaches a maximum value at a bed temperature of 460°C for the SP-1 particles and 500°C for the SP-2 particles and then begins to decrease gradually for both types. The SP-2 particles have a larger emissivity than the SP-1 particles at all bed temperatures; however, the emissivity, in both cases, always remains less than one. Il'chenko et al. [8] also predicted that the bed emissivity was less than one when they found their experimental values for radiative heat flux were less than the calculated black body values. Thring [16] and Vedamurthy and Sastri [18], on the other hand, assumed that the bed emissivity was very close to that of a black body and used  $\epsilon_{bed} = 1$  in their analyses. The experimental results of this study support Il'chenko's prediction.

#### F. Error Analysis

The accuracy of the results obtained in this study is determined by calculating the standard deviation from the mean for each of the following parameters: radiation heat flux, percentage of the total heat flux due to radiation, total heat transfer coefficient and radiative heat transfer coefficient. Two data points at the same fluidizing velocity and bed temperature are found and then the mean value of the parameter and the standard deviation are calculated. This procedure is repeated for several combinations of bed temperature and fluidizing velocity for each parameter. The largest deviation and the average deviation from the mean for each

parameter for each particle type are determined. The following results are obtained:

	Maximum Deviation (%)	Average Deviation (%)
<u>SP-1 Particles</u>		
$q_r$	3.0	1.1
% Radiation	5.4	1.6
$h_t$	7.6	3.7
$h_r$	3.6	1.3
<u>SP-2 Particles</u>		
$q_r$	1.1	0.6
% Radiation	1.8	1.3
$h_t$	2.0	1.0
$h_r$	0.8	0.6

The datalogger used to record temperature and emf readings at critical points in the test setup rounds off readings to the nearest tenth producing a maximum error of 0.05°C or 0.05 mv. This accuracy in reading the emf output of the thermopile results in a maximum error of 90 W/m<sup>2</sup> for  $q_r$ .

The flowmeters used to measure the flow of the coolant air and water to the probe have a  $\pm 2.0$  percent accuracy and the K-type thermocouples used are accurate to within  $\pm 2.2^\circ\text{C}$ .

## 6. CONCLUSIONS

The radiation heat flux, percentage of total heat flux due to radiation, total heat transfer coefficient, radiative heat transfer

coefficient, and bed emissivity for two sizes of silica sand particles are studied in order to determine the effect of particle size on the radiative component of heat transfer in high temperature fluidized beds.

Radiation is found to be a significant part of the overall heat transfer process in high temperature fluidized beds. For both particle sizes tested, the radiative component becomes significant for bed temperatures greater than 400°C. This study defines "significant" to mean at least 10 percent of the total heat flux. The percentage of total heat transfer due to radiation for the large particles is greater than that for the small particles at all bed temperatures. Therefore, the radiative component of total heat transfer becomes significant at lower bed temperatures for the large particles. At a bed temperature of 750°C, the radiative component is 30 percent of the total heat flux for the larger SP-2 particles and 20 percent for the SP-1 particles.

While the percentage of total heat transfer due to radiation varies with particle size, the absolute quantity of radiant heat flux does not. The radiation heat flux is found to be approximately the same for both particle sizes tested at all bed temperatures.

The total heat transfer coefficient increases gradually with increasing bed temperature for both particle types. After initially increasing with fluidizing velocity,  $h_t$  reaches a maximum value and then slowly decreases as the velocity continues to increase. The

radiative heat transfer coefficient increases linearly with bed temperature and is independent of particle size, having the same value for both particle types at all bed temperatures.

The bed emissivity increases with bed temperature and after reaching a maximum value slowly decreases for both particle types. The larger particles have a higher emissivity than the small particles at all bed temperatures; however, the emissivity for both particle types remains in the 0.7 to 0.8 range at high temperatures.

The significant contribution that radiative heat transfer makes in the overall heat transfer process in high temperature fluidized beds cannot be neglected. Analytical models for heat transfer in high temperature fluidized bed combustors must include not only the conduction-convection mechanism but the radiation mechanism as well.

This study has determined the significance of radiation in high temperature fluidized beds using only two sizes of silica sand particles. Future studies should investigate the effect other size particles would have on radiation, particularly much larger sizes (3000  $\mu\text{m}$ ). Different types of materials such as silicon carbide, fused magnesite, corundum, etc. could also be used to determine their effect on the radiative component. A high temperature fluidized bed in which coal is actually being combusted could also be analyzed to determine the effect carbon particles have on radiation.

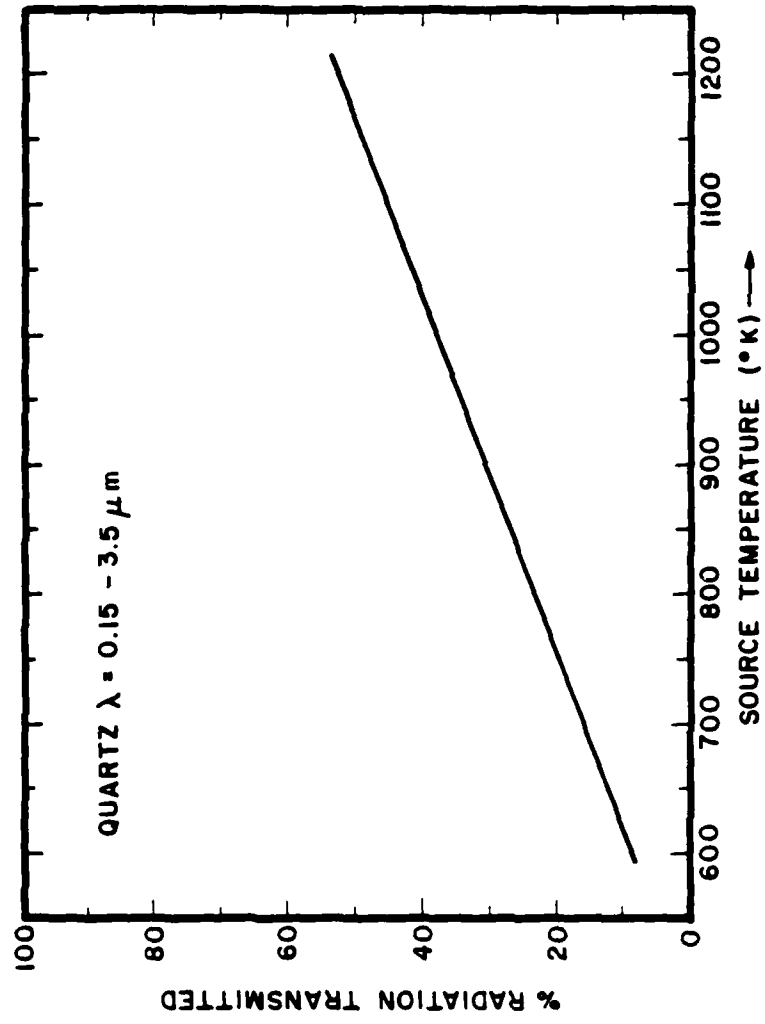


Figure 1 Percentage of radiation transmitted by a quartz window

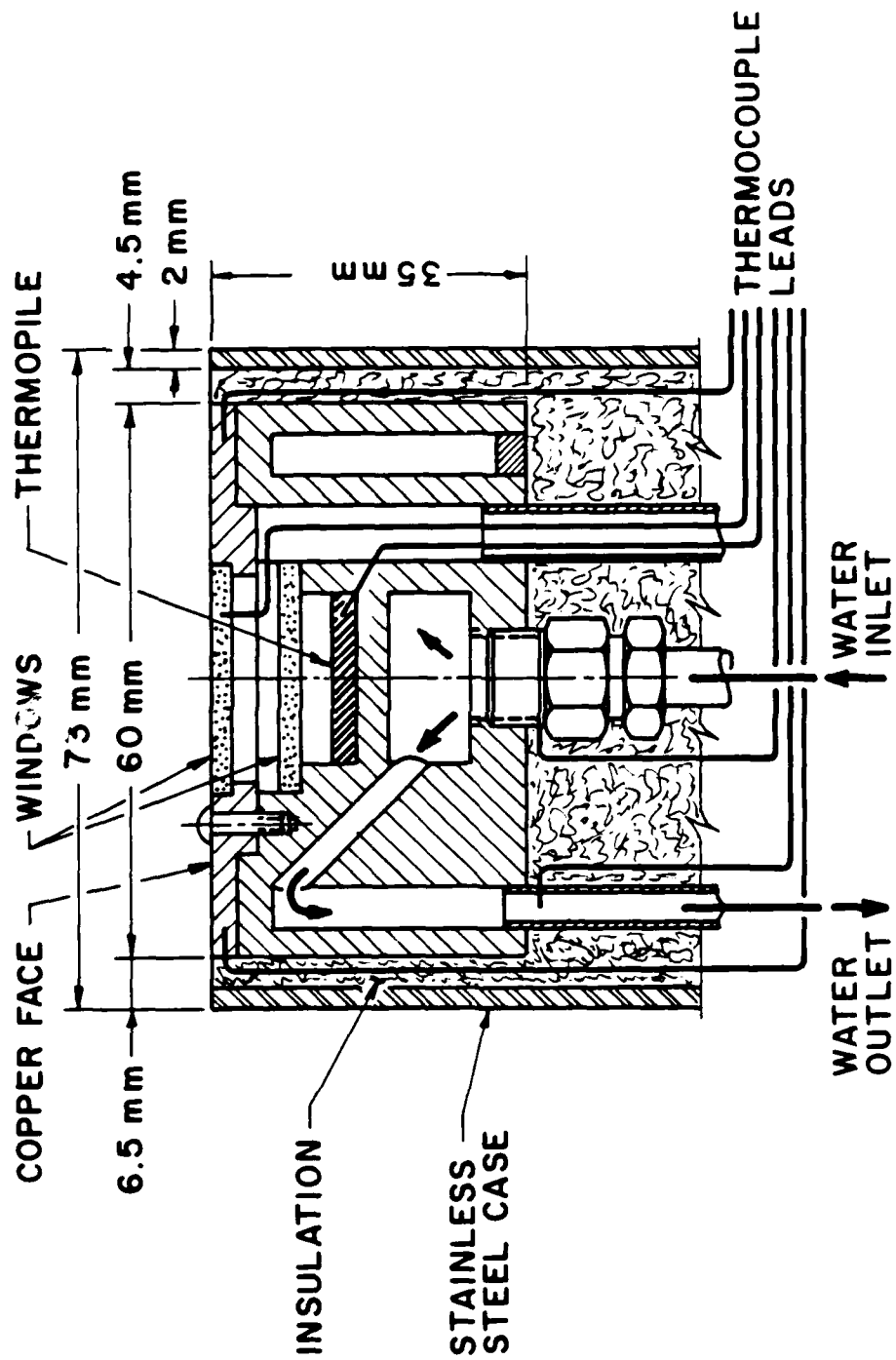


Figure 2 Configuration of the probe with the zinc selenide window

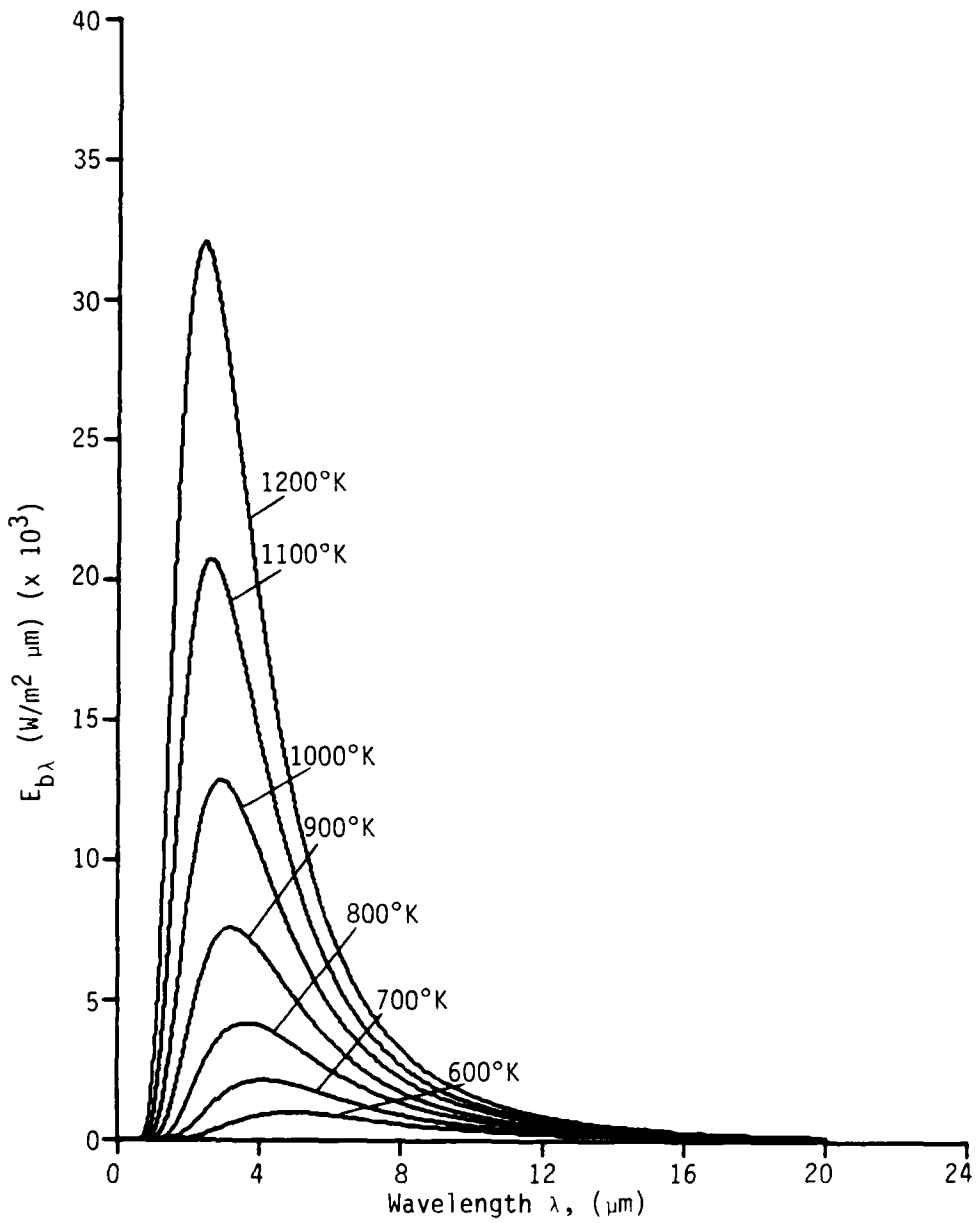


Figure 3 Monochromatic emissive power of a black body as a function of wavelength and temperature

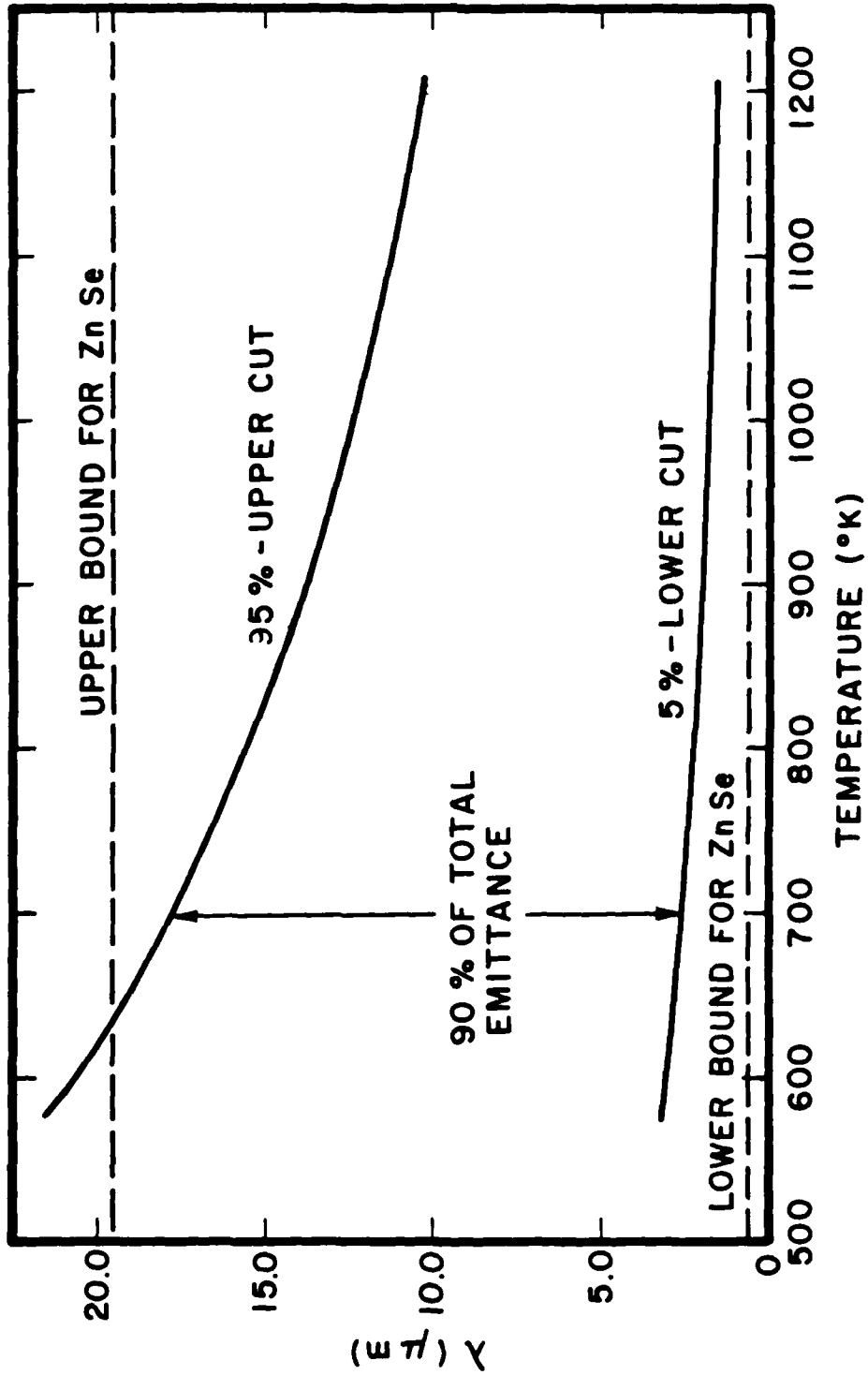


Figure 4 Wavelength range required for the window transmittance

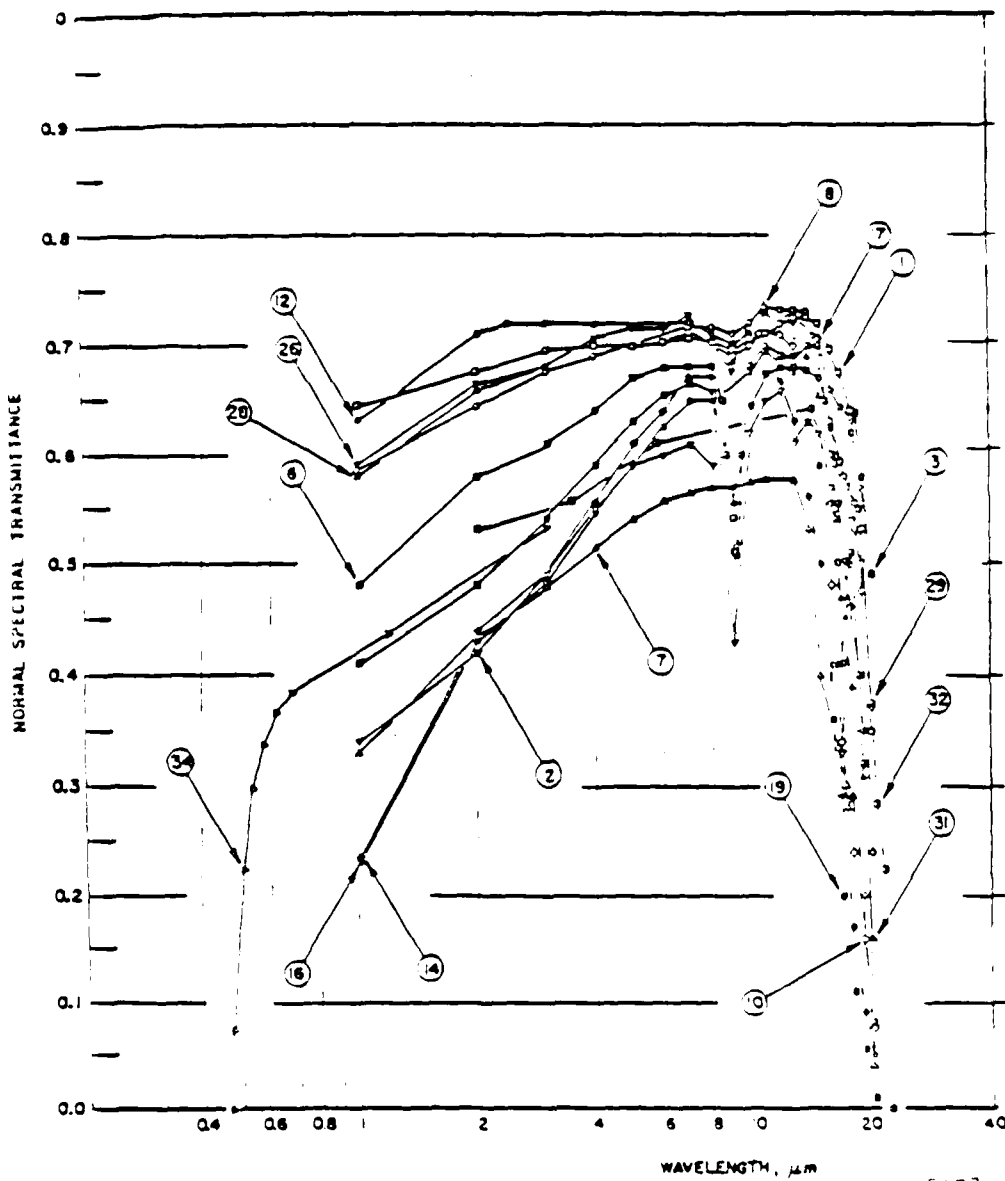


Figure 5 Normal spectral transmittance of zinc selenide [17]

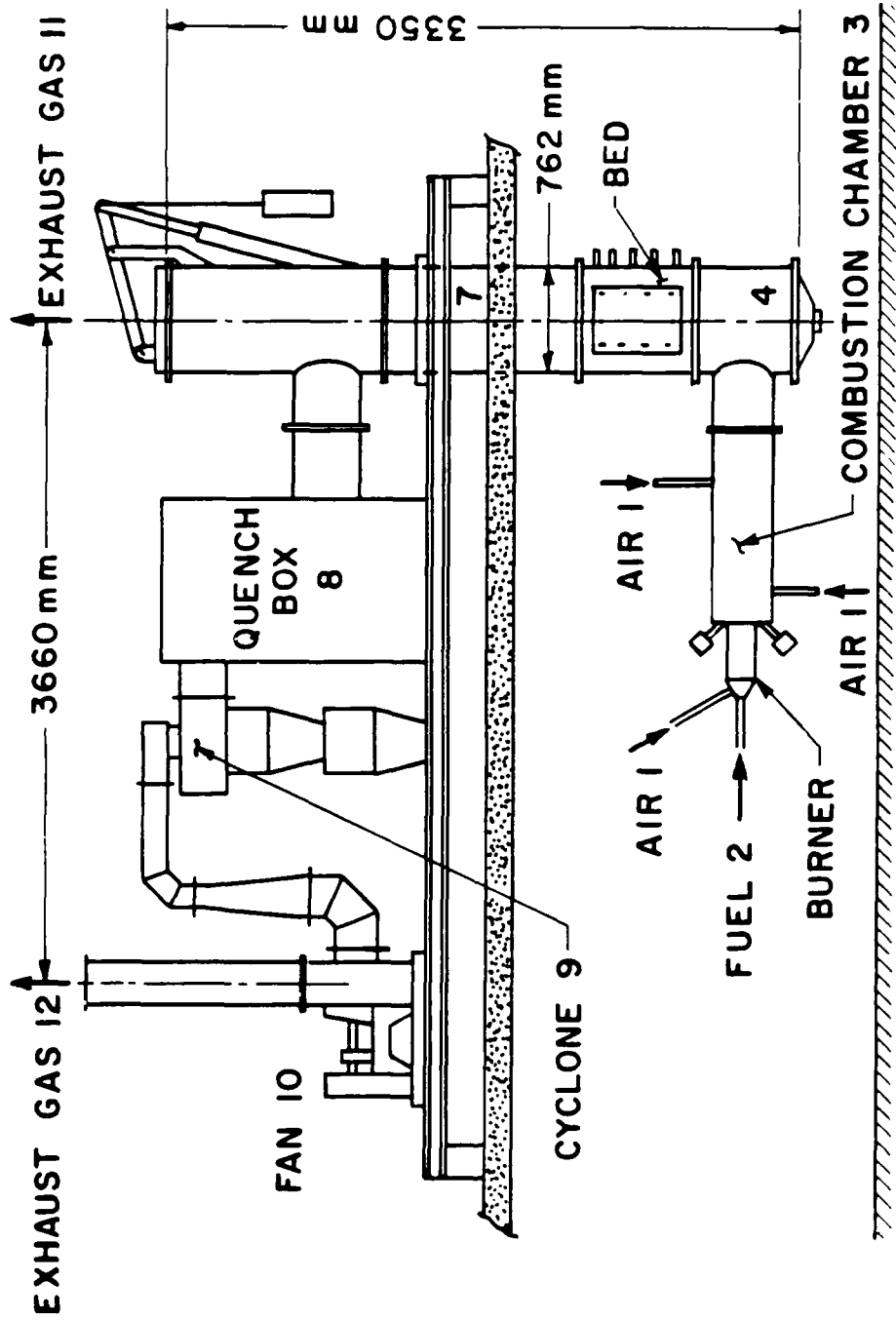


Figure 6 Diagram of the hot bed facility

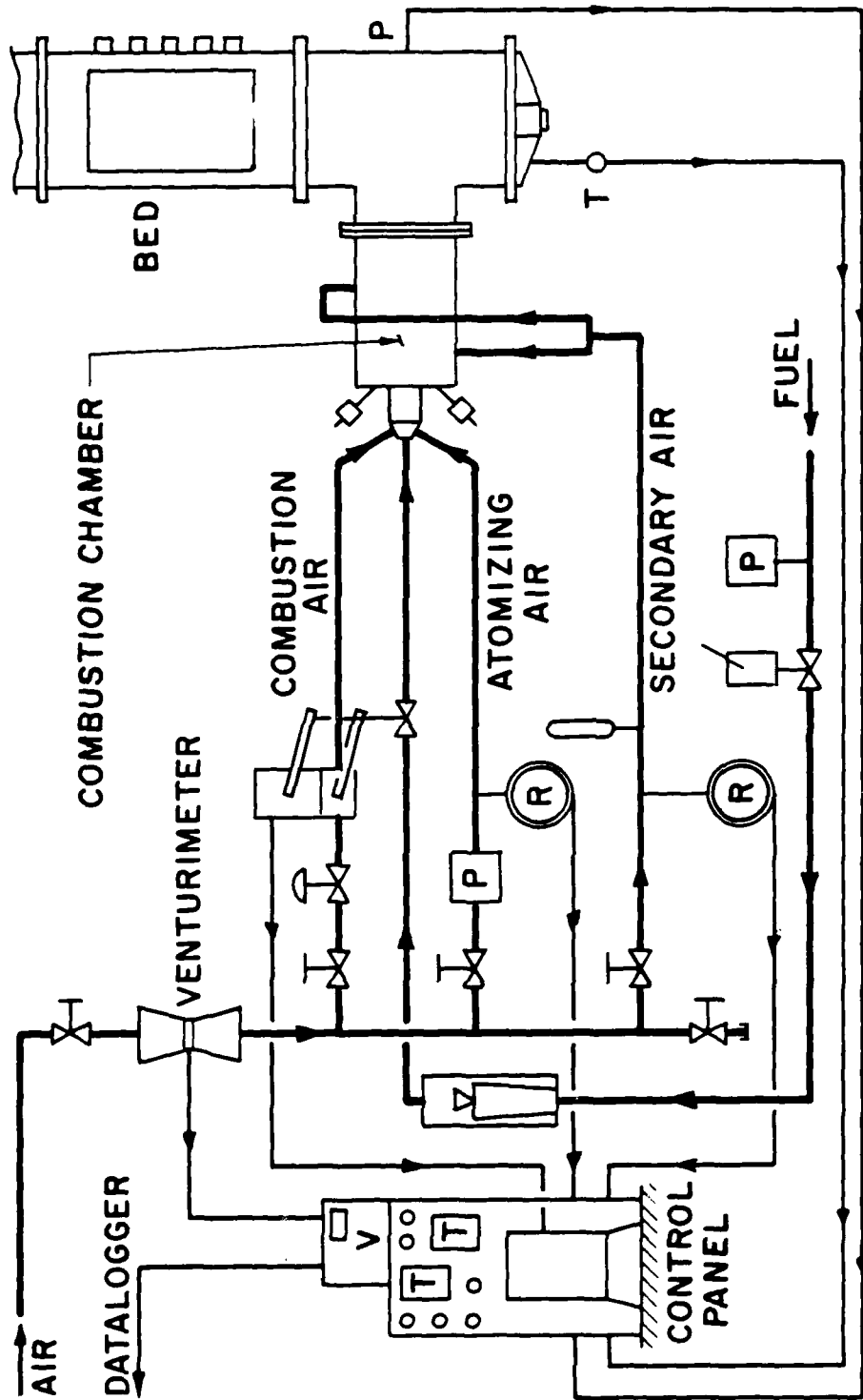


Figure 7 Schematic diagram of the control panel and air and fuel lines of the hot bed facility

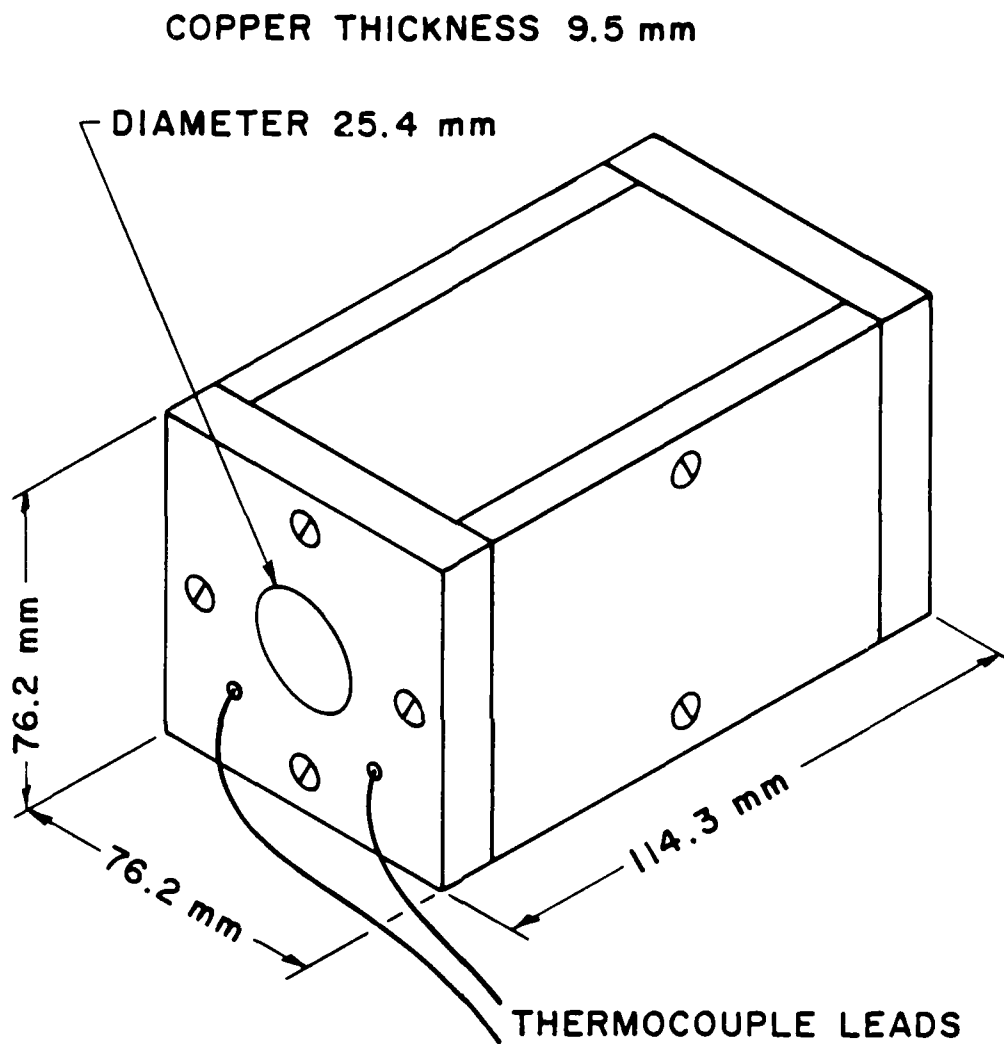


Figure 8 The black cavity used for calibration of the probe

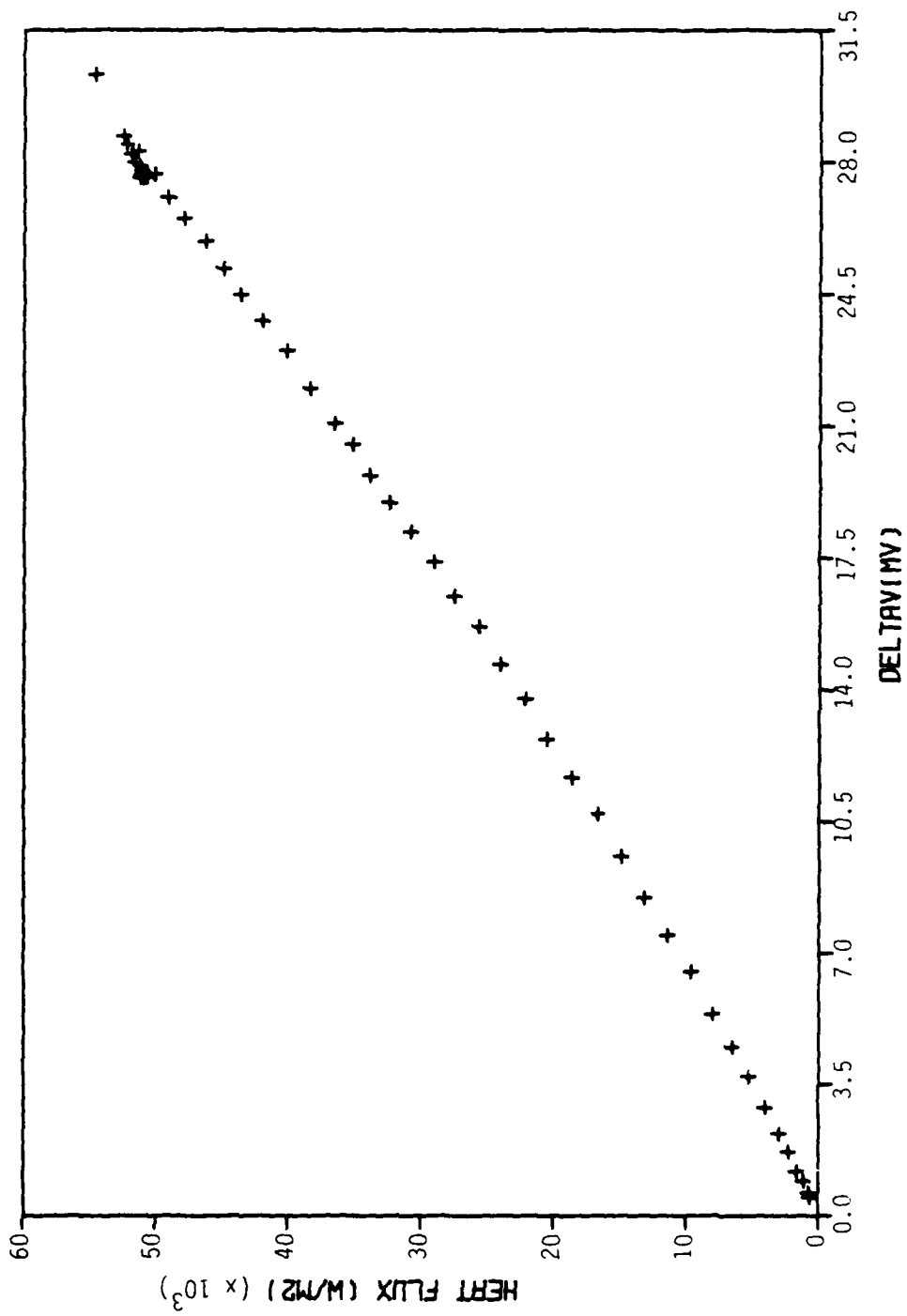


Figure 9 Calibration curve for the probe

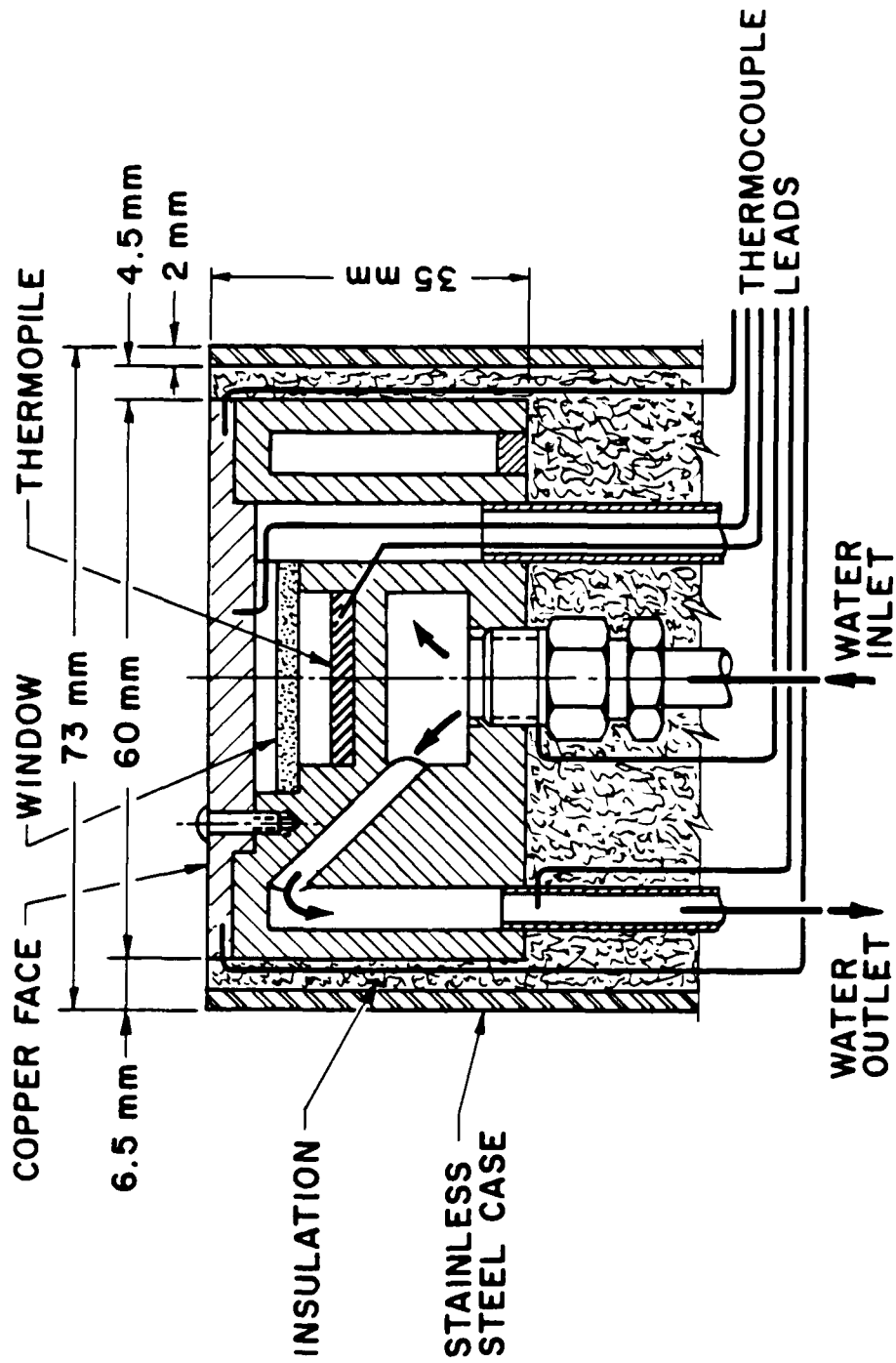
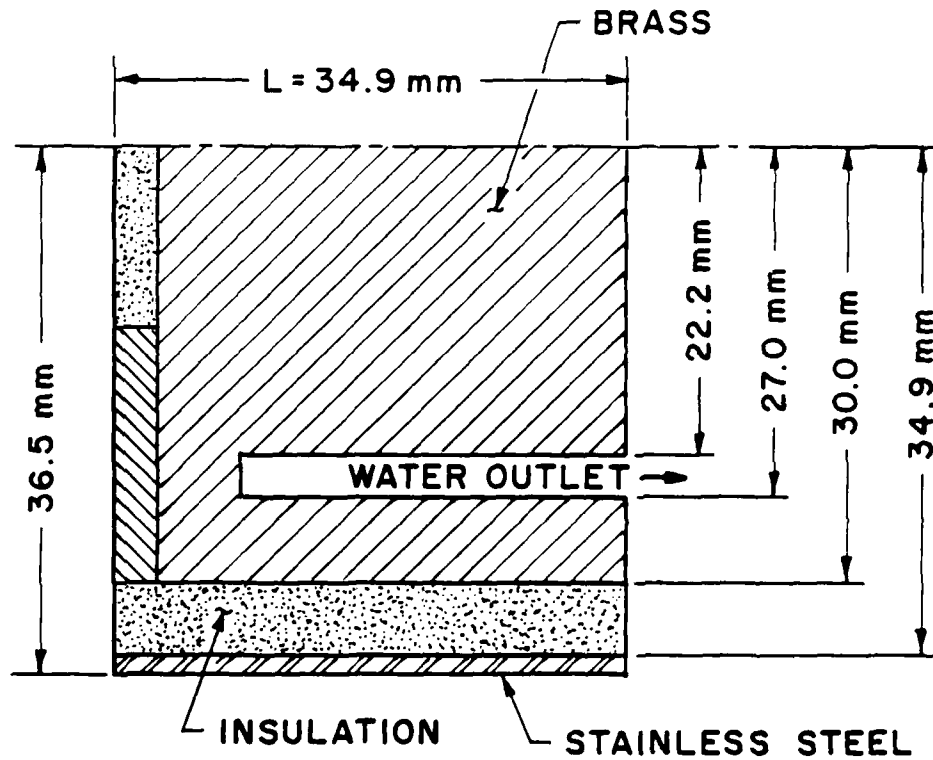


Figure 10 Configuration of the probe with the solid copper face



Brass  
 $r_i = 27.0 \text{ mm}$   
 $r_o = 30.0 \text{ mm}$   
 $k = 111.0 \text{ W/m}^\circ\text{C}$

Insulation  
 $r_i = 30.0 \text{ mm}$   
 $r_o = 34.9 \text{ mm}$   
 $k = 0.0502 \text{ W/m}^\circ\text{C}$

Stainless Steel  
 $r_i = 34.9 \text{ mm}$   
 $r_o = 36.5 \text{ mm}$   
 $k = 16.27 \text{ W/m}^\circ\text{C}$

$$A_o = 2\pi r_{oSS} L = 80.04 \text{ cm}^2$$

$$A_i = 2\pi r_{iBr} L = 59.21 \text{ cm}^2$$

Figure 11 Dimensions and conductivities of probe materials

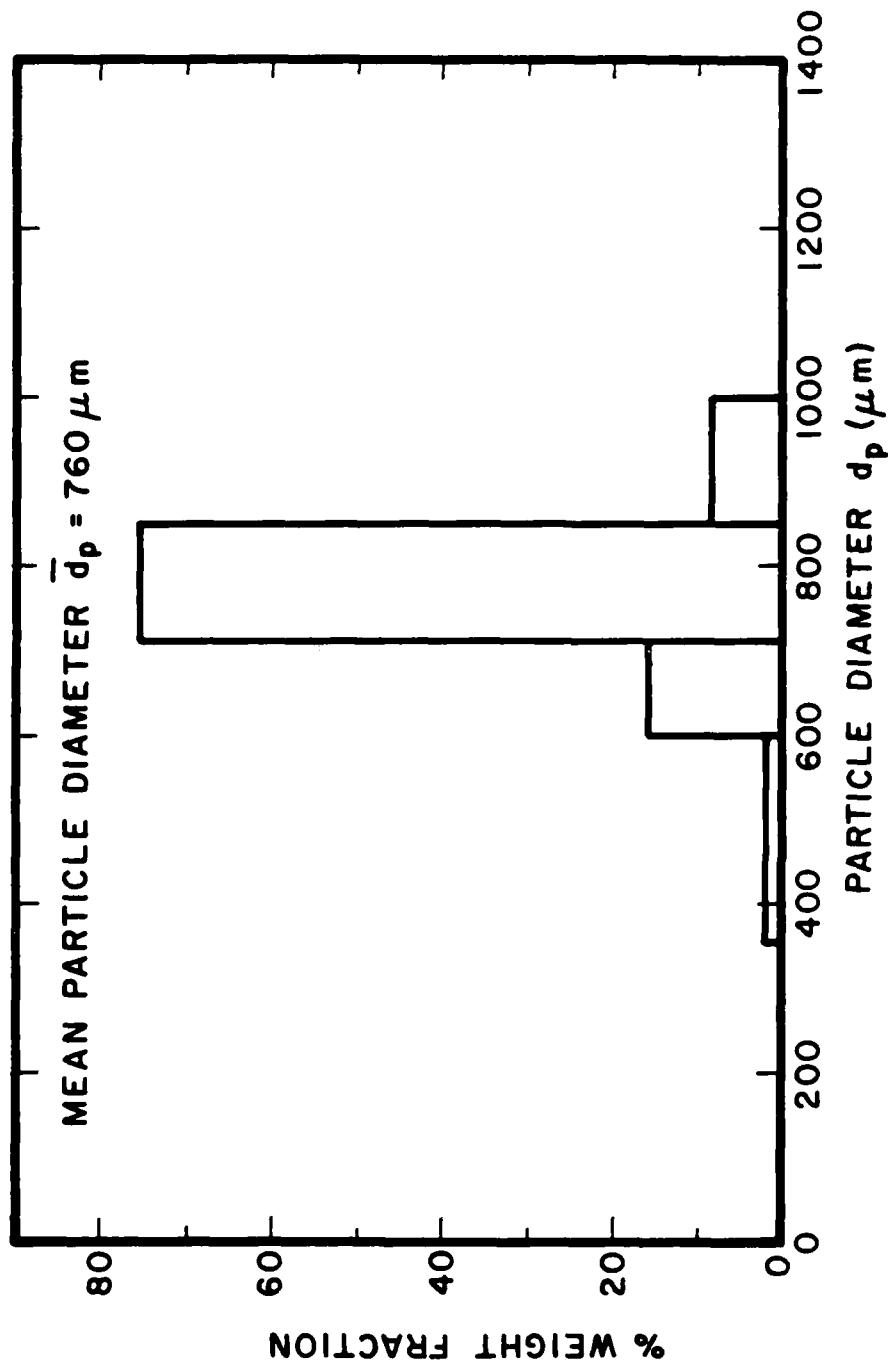


Figure 12 Size distribution of the SP-1 particles

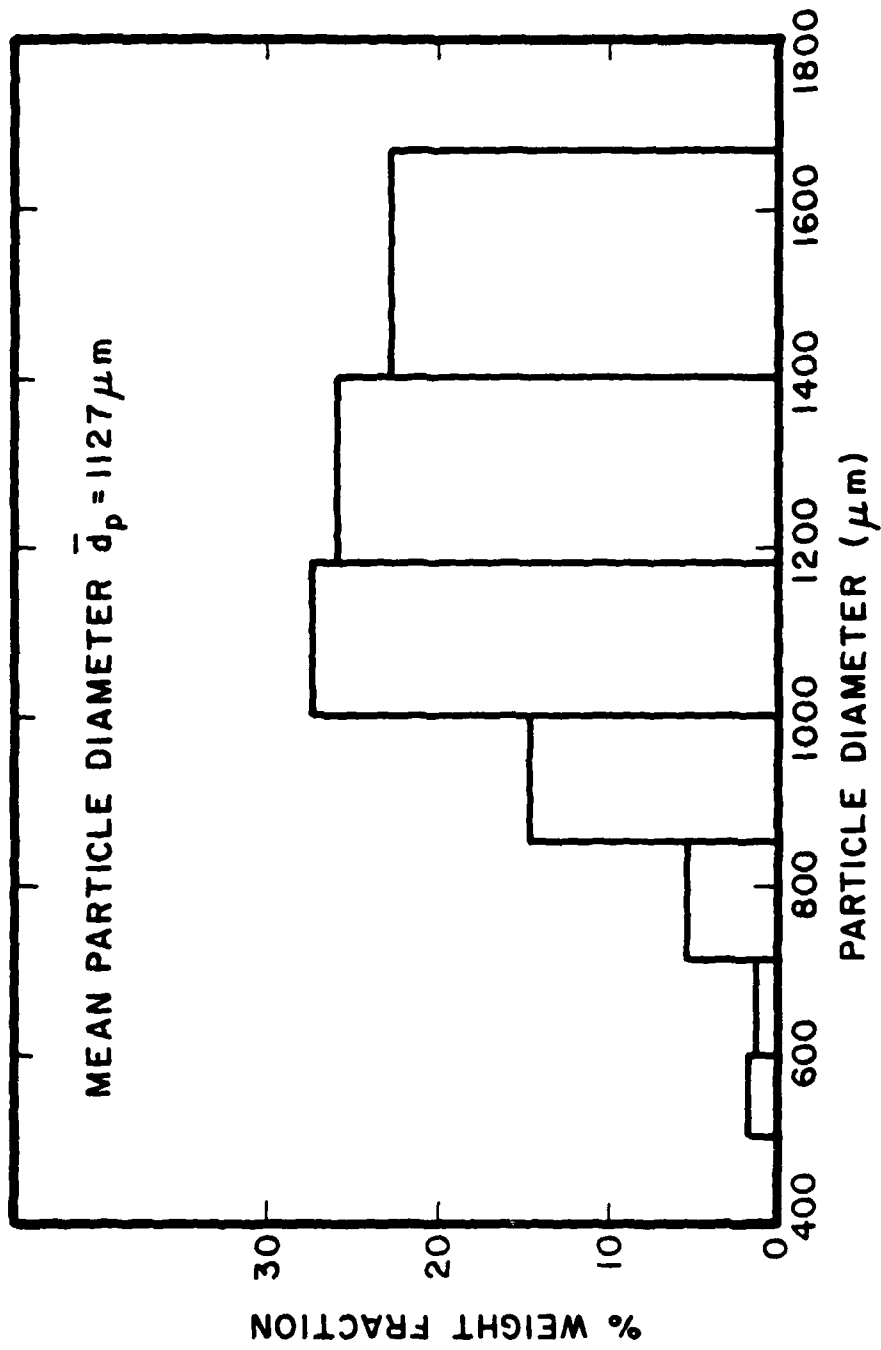


Figure 13 Size distribution of the SP-2 particles

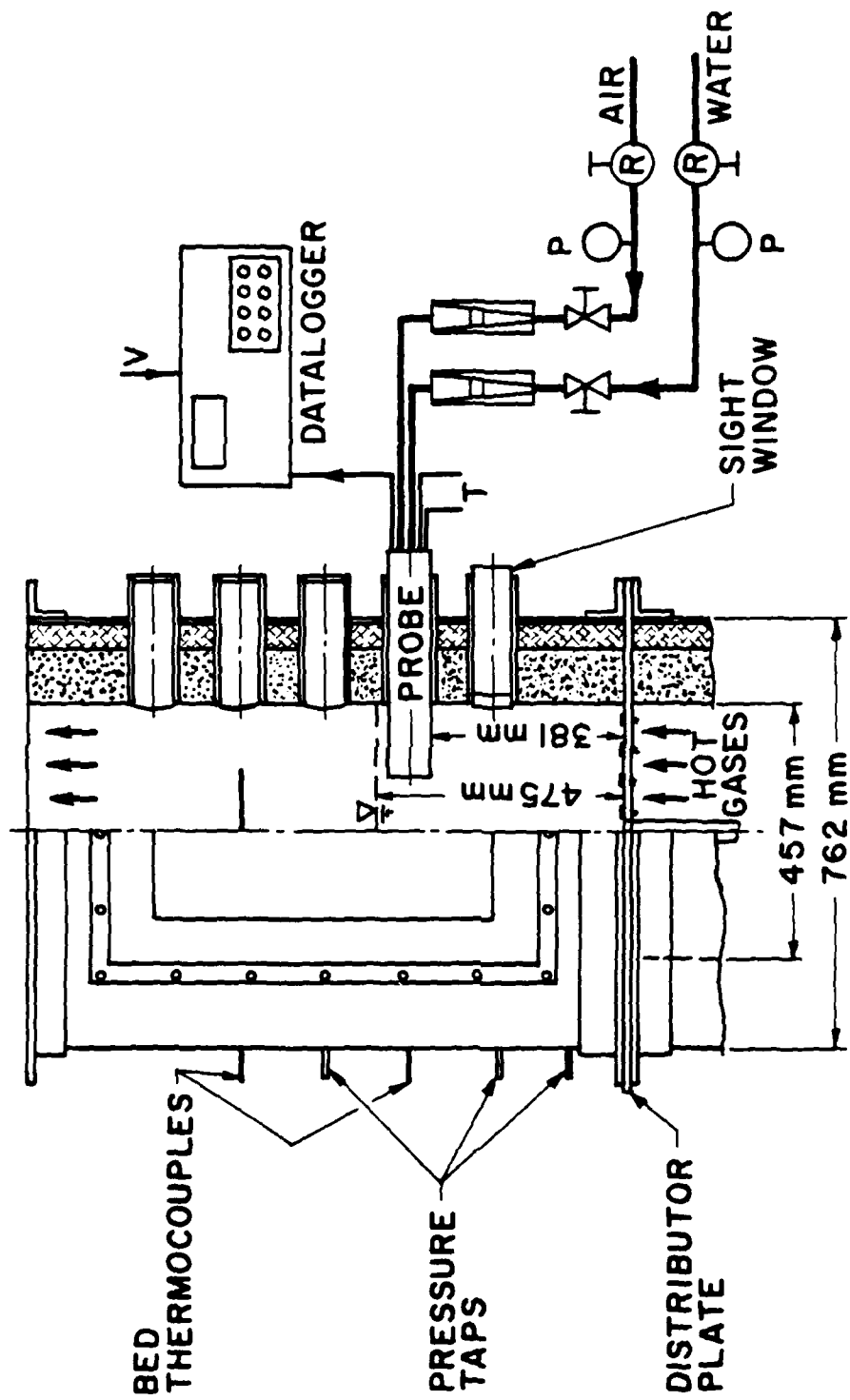


Figure 14 Probe in the test section

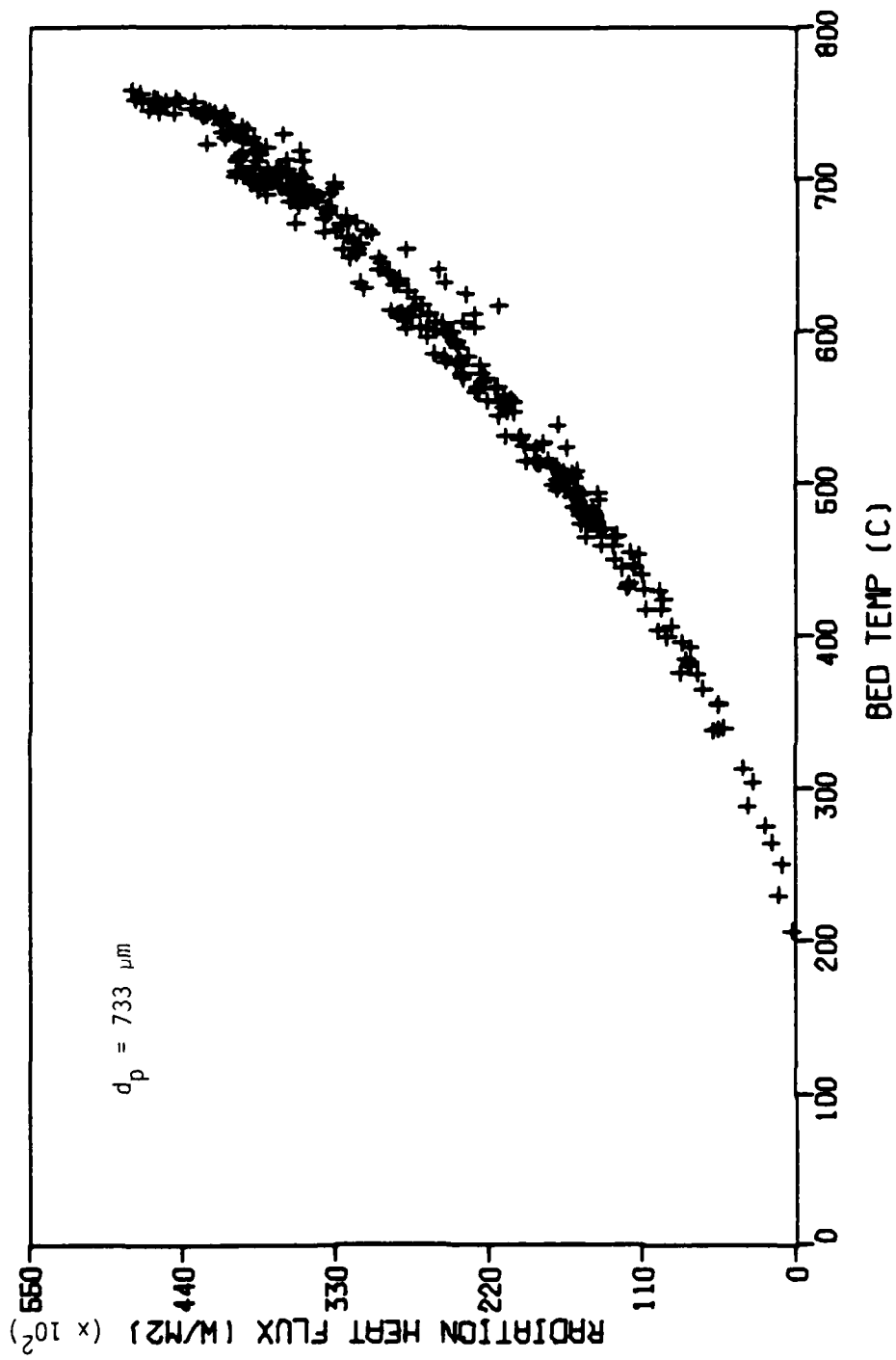


Figure 15 Radiation heat flux, SP-1 particles

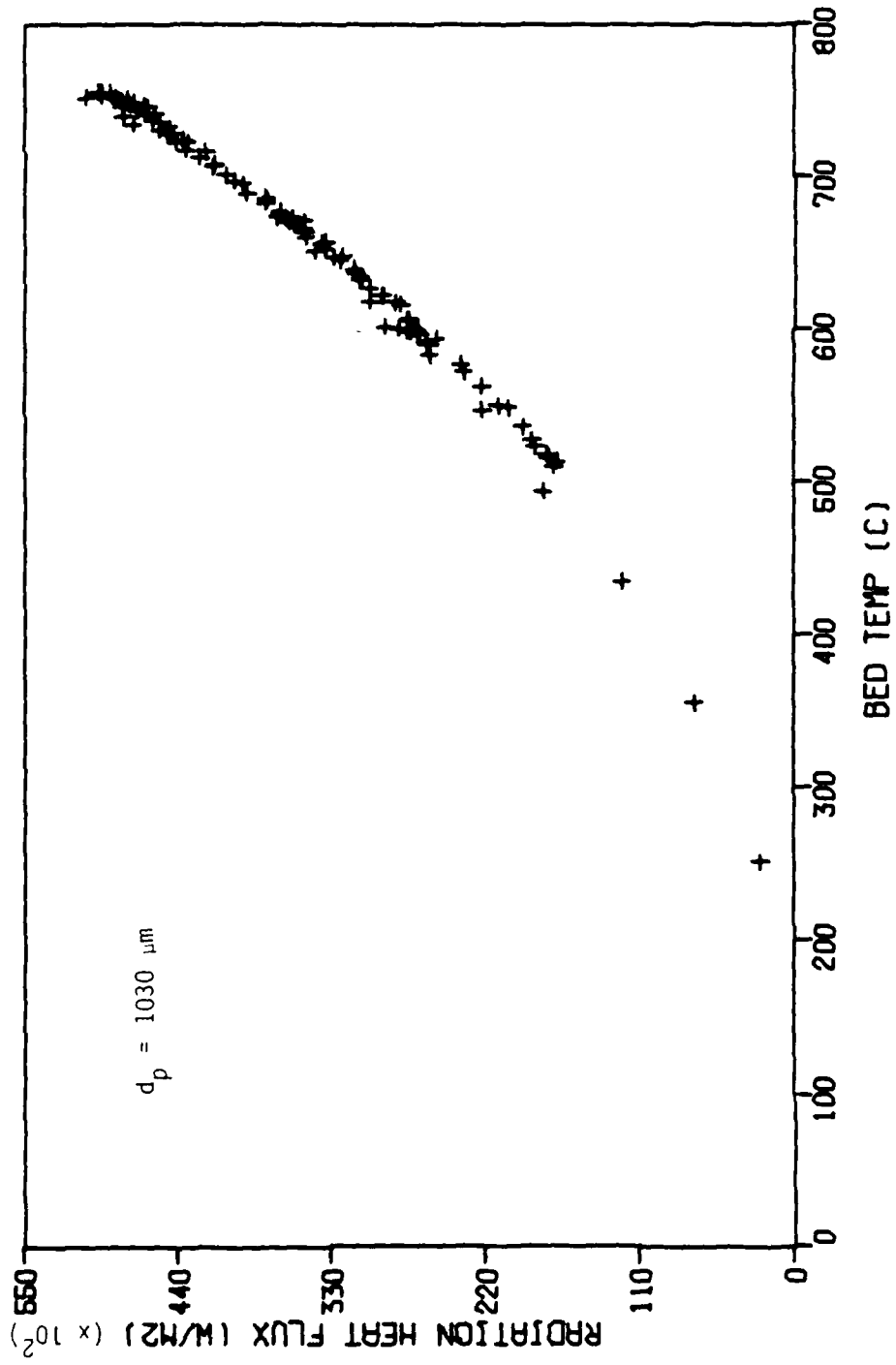


Figure 16 Radiation heat flux, SP-2 particles

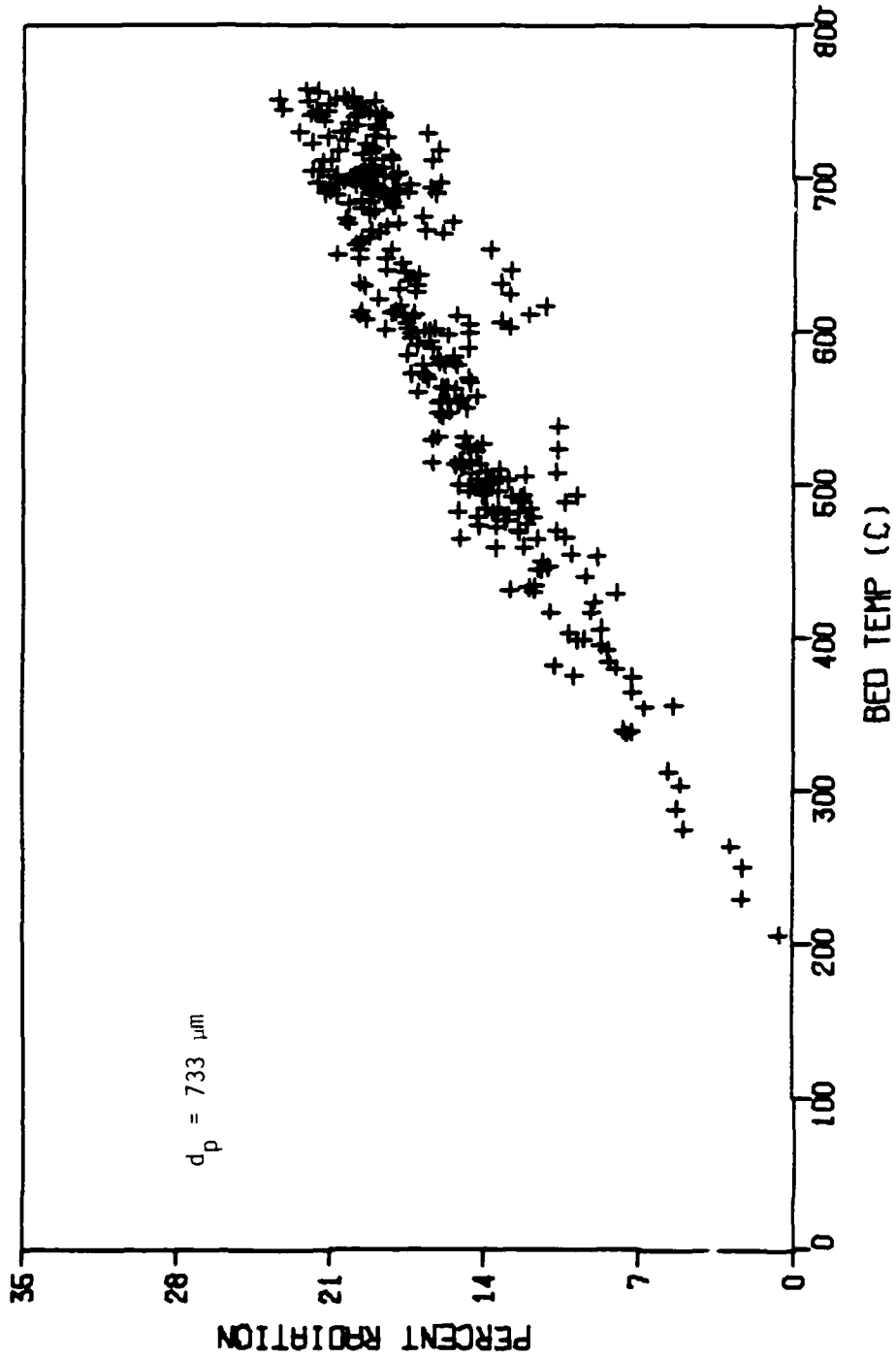


Figure 17 Percentage of total heat flux due to radiation, SP-1 particles

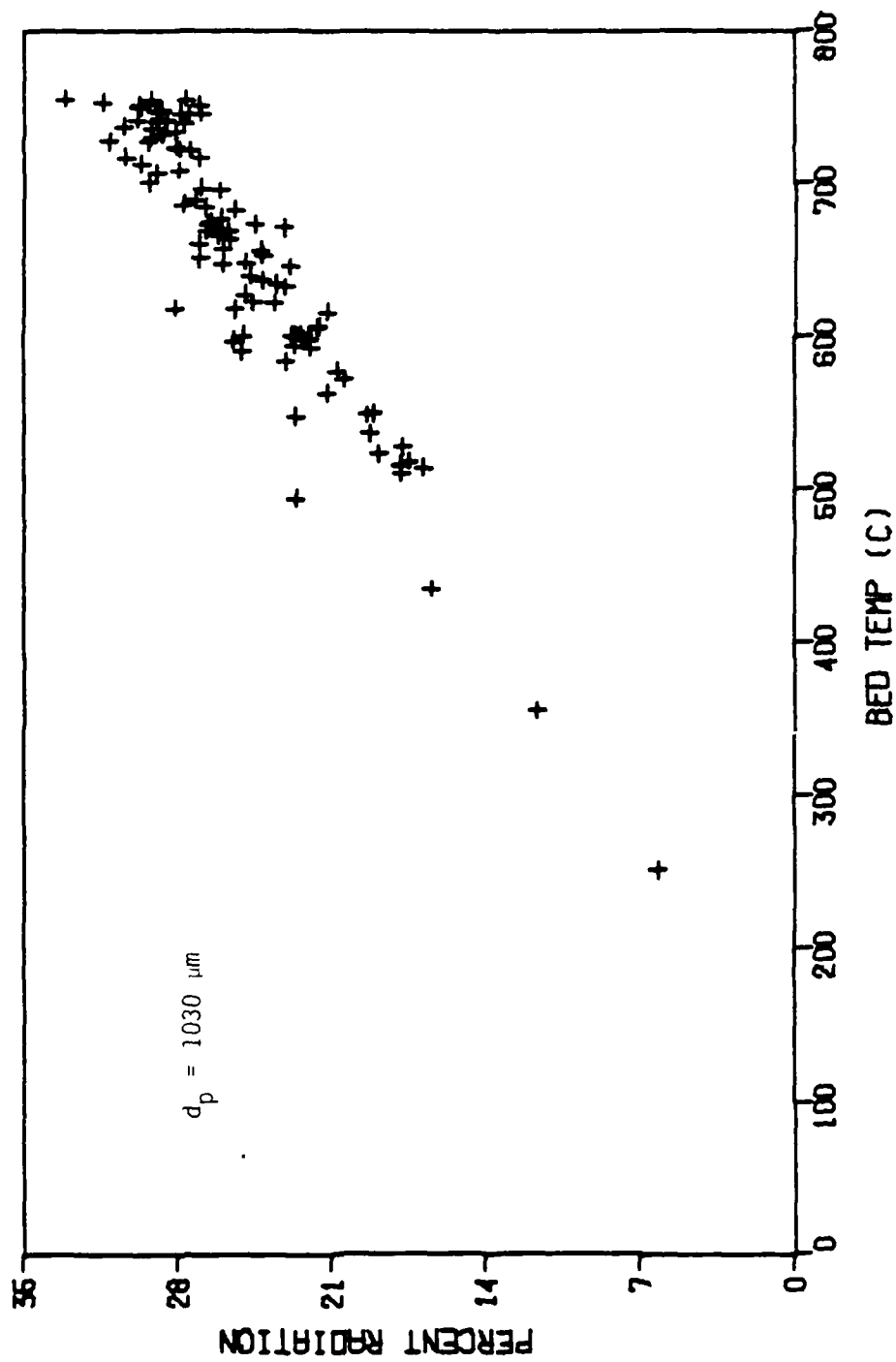


Figure 18 Percentage of total heat flux due to radiation, SP-2 particles

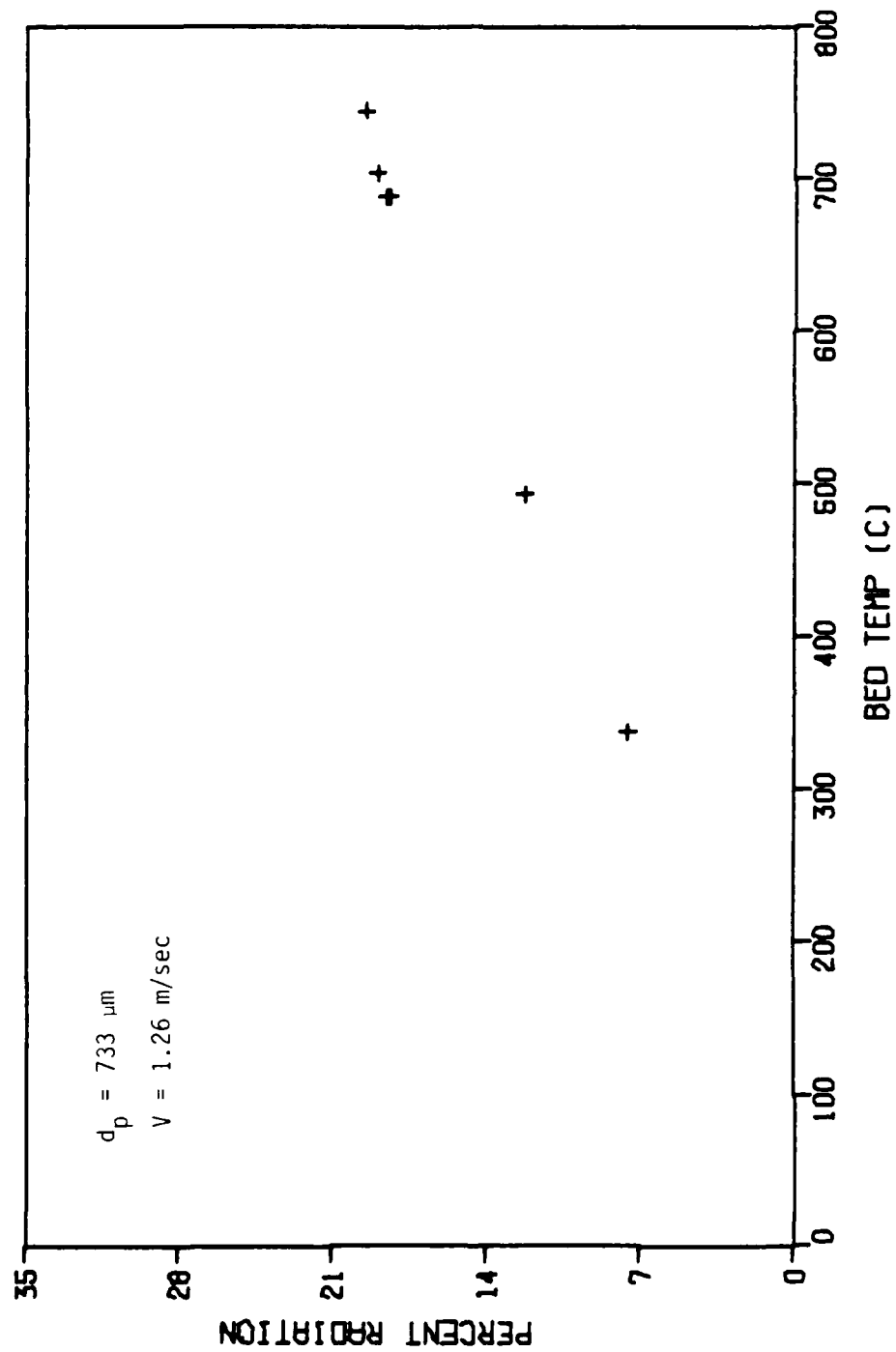


Figure 19 Percent radiation, SP-1 particles at constant fluidizing velocity,  
 $V = 1.26 \text{ m/sec}$

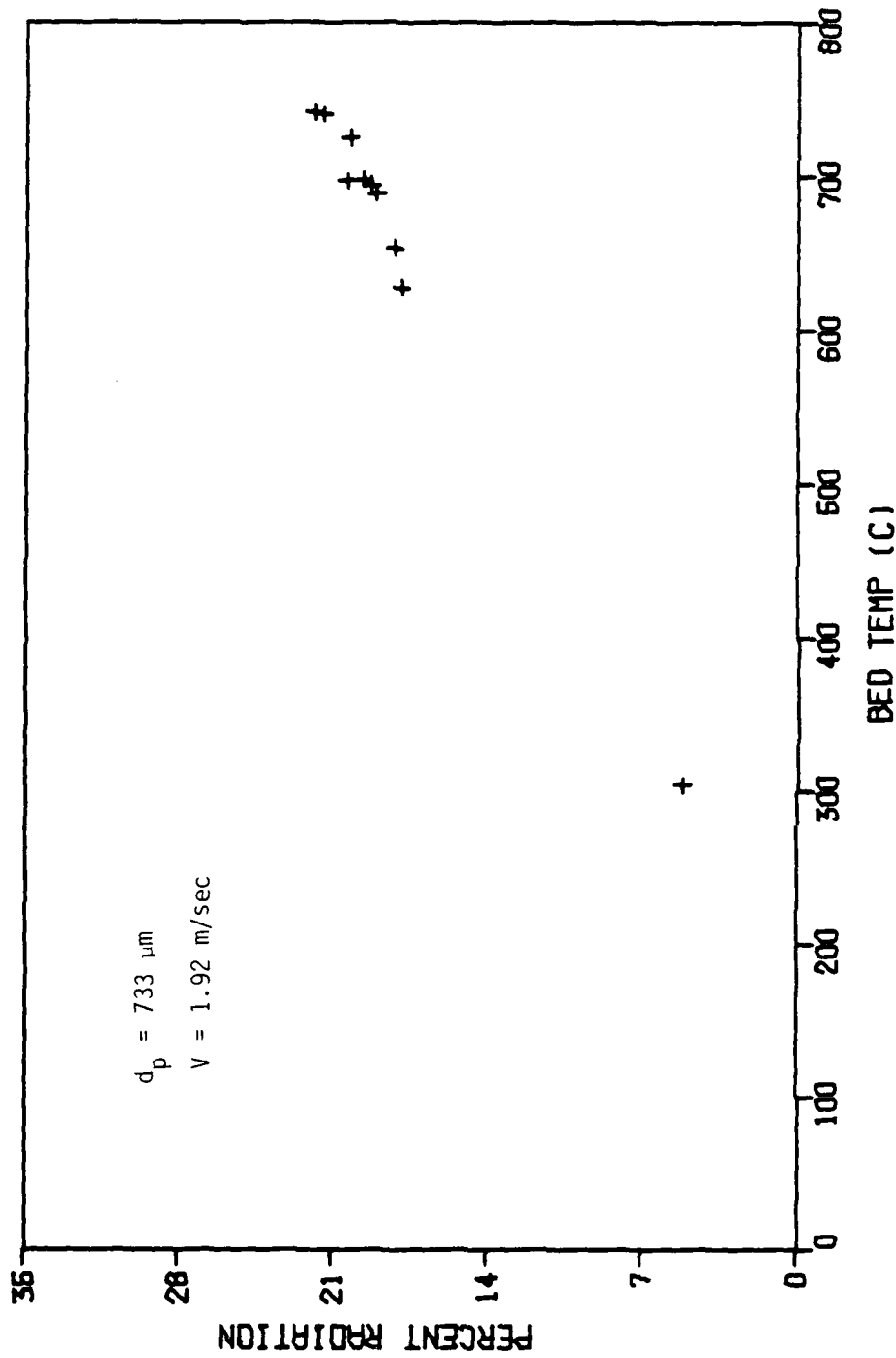


Figure 20 Percent radiation, SP-1 particles at constant fluidizing velocity,  $V = 1.92 \text{ m/sec}$

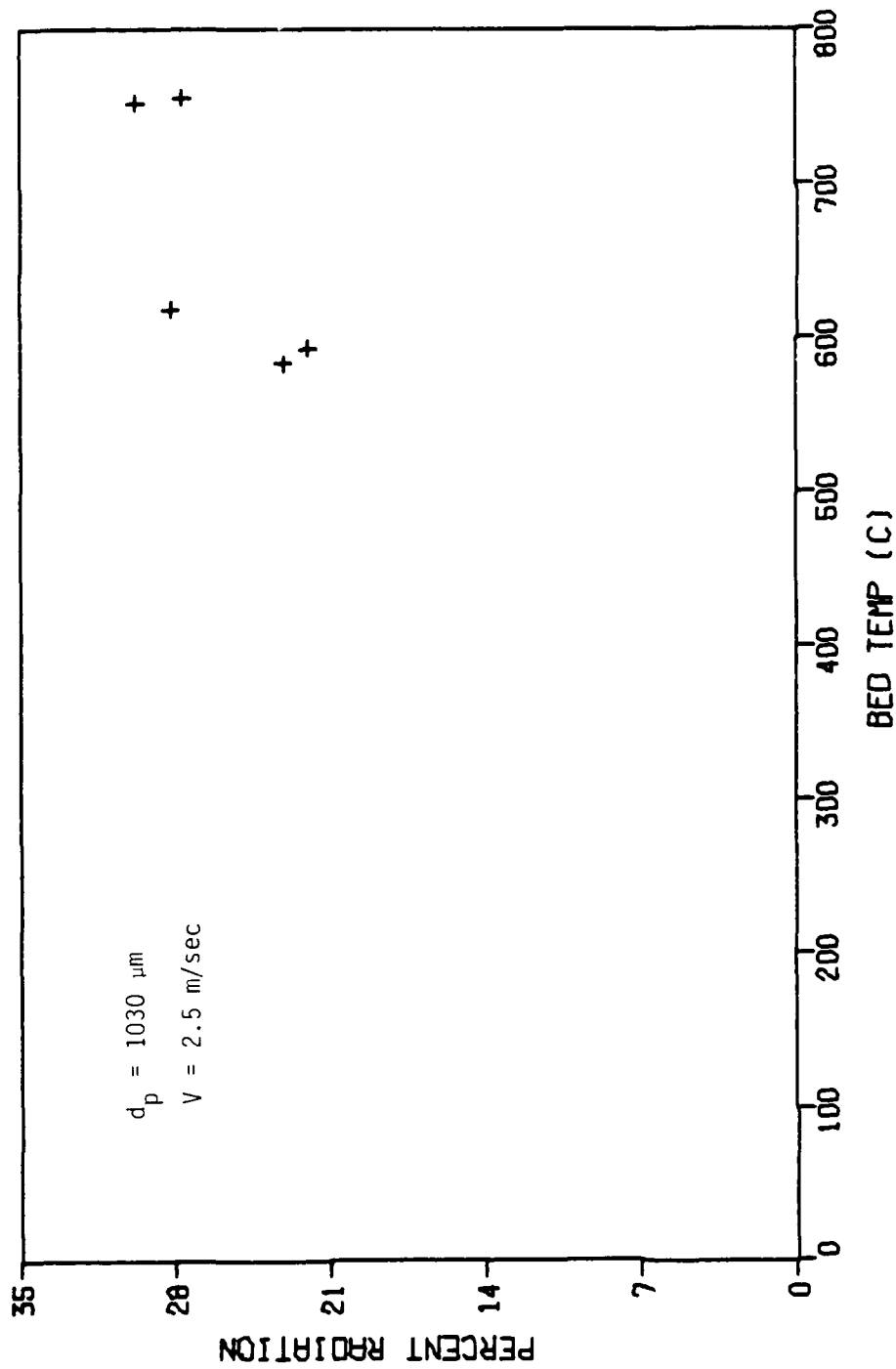


Figure 21 Percent radiation, SP-2 particles, at constant fluidizing velocity,  $V = 2.5 \text{ m/sec}$

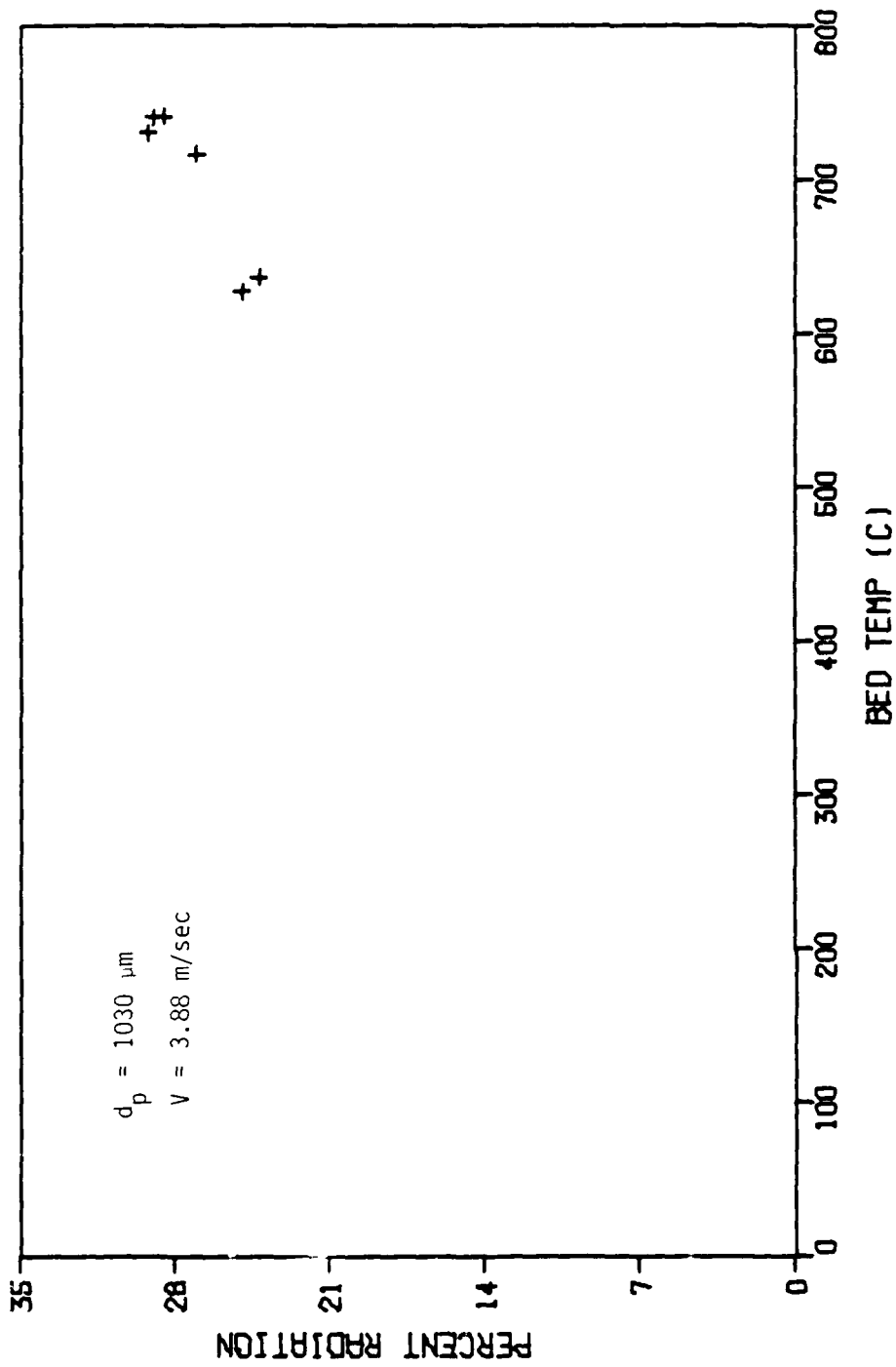


Figure 22 Percent radiation, SP-2 particles, at constant fluidizing velocity,  $V = 3.88 \text{ m/sec}$

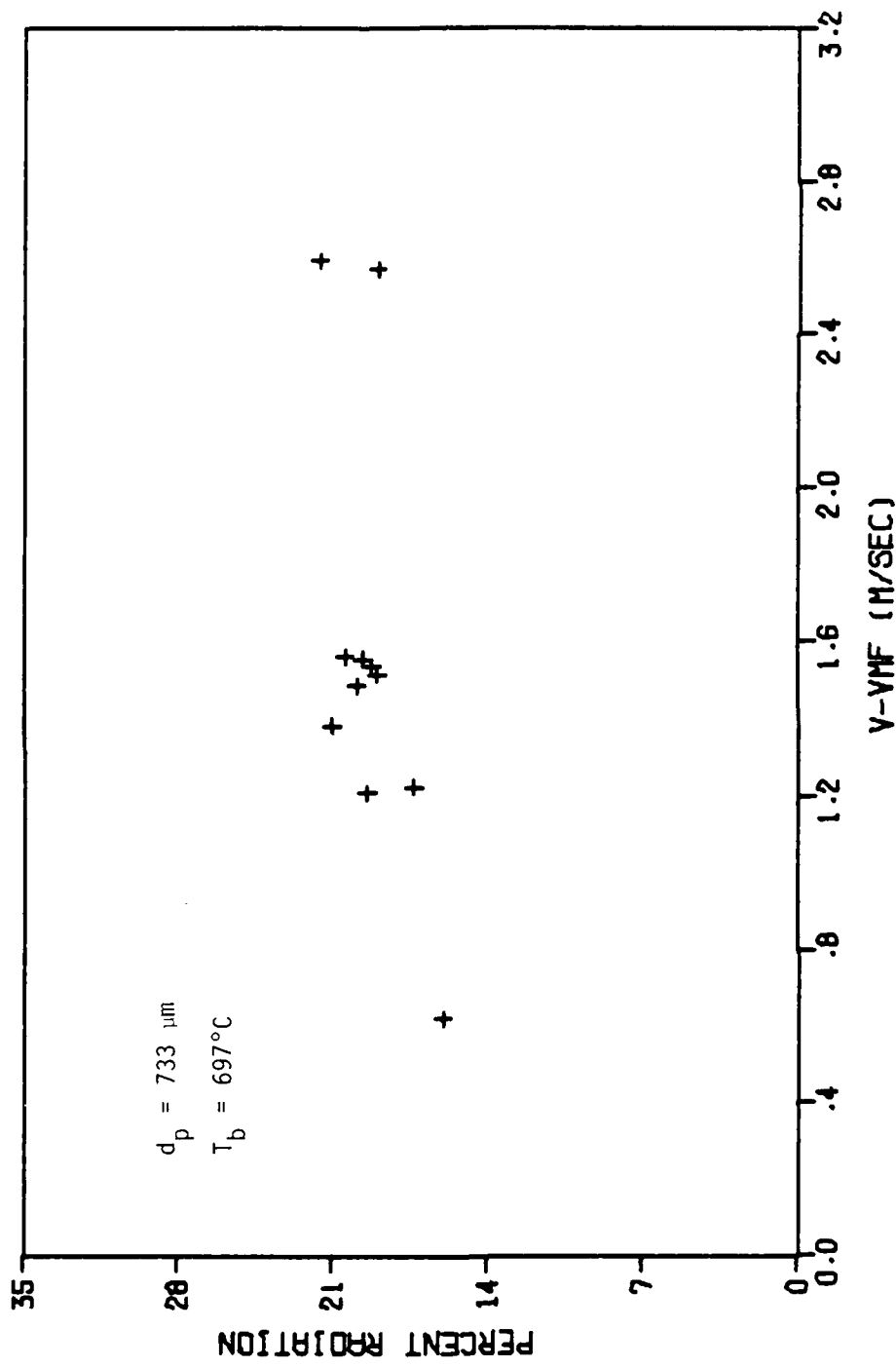


Figure 23 Percent radiation, SP-1 particles, at constant bed temperature,  $T_b = 697^\circ\text{C}$

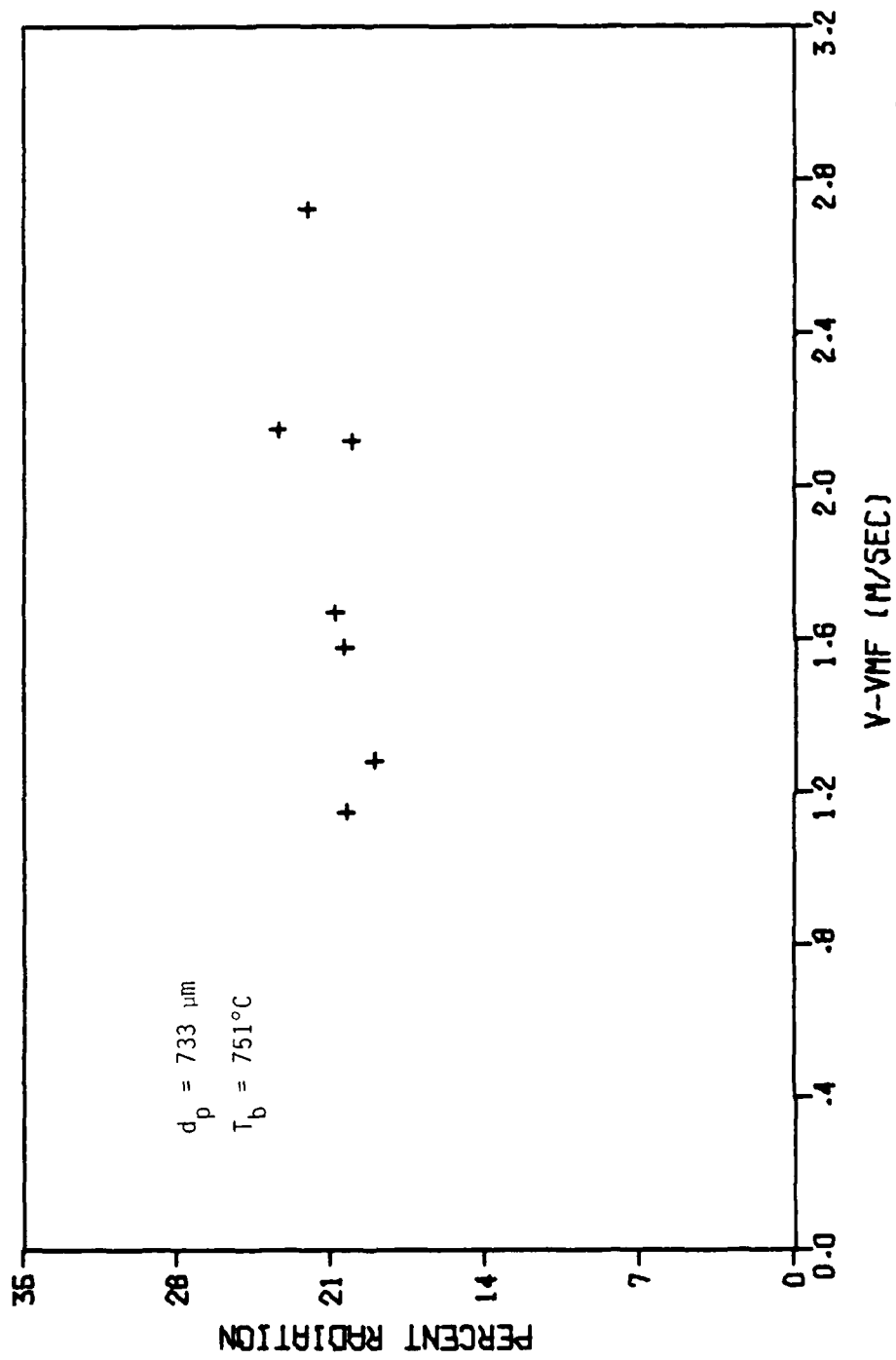


Figure 24 Percent radiation, SP-1 particles, at constant bed temperature,  $T_b = 751^\circ\text{C}$

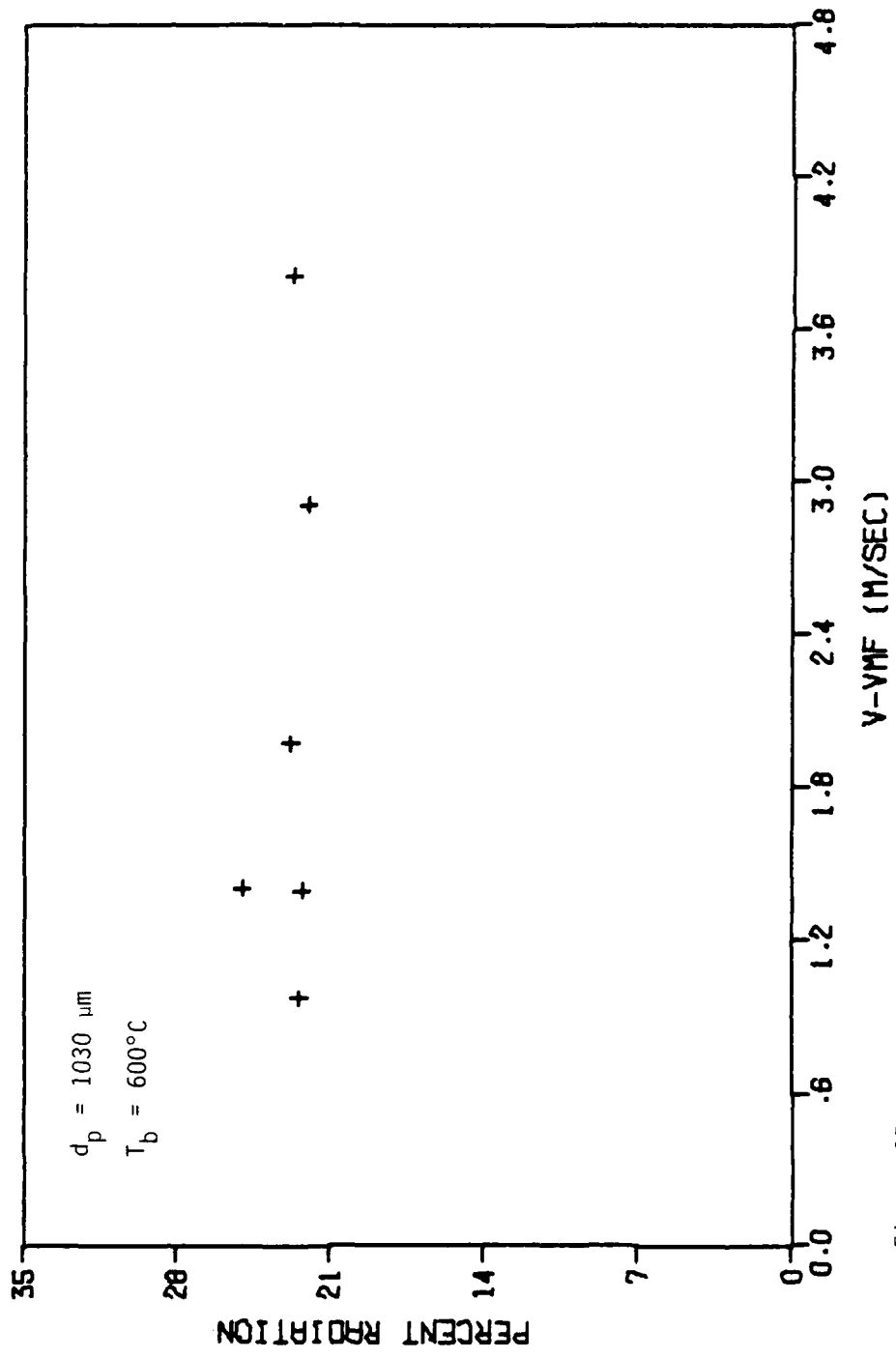


Figure 25 Percent radiation, SP-2 particles, at constant bed temperature,  $T_b = 600^\circ\text{C}$

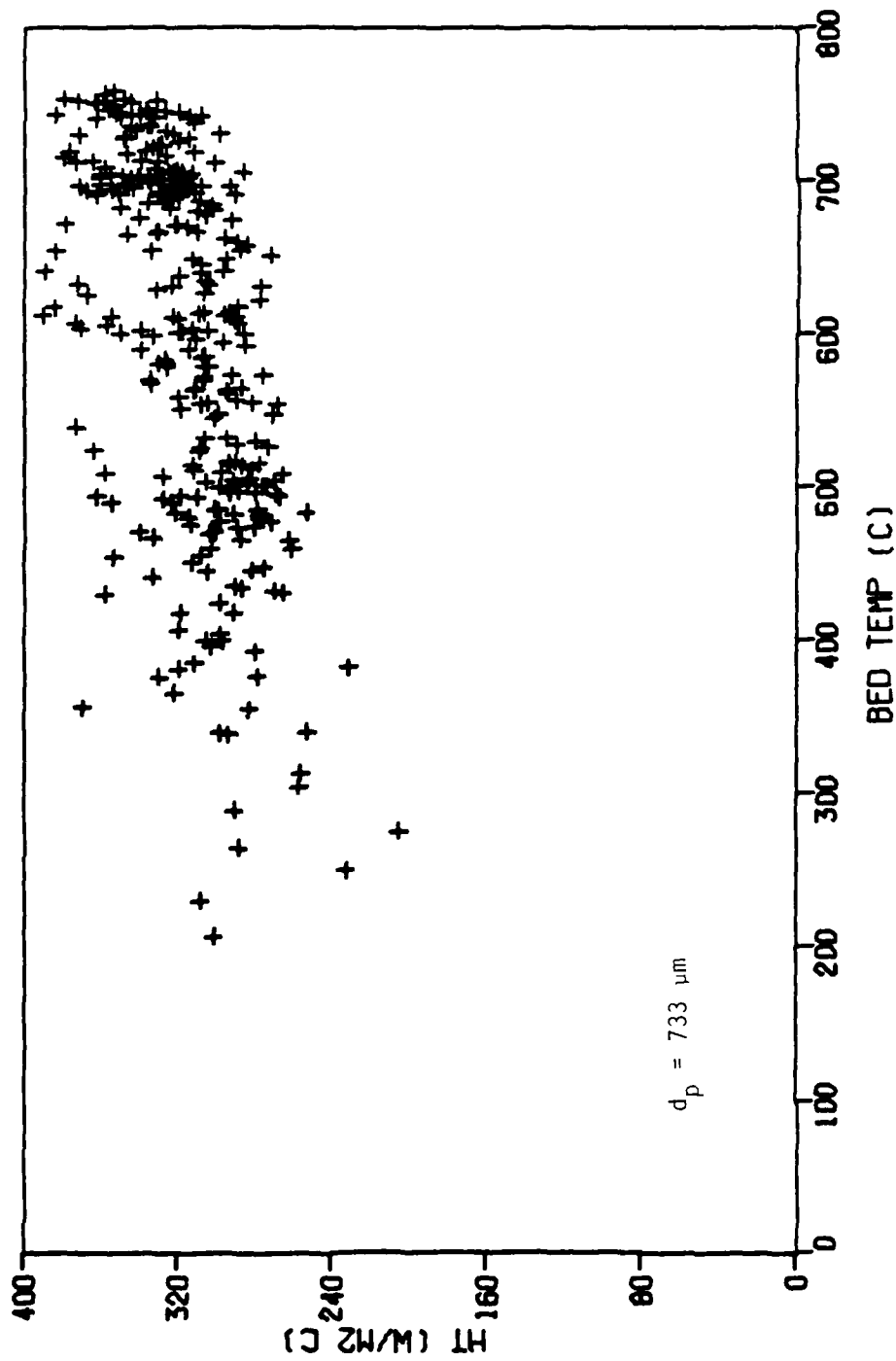


Figure 26 Total heat transfer coefficient as a function of bed temperature, SP-1 particles

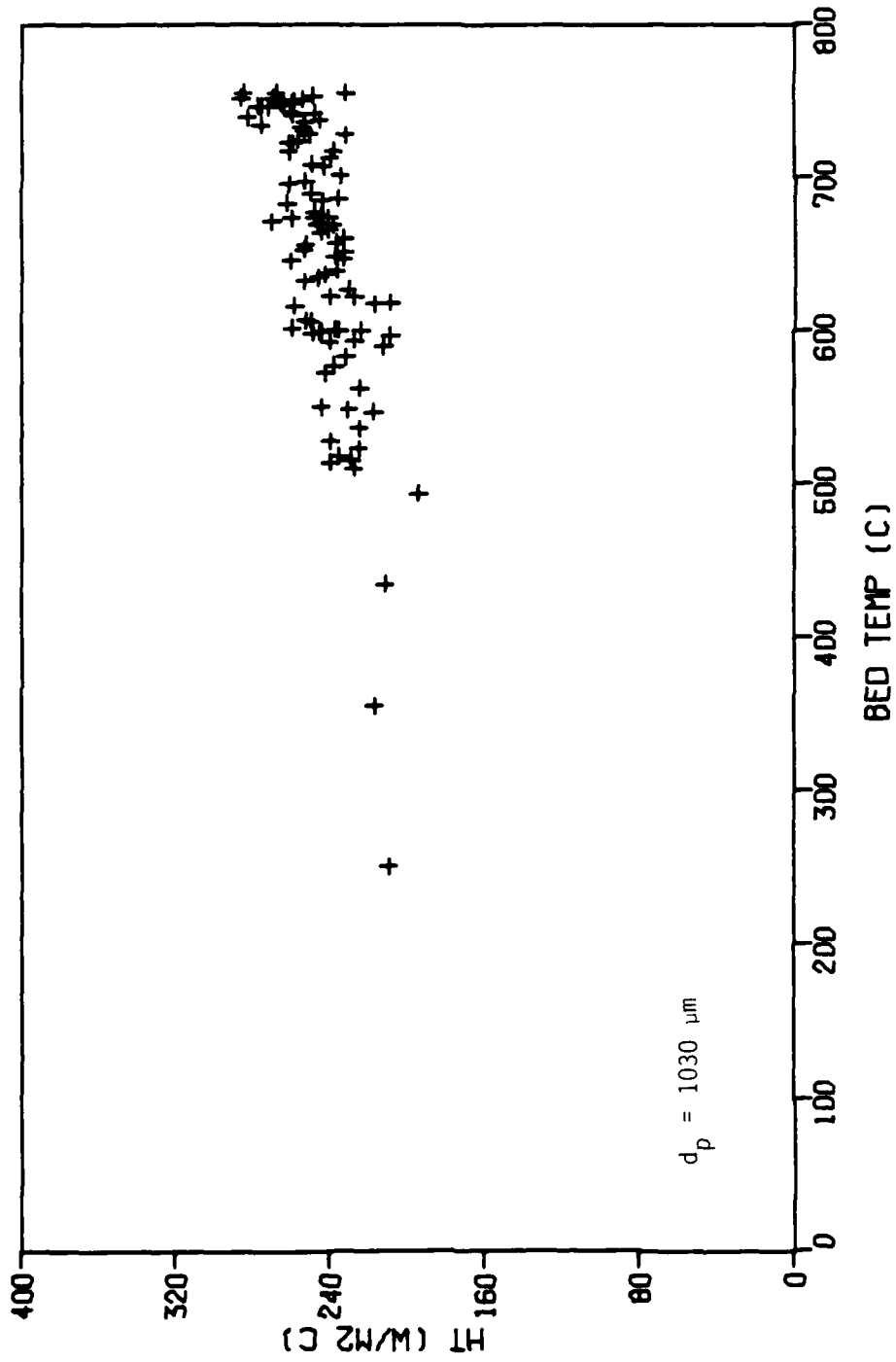


Figure 27 Total heat transfer coefficient as a function of bed temperature, SP-2 particles

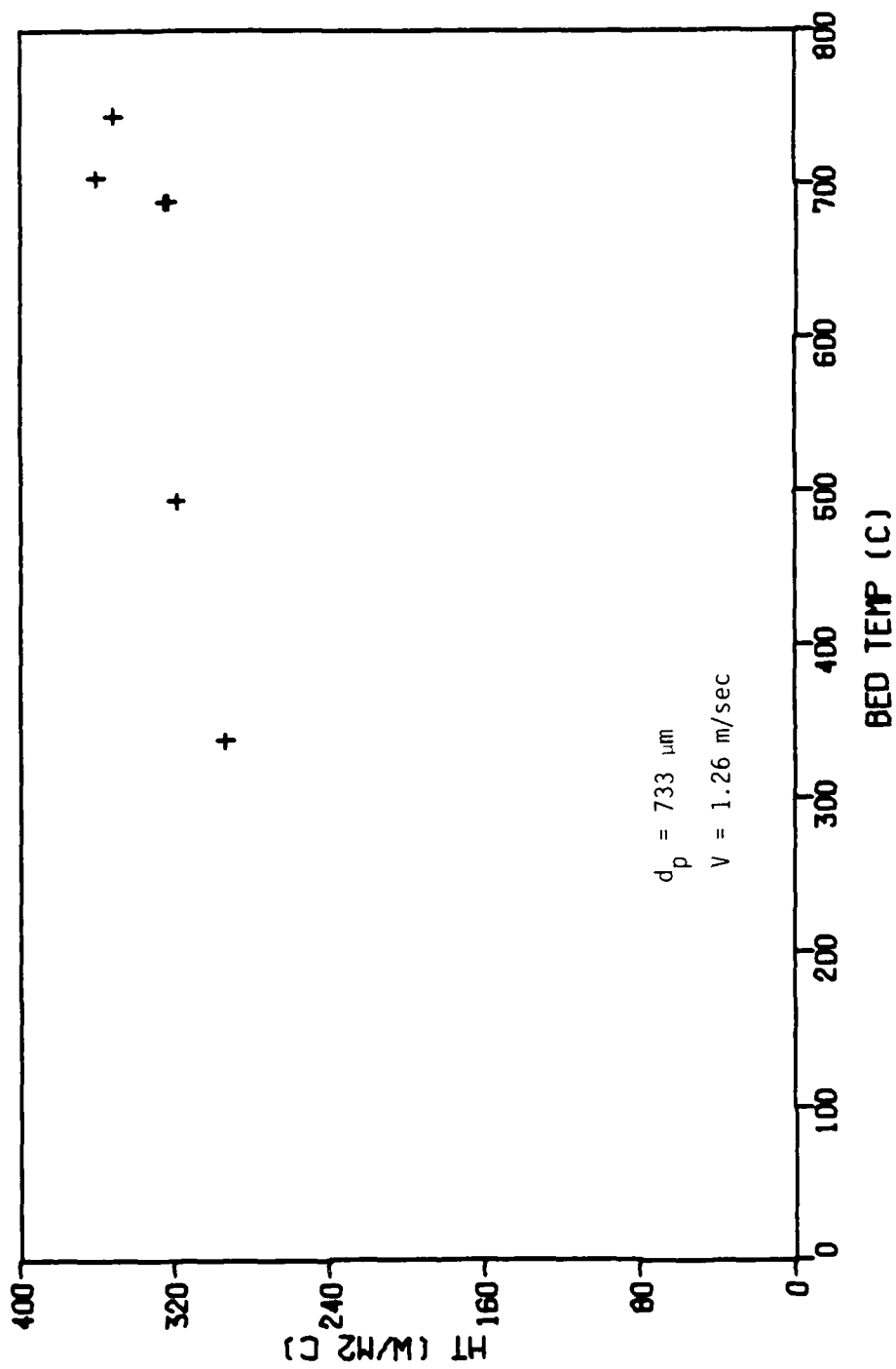


Figure 28 Total heat transfer coefficient, SP-1 particles, at constant fluidizing velocity,  $V = 1.26 \text{ m/sec}$

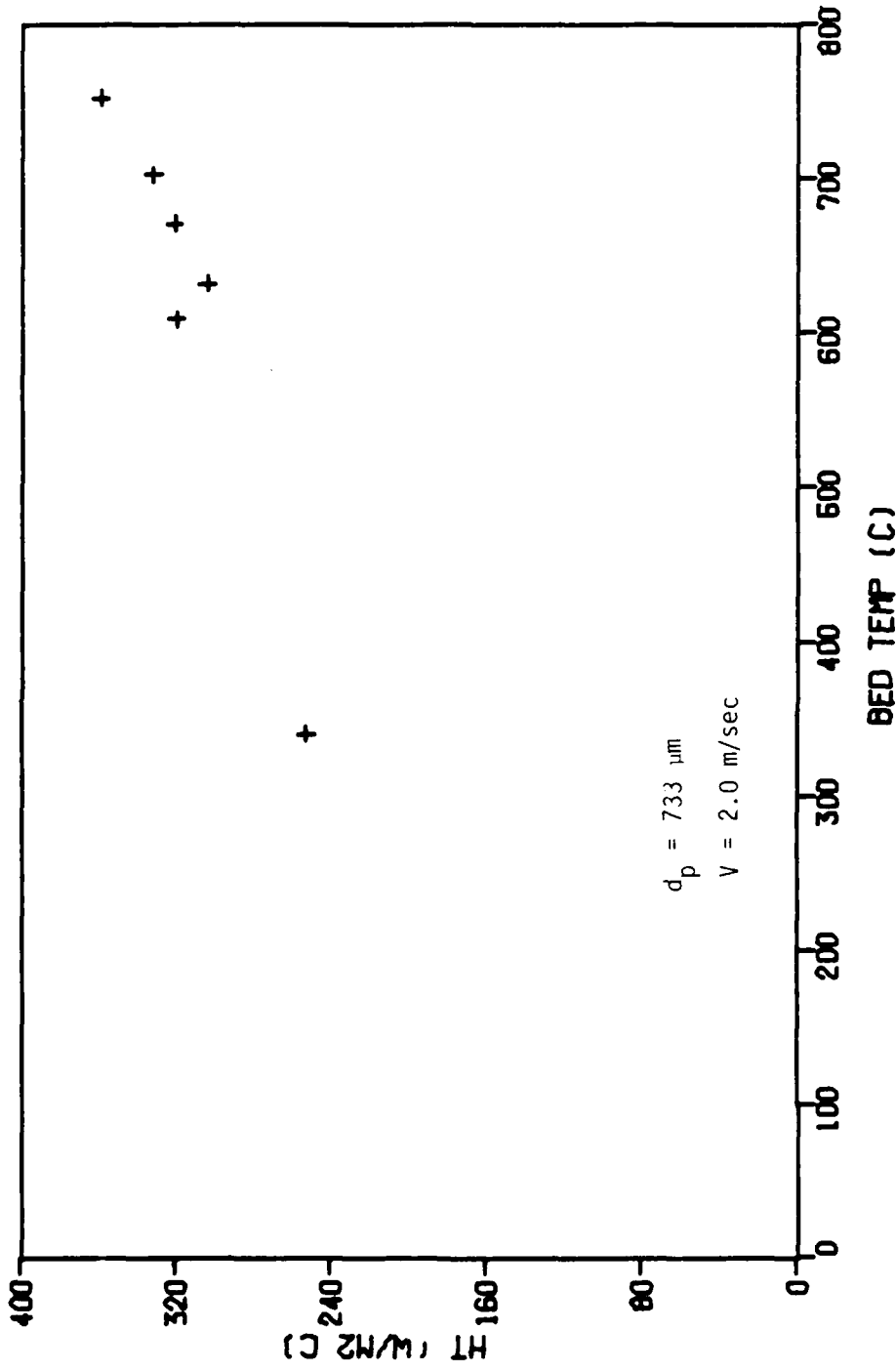


Figure 29 Total heat transfer coefficient, SP-1 particles, at constant fluidizing velocity,  $V = 2.0 \text{ m/sec}$

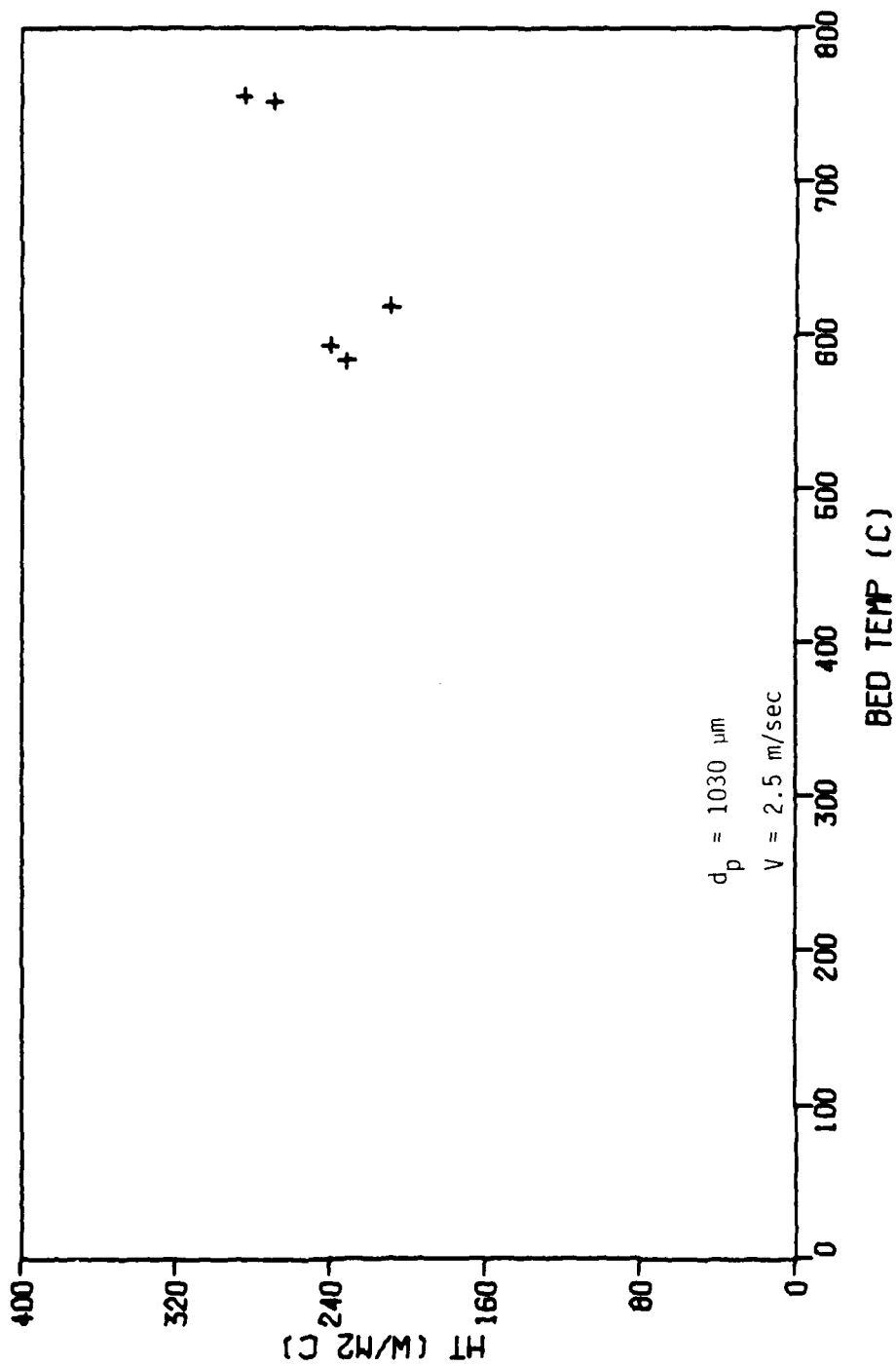


Figure 30 Total heat transfer coefficient, SP-2 particles, at constant fluidizing velocity,  $V = 2.5 \text{ m/sec}$

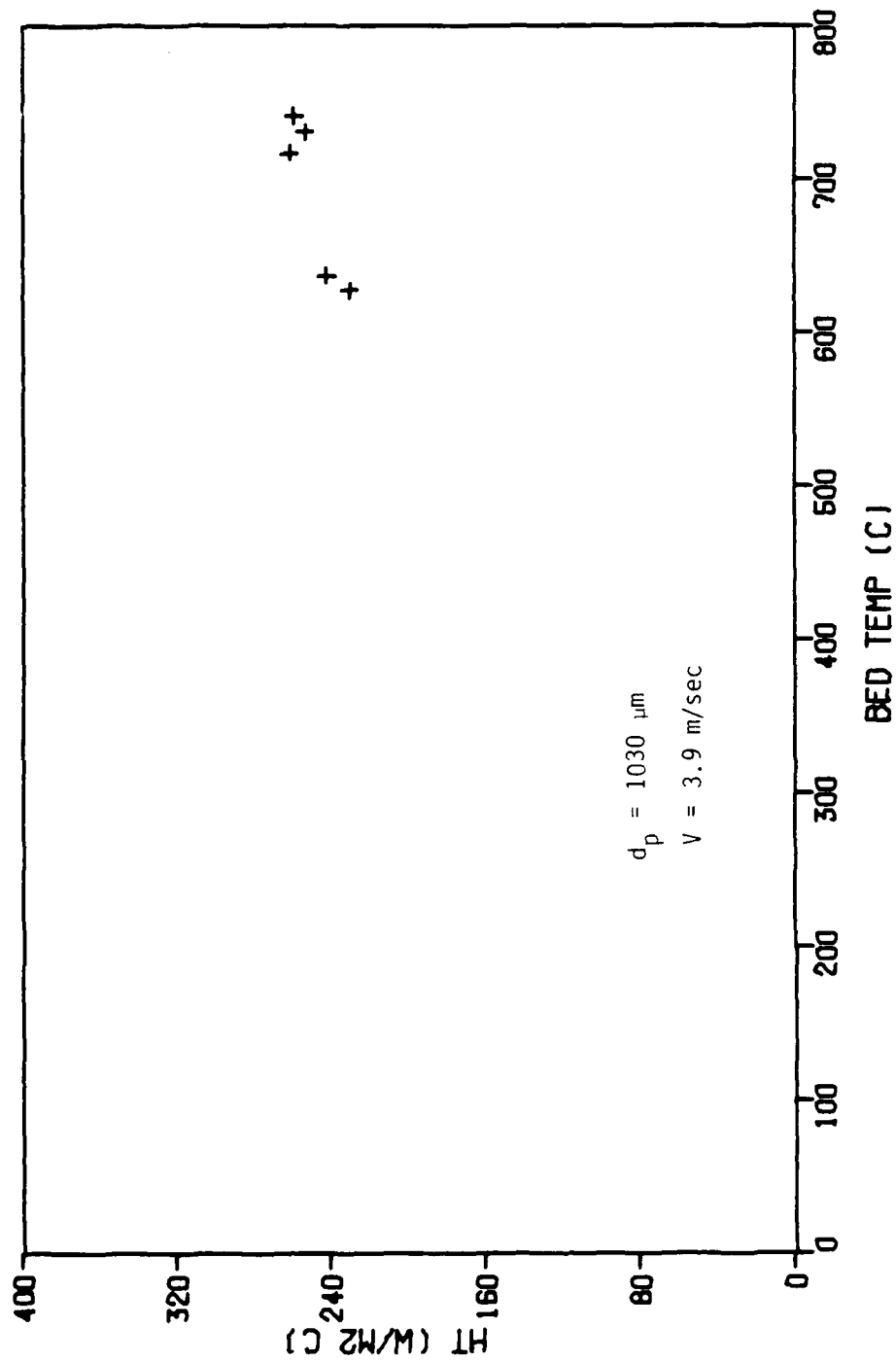


Figure 31 Total heat transfer coefficient, SP-2 particles, at constant fluidizing velocity,  $V = 3.9 \text{ m/sec}$

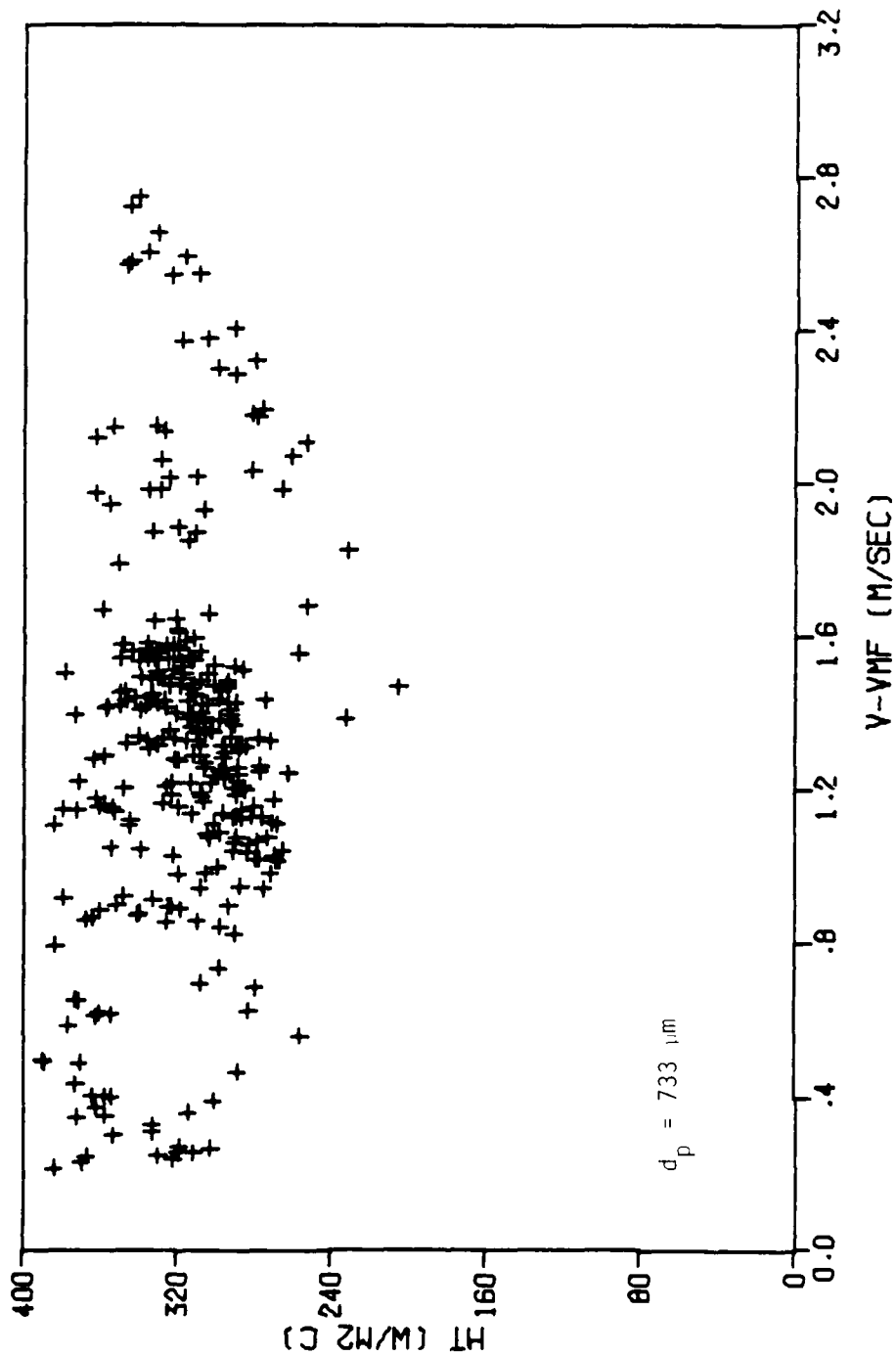


Figure 32 Total heat transfer coefficient as a function of fluidizing velocity, SP-1 particles

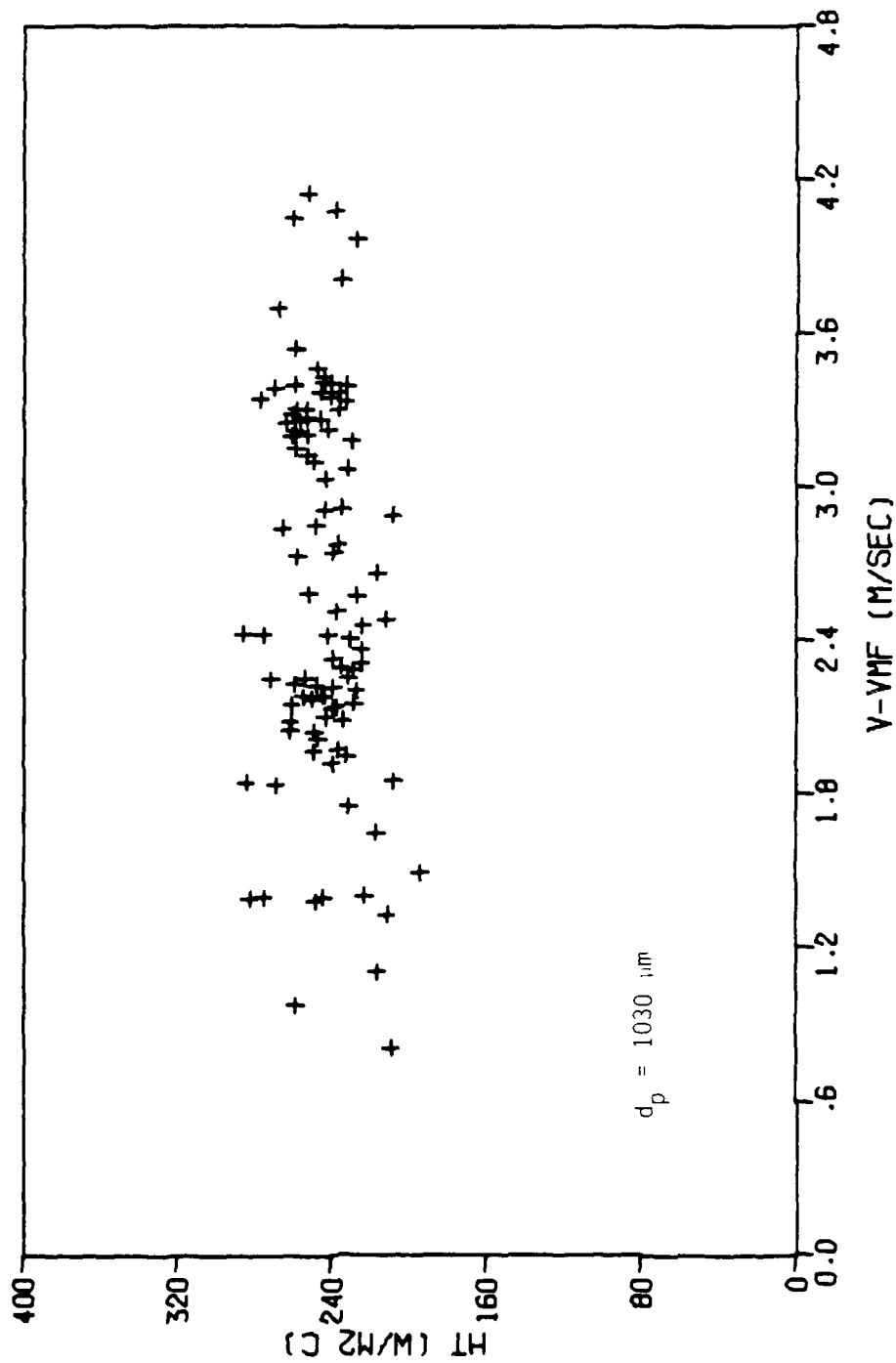


Figure 33 Total heat transfer coefficient as a function of fluidizing velocity, SP-2 particles

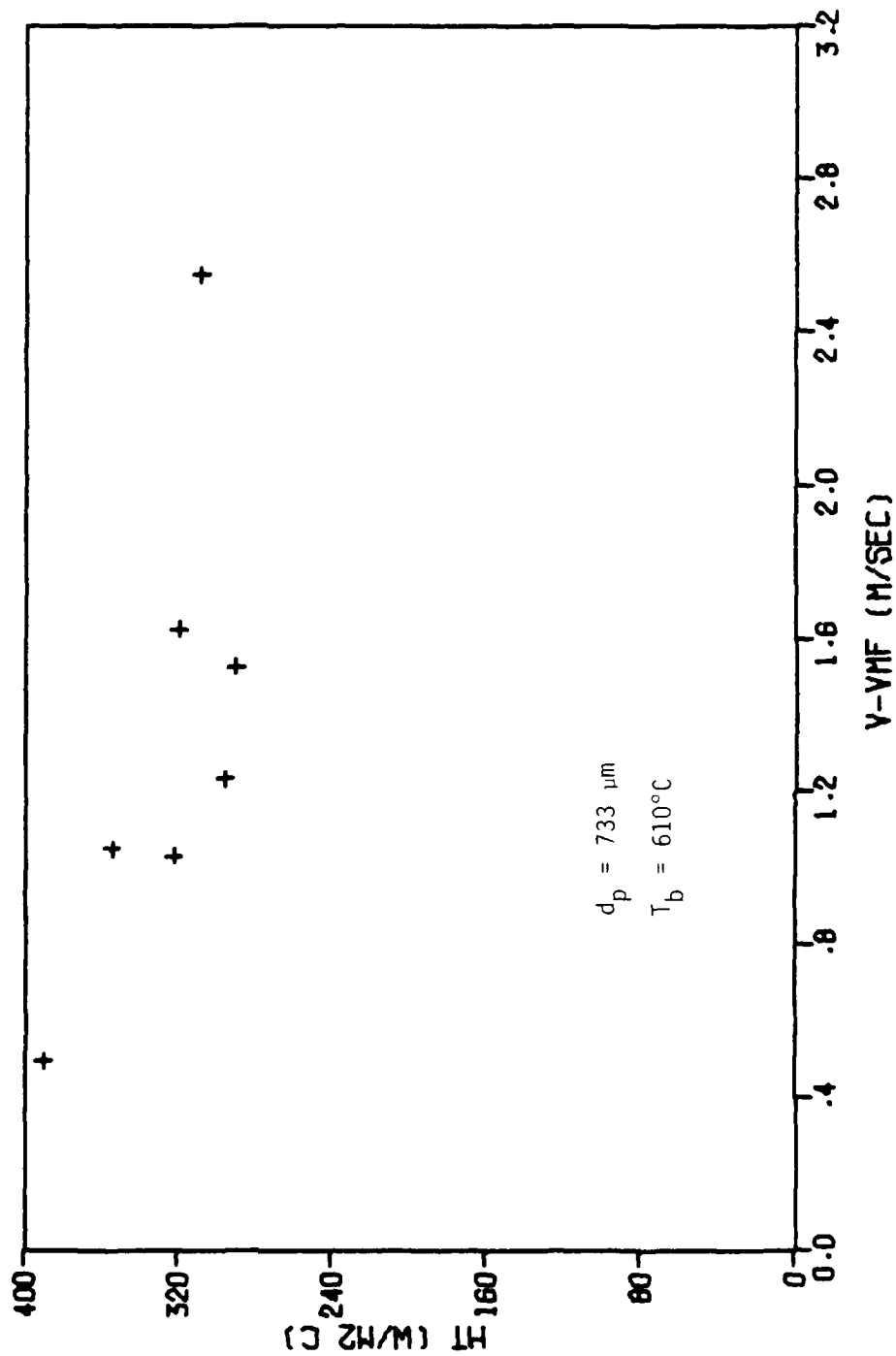


Figure 34 Total heat transfer coefficient, SP-1 particles, at constant bed temperature,  $T_b = 610^\circ\text{C}$

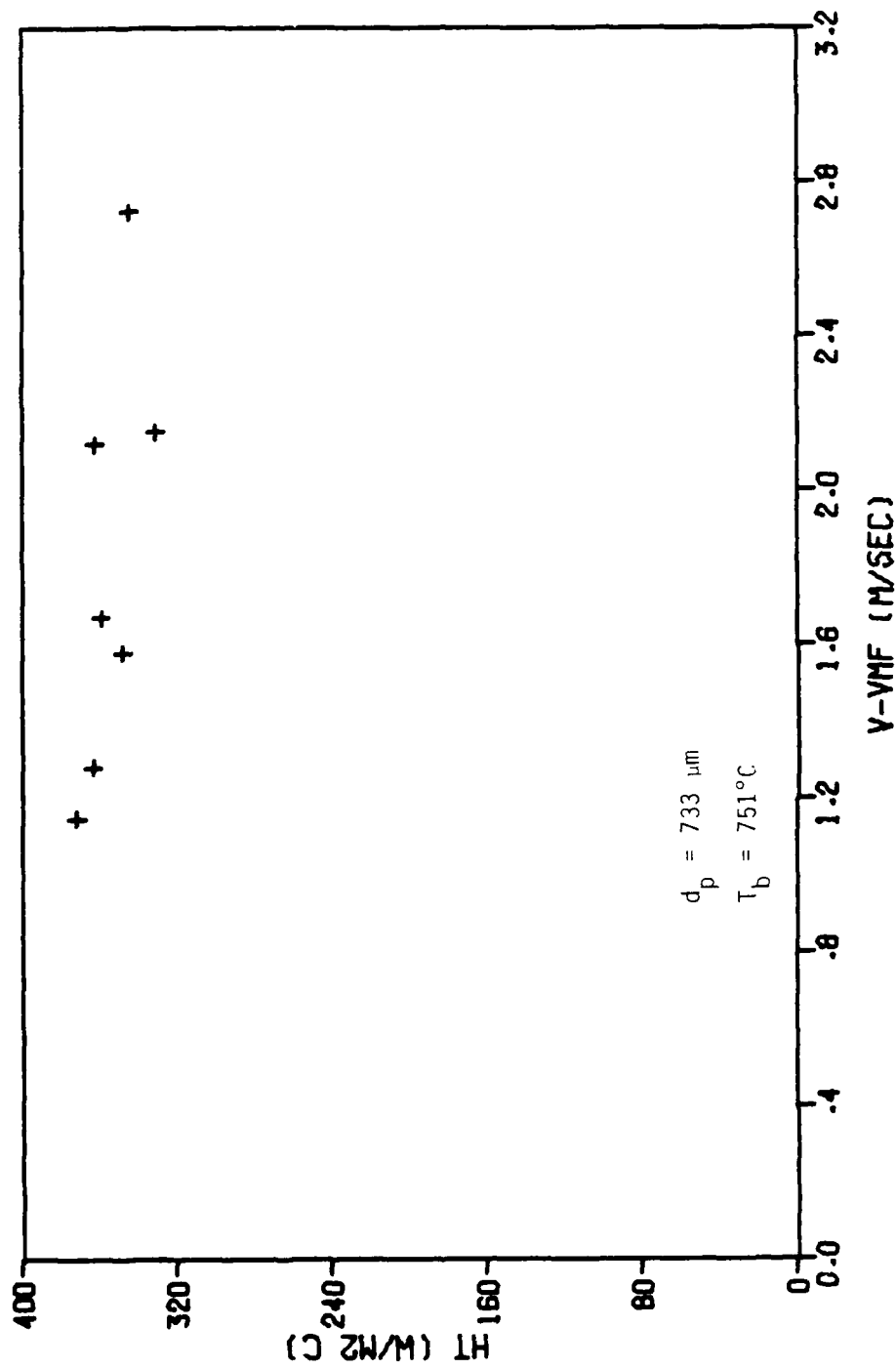


Figure 35 Total heat transfer coefficient, SP-1 particles, at constant bed temperature,  $T_b = 751^\circ\text{C}$

AD-A099 037

ARMY MILITARY PERSONNEL CENTER ALEXANDRIA VA  
THE EFFECT OF PARTICLE SIZE ON RADIATIVE HEAT TRANSFER IN HIGH --ETC(U)  
MAY 81 Y R FRANKENFIELD

F/G 20/13

UNCLASSIFIED

NL

2 OF 2

AD A  
39 500 07

END

DATE

FILED

6-81

DTIC

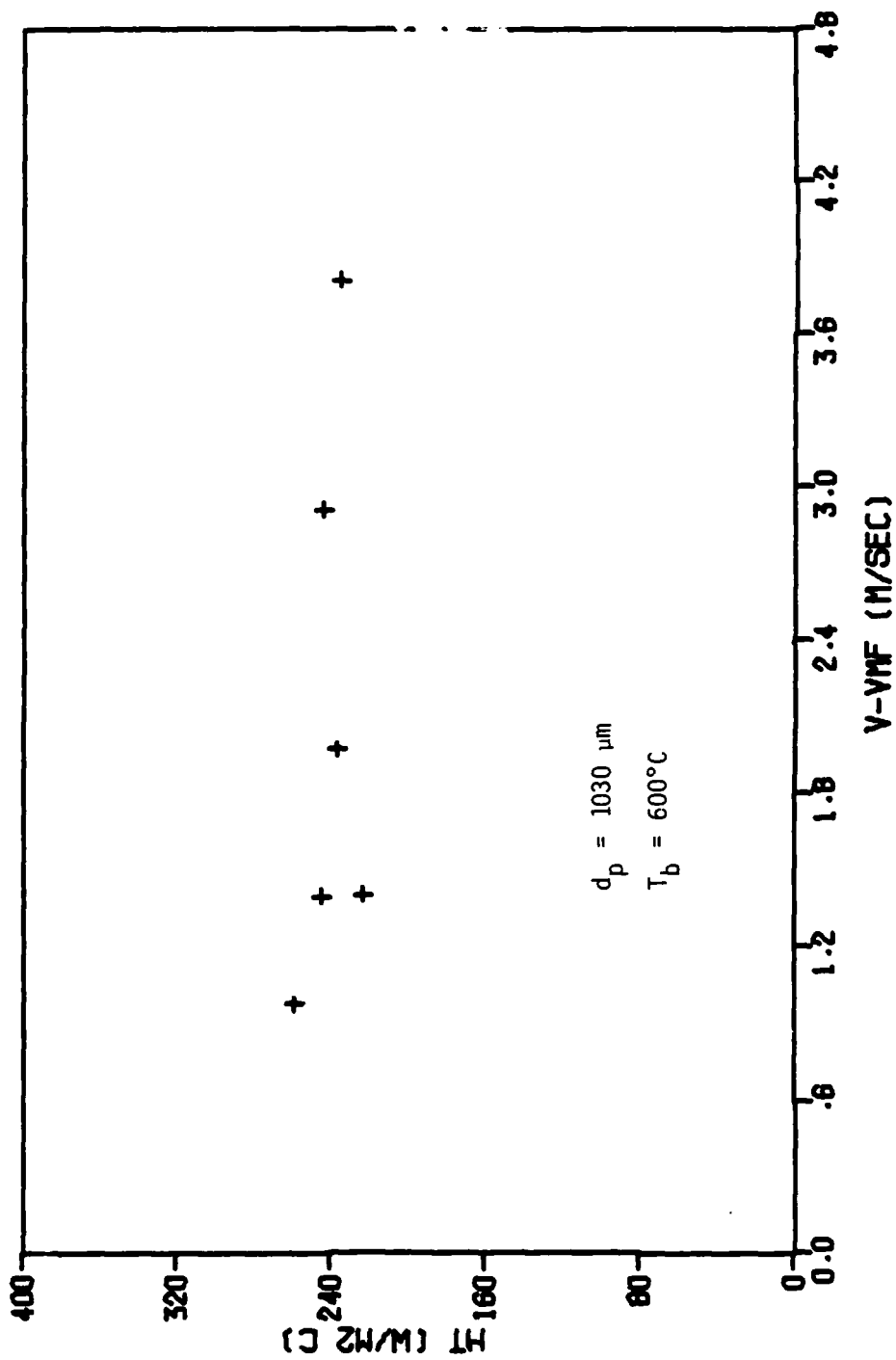


Figure 36 Total heat transfer coefficient, SP-2 particles, at constant bed temperature,  $T_b = 600^\circ\text{C}$

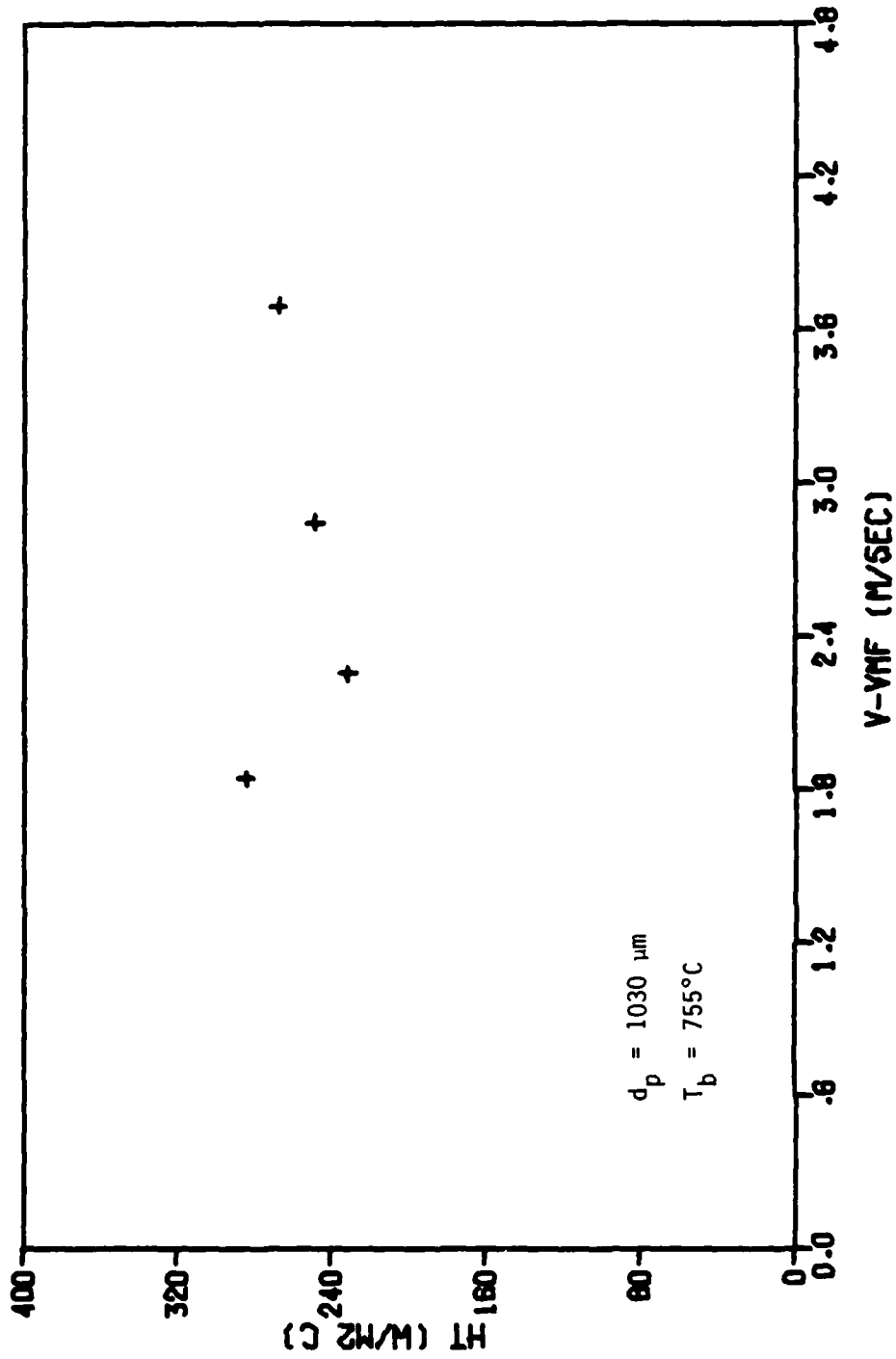


Figure 37 Total heat transfer coefficient, SP-2 particles, at constant bed temperature,  $T_b = 755^\circ\text{C}$

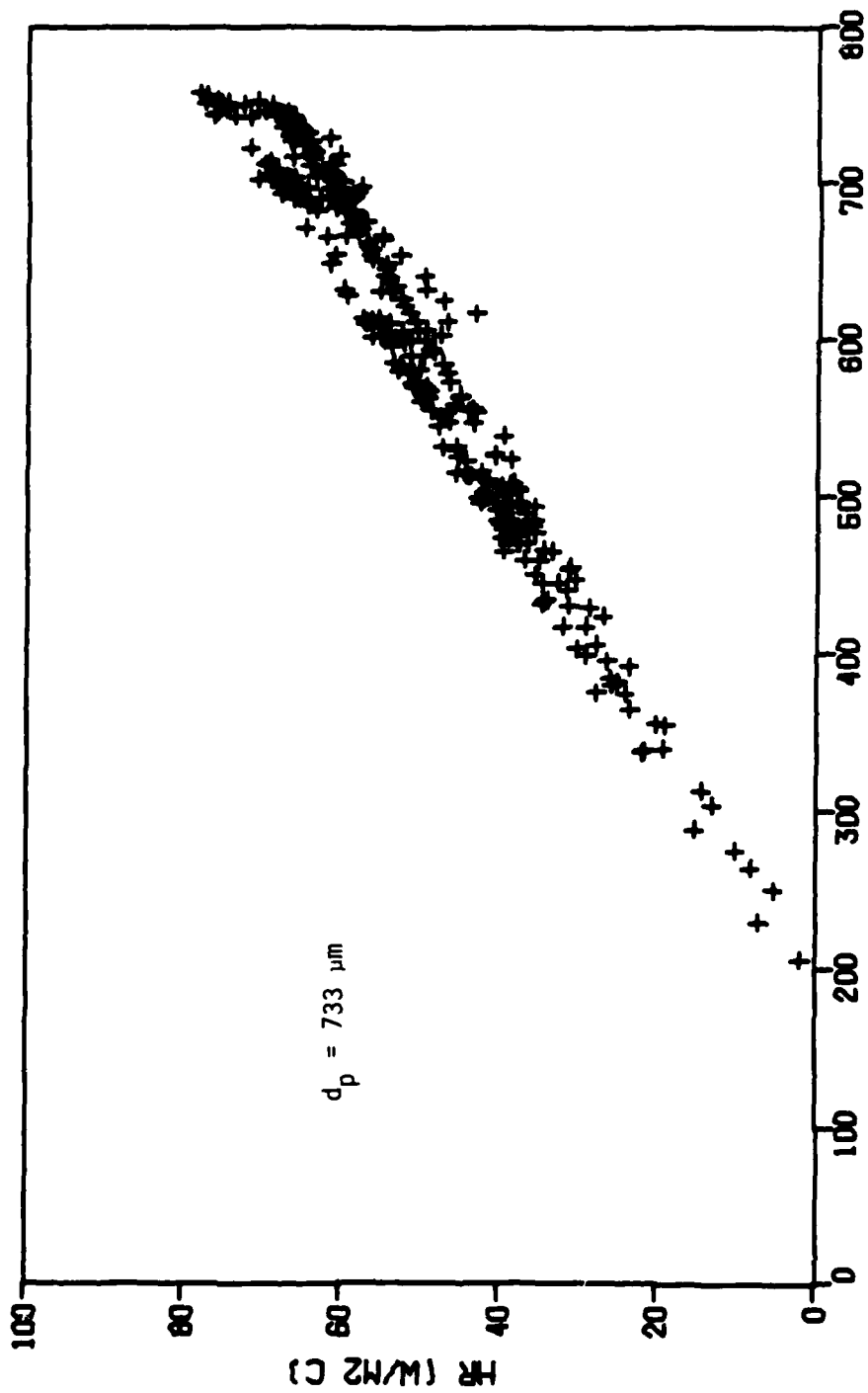


Figure 38 Radiative heat transfer coefficient, SP-1 particles

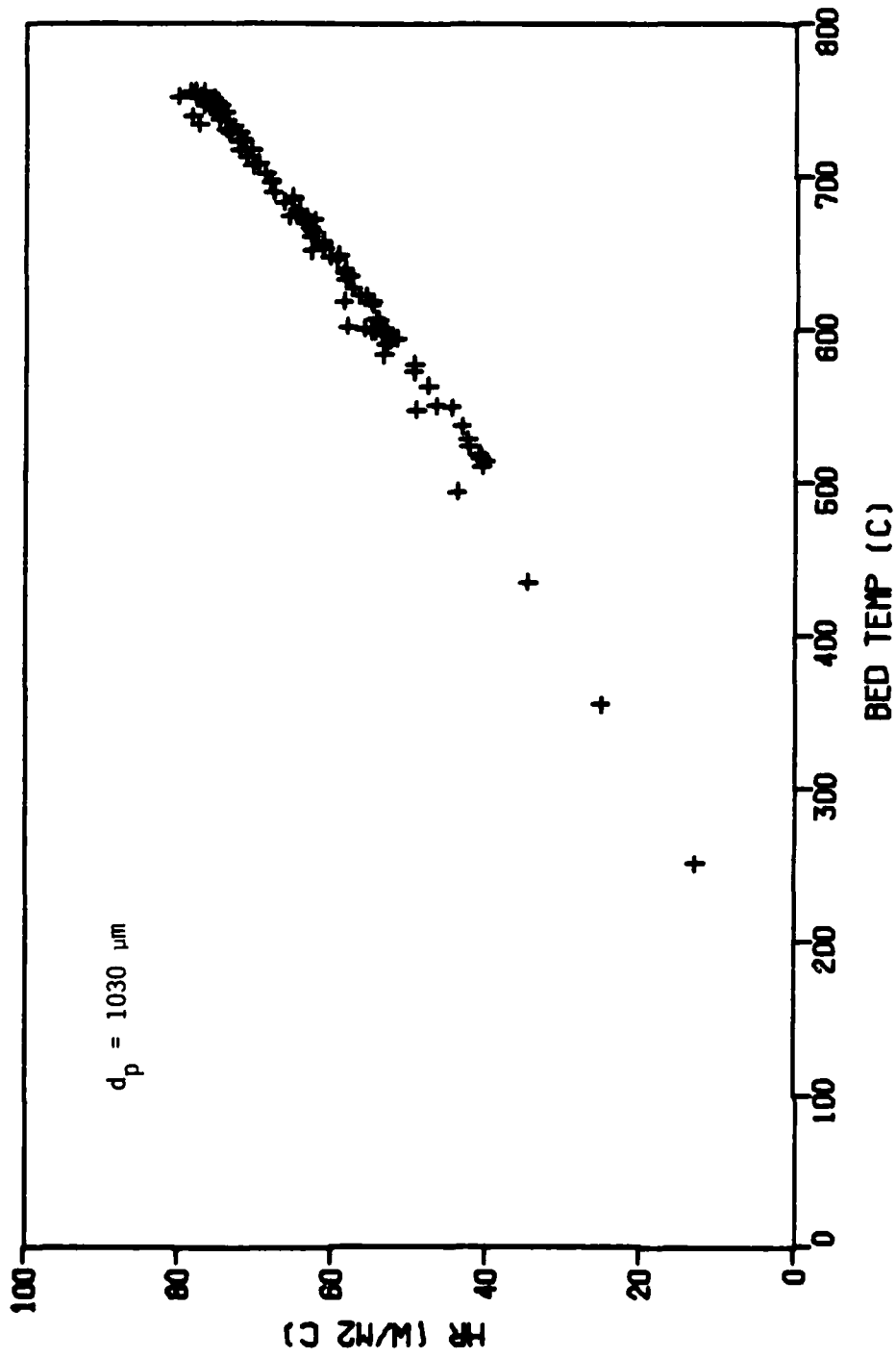


Figure 39 Radiative heat transfer coefficient, SP-2 particles

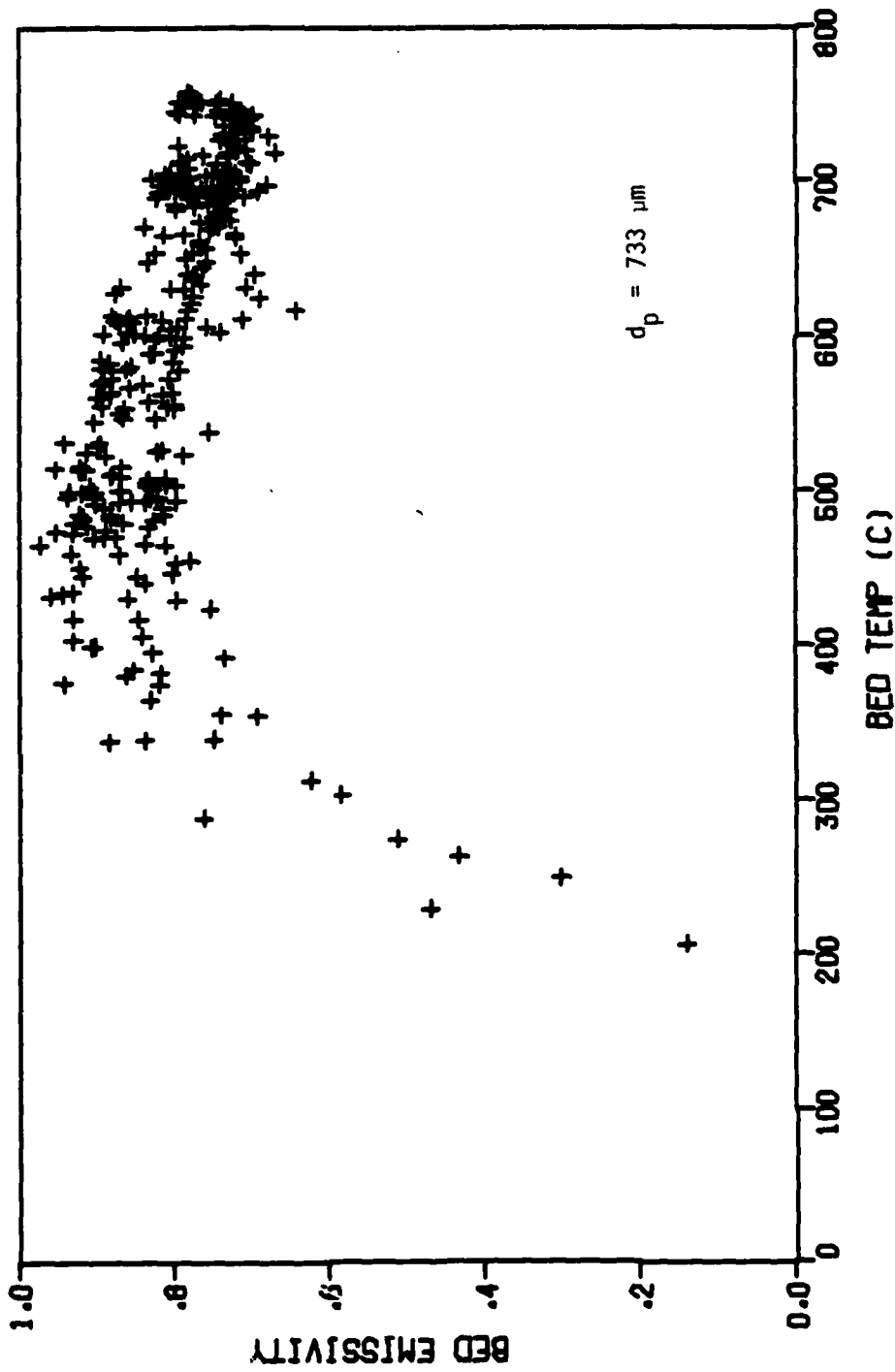


Figure 40 Bed emissivity, SP-1 particles

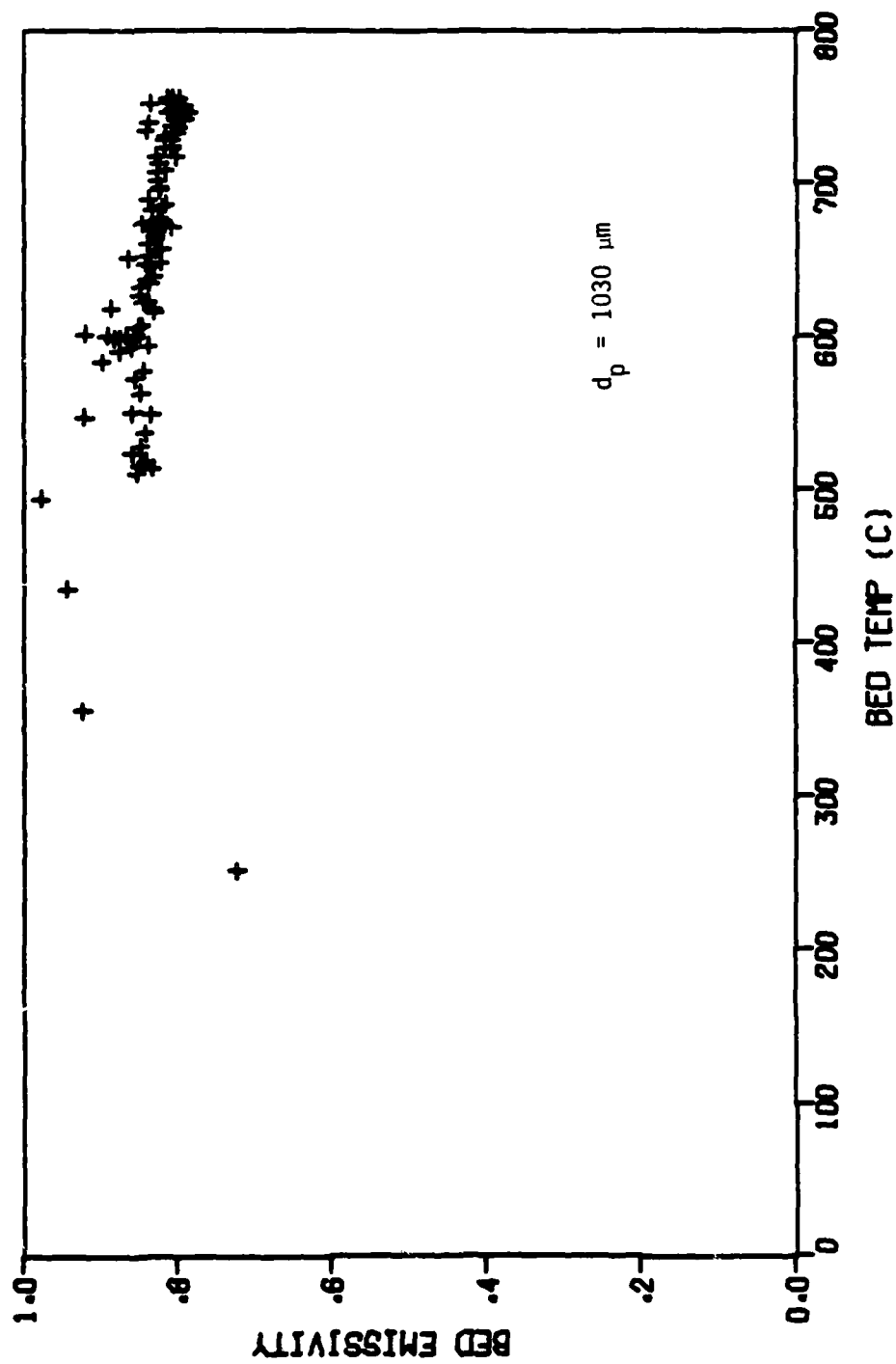


Figure 41 Bed emissivity, SP-2 particles

TABLE 3: Test Data, SP-1 Particles, Probe with ZnSe Window

EXPER NO	DATA NO	V (M/SEC)	T8 (C)	TM (C)	TMO (C)	QR (W/M2)	QT (W/M2)	HT (W/M2.K)
1	1	1.062	229.9	52.0	77.7	1303.3	54580.5	308.2
1	2	1.191	288.5	61.7	92.6	3526.3	65825.9	290.2
1	3	1.264	338.3	67.0	100.4	6020.4	7595.0	293.4
1	4	1.346	380.6	80.5	120.5	7746.1	95931.3	319.7
1	5	1.349	399.9	79.4	113.6	9340.0	97974.5	305.7
1	6	1.495	417.3	81.5	114.0	10796.0	97722.6	291.0
1	7	1.430	434.9	82.4	118.2	12024.3	102317.0	290.3
1	8	1.452	444.5	85.3	122.2	12523.2	109399.8	304.6
1	9	1.503	450.4	85.7	122.8	13031.2	114055.9	312.7
1	10	1.585	459.9	83.0	123.5	13949.1	113899.3	302.8
1	11	1.441	469.8	94.7	134.8	14198.9	113971.7	303.8
1	12	1.443	473.3	87.7	126.2	15012.4	111416.1	288.9
1	13	1.587	475.2	96.3	136.8	14378.3	118747.7	313.4
1	14	1.614	477.6	88.6	127.7	15108.2	115972.9	298.1
1	15	1.570	482.0	91.2	133.6	15486.1	113741.1	291.0
1	16	1.748	496.0	92.3	134.1	16500.7	118244.8	292.9
1	17	1.750	513.8	94.2	135.5	18434.3	122743.3	292.5
1	18	1.743	531.2	99.0	144.0	19708.4	132205.4	305.9
1	19	1.840	545.0	98.9	144.4	21366.0	134405.4	301.3
1	20	1.837	550.2	105.5	154.7	21007.9	141589.0	318.4
1	21	1.791	554.8	98.5	145.2	22220.8	138851.4	304.3
1	22	1.961	562.5	100.7	148.1	22796.2	143749.1	311.3
1	23	1.854	566.9	107.9	156.7	22527.0	153319.5	334.0
1	24	1.790	568.9	101.2	149.5	23895.4	143621.3	307.1
1	25	1.745	571.2	102.5	150.9	24011.0	143594.6	306.4
1	26	1.762	572.7	102.1	153.5	23878.6	137488.7	292.2
1	27	1.811	563.5	102.7	152.4	22832.4	143141.0	310.6
1	28	1.682	525.1	95.2	137.9	19537.7	132488.4	308.2
1	29	.764	488.9	105.1	147.6	14121.8	136095.5	354.6
1	30	1.702	492.0	94.4	134.3	16120.3	130148.6	327.3

TABLE 3 (Continued)

EXPER NO	DATA NO	V (M/SEC)	TB (C)	TW (C)	FWD (C)	QR (W/M2)	QT (W/M2)	HT (W/M2.K)
1	31	1.243	470.4	94.6	135.6	13769.6	127898.3	340.3
1	32	1.524	473.6	88.2	123.7	15434.3	107948.7	280.1
1	33	1.637	503.1	95.7	139.5	17196.1	124399.0	305.3
1	34	1.833	516.1	93.8	135.8	18793.7	124152.0	294.0
1	35	1.556	489.5	94.7	136.5	15641.0	127431.7	322.8
1	36	1.792	499.0	94.4	137.5	17053.2	118881.4	293.8
1	37	1.645	483.0	94.5	135.9	15549.4	124697.7	321.0
1	38	1.702	514.9	89.1	130.4	19409.3	118437.2	278.2
1	39	1.626	496.5	93.7	137.2	17142.9	116156.8	288.4
1	40	1.610	465.1	85.2	121.3	15049.9	99632.0	262.3
1	41	1.492	433.4	84.1	118.5	12058.2	100133.8	286.7
1	42	1.456	403.4	75.9	107.1	9943.0	97542.3	297.8
1	43	1.433	375.9	74.6	104.5	8383.8	84067.6	279.0
1	44	1.506	399.0	78.4	111.4	9365.9	95053.8	296.5
1	45	1.541	431.7	81.5	115.7	12181.5	94534.9	269.9
1	46	1.702	479.4	90.1	131.5	15472.6	107978.1	277.4
1	47	1.684	513.8	91.6	132.8	18583.8	121200.4	287.1
1	48	1.764	513.5	97.4	140.8	18460.9	129918.3	312.2
1	49	1.841	531.5	92.1	138.0	20835.1	129381.2	294.4
1	50	1.751	499.5	92.2	133.8	17442.2	121517.2	298.3
1	51	1.604	485.5	90.4	129.1	15942.0	118826.9	300.8
1	52	1.694	522.8	103.1	146.0	18663.6	129775.5	309.2
1	53	1.851	560.6	102.7	148.8	22986.4	134671.5	294.1
1	54	1.575	577.8	105.1	157.3	24432.9	154008.8	325.8
1	55	1.753	585.4	101.4	148.1	25930.3	148077.8	305.9
1	56	1.732	602.7	110.9	160.1	26948.2	153662.6	312.4
1	57	1.778	613.4	108.3	158.1	29033.6	147832.7	292.7
1	58	1.889	610.6	110.0	158.4	28553.7	145088.5	289.8
1	59	1.869	601.9	106.5	153.6	27940.4	150645.1	304.1
1	60	1.799	583.3	104.8	155.1	25246.8	156503.4	327.1

TABLE 3 (Continued)

EXPER NO	DATA NO	V (M/SEC)	TB (C)	TW (C)	TMD (C)	OR (W/M2)	QT (W/M2)	HT (W/M2.KI)
1	61	1.859	579.6	105.0	151.1	25137.1	156541.4	329.8
1	62	1.986	609.3	112.1	165.7	27542.3	158959.2	319.7
1	63	2.026	632.0	109.9	161.0	31241.4	158596.9	303.8
1	64	1.921	628.1	106.5	159.0	30982.7	172521.3	330.8
1	65	1.921	653.6	120.2	177.3	32498.7	177909.6	333.5
1	66	1.873	665.1	119.6	171.7	33842.0	180460.5	330.8
1	67	2.013	671.1	117.6	170.9	35868.2	177427.7	320.6
1	68	1.908	681.9	119.1	178.7	35661.6	196842.0	349.8
1	69	1.975	688.9	116.5	176.7	37936.6	182728.5	319.2
1	70	1.952	694.2	124.1	184.0	37964.5	180146.9	316.0
1	71	1.920	697.9	126.9	186.8	37539.7	191187.1	334.8
1	72	2.006	702.3	127.1	183.4	38022.7	190964.6	332.0
1	73	1.855	705.1	121.4	178.9	39799.3	185318.1	317.5
1	74	1.658	510.1	94.3	141.8	17311.4	129495.0	311.4
1	75	1.560	553.6	99.3	148.6	21298.7	139963.1	308.1
1	76	1.859	589.2	104.2	157.7	24249.5	164498.3	339.2
1	77	1.586	630.6	113.6	171.8	28558.0	166922.5	322.9
1	78	2.384	666.0	112.7	166.1	32956.8	171638.5	310.2
1	79	2.154	690.6	121.7	185.2	34839.8	199359.2	350.4
1	80	2.310	703.5	119.2	183.9	37119.7	207342.5	354.9
1	81	1.800	716.9	119.5	181.9	39644.8	207024.6	346.5
1	82	1.823	728.8	124.5	190.9	39912.4	209867.1	347.3
1	83	1.695	735.7	126.6	189.4	41209.3	204290.1	335.4
1	84	2.340	740.0	129.9	198.9	41073.7	221063.8	362.3
1	85	1.783	746.2	126.2	191.0	43383.0	220680.6	355.9
1	86	1.944	752.8	126.2	195.5	44410.6	217866.0	347.7
1	87	1.647	751.1	128.0	199.4	43054.5	226285.7	363.2
1	88	1.266	744.1	131.1	199.1	41967.8	215456.5	351.5
1	89	1.016	729.4	133.4	204.6	36707.2	221316.7	371.3
1	90	1.017	711.5	131.6	199.4	35309.9	216107.1	372.7

TABLE 3 (Continued)

EXPER NO	DATA NO	V (M/SEC)	T8 (C)	TW (C)	TWD (C)	QR (M/M2)	QT (M/M2)	MT (M/M2.K)
1	91	1.931	669.0	118.6	183.0	35906.6	186190.3	329.9
1	92	1.160	653.5	124.1	191.1	27908.7	203018.6	383.5
1	93	.855	640.3	125.1	186.3	25640.5	200361.0	388.9
1	94	.710	632.0	122.9	182.9	25134.0	189381.0	372.0
1	95	.609	624.8	123.7	181.8	23695.8	183911.1	367.0
1	96	.578	616.9	123.4	178.6	21316.2	189469.5	383.9
1	97	.860	611.4	118.6	173.3	23062.8	192203.6	390.0
1	98	.853	603.3	120.7	176.0	23001.7	178682.4	370.2
1	99	1.222	580.7	102.0	154.9	24135.3	156143.0	326.2
1	100	1.522	558.0	102.1	153.9	20933.1	145483.3	319.1
1	101	.798	538.7	109.4	159.3	17058.7	159923.3	372.5
1	102	.767	523.4	99.0	154.7	16466.7	154435.6	363.9
1	103	.715	508.5	99.4	147.9	15711.1	146218.2	357.4
1	104	.738	493.8	96.8	147.6	14195.6	143765.0	362.1
1	105	.724	479.8	93.4	136.6	14379.3	121538.7	314.5
1	106	.690	466.6	92.6	135.8	12889.8	124595.2	333.1
1	107	.665	453.7	92.8	135.8	11348.0	127418.2	353.1
1	108	.673	441.1	90.9	132.3	11063.8	116610.4	333.0
1	109	.767	429.7	88.4	128.0	9844.8	122168.9	358.0
1	110	.634	417.5	86.4	123.8	9710.6	105637.8	319.1
1	111	.619	406.5	83.5	119.5	9040.8	103113.5	319.2
1	112	.631	395.8	82.0	116.6	8303.9	94859.2	302.3
1	113	.619	384.9	80.1	115.6	7954.7	94931.0	311.5
1	114	.611	375.2	78.5	111.5	7181.3	97921.0	330.0
1	115	.601	365.1	77.8	111.6	6778.8	92453.9	321.8
1	116	.592	355.8	75.7	106.9	5675.1	103531.7	369.6
2	1	.755	206.3	37.9	33.0	353.3	50692.1	301.0
2	2	.831	264.4	47.5	39.2	1817.8	62566.5	288.5
2	3	.923	313.0	51.7	42.5	3823.4	66950.7	256.2
2	4	.990	354.8	58.2	48.7	5678.7	83842.7	282.7

TABLE 3 (Continued)

EXPER NO	DATA NO	V (M/SEC)	TB (C)	TM (C)	TWD (C)	QR (M/M2)	QT (M/M2)	HT (M/M2.K)
2	5	1.051	392.5	67.4	53.3	7695.4	90980.9	279.9
2	6	1.101	424.0	70.7	58.2	9563.4	105454.7	298.5
2	7	1.308	447.1	65.5	57.2	11685.8	105020.2	275.2
2	8	1.310	455.3	73.9	62.4	11871.0	117492.5	308.1
2	9	1.314	465.4	74.3	61.1	13090.4	112354.8	287.3
2	10	1.349	477.1	73.2	60.3	14380.5	109751.5	271.7
2	11	1.386	481.5	76.8	62.7	14568.3	112306.3	277.5
2	12	1.365	485.0	76.7	64.7	14624.5	122118.5	299.1
2	13	1.381	493.8	74.4	61.5	15823.7	112146.3	267.4
2	14	1.384	495.2	78.2	62.9	15794.1	112228.0	269.1
2	15	1.386	496.4	77.3	63.7	15709.2	117170.4	279.6
2	16	1.407	503.5	83.5	67.0	15832.1	122210.6	291.0
2	17	1.404	501.7	80.4	65.4	16294.9	119564.9	283.8
2	18	1.424	504.7	82.4	91.9	15994.9	119382.2	282.7
2	19	1.409	507.8	77.6	89.6	16720.0	114298.0	265.7
2	20	1.394	503.6	80.7	88.9	16413.6	114324.2	270.2
2	21	1.442	526.0	81.3	93.7	18160.1	121466.9	273.1
2	22	1.481	547.1	81.3	93.9	20273.3	126065.7	270.6
2	23	1.498	556.0	86.6	100.8	20494.1	136001.7	289.7
2	24	1.478	553.4	83.9	96.6	20278.3	126011.6	268.4
2	25	1.497	554.6	87.9	100.1	20599.0	131113.5	280.9
2	26	1.514	563.9	90.2	102.8	21402.7	135905.4	286.9
2	27	1.496	572.4	88.8	102.0	22464.5	133386.4	275.8
2	28	1.537	578.1	95.0	107.9	22615.7	148131.1	306.6
2	29	1.550	584.1	86.5	106.8	23561.1	152946.2	307.4
2	30	1.565	592.1	89.8	105.1	24417.3	142879.5	284.5
2	31	1.576	599.2	98.1	110.7	24832.9	143146.2	285.7
2	32	1.588	605.6	94.3	106.9	25895.1	147576.8	288.6
2	33	1.598	611.7	95.0	111.0	26280.6	152562.6	295.3
2	34	1.606	616.8	96.3	110.2	26784.3	149944.3	288.1

TABLE 3 (Continued)

EXPER NO	DATA NO	V (M/SEC)	TB (C)	TW (C)	TMD (C)	QR (W/M2)	QT (W/M2)	HT (W/M2.K)
2	35	1.616	622.0	98.4	111.0	27306.3	144987.9	276.9
2	36	1.623	626.6	97.2	113.6	27782.6	162077.7	306.2
2	37	1.631	630.4	97.7	111.7	28729.0	147392.5	276.7
2	38	1.638	634.4	103.0	118.2	28363.3	162391.1	305.6
2	39	1.644	637.4	98.1	117.5	29194.1	172115.2	319.1
2	40	1.650	641.1	94.4	112.6	29915.3	161978.3	296.3
2	41	1.657	644.7	102.1	117.5	29655.0	167819.5	307.8
2	42	1.663	647.9	99.1	116.1	29897.2	161848.5	294.9
2	43	1.695	650.8	92.2	108.4	31453.8	151795.4	271.7
2	44	1.675	654.0	99.4	116.0	31420.2	159420.1	287.5
2	45	1.680	657.3	105.0	118.2	31175.5	156888.5	284.1
2	46	1.683	659.0	100.3	118.2	31764.9	161684.6	289.4
2	47	1.684	661.7	97.7	117.3	32097.4	166530.8	295.3
2	48	1.689	663.9	110.4	129.1	30390.4	191480.6	345.9
2	49	1.684	665.9	108.5	125.9	30694.7	184038.9	330.2
2	50	1.696	668.9	109.3	123.4	32550.7	176571.4	315.5
2	51	1.702	671.0	106.3	123.7	32590.6	181479.0	321.4
2	52	1.707	673.6	103.6	117.9	33812.2	166292.4	291.7
2	53	1.707	675.2	111.4	130.3	32210.1	191518.9	339.7
2	54	1.714	677.2	107.9	125.0	33501.4	174075.3	305.8
2	55	1.717	679.1	109.7	125.9	33544.5	176453.1	309.9
2	56	1.719	680.7	112.1	124.8	33566.8	171581.1	301.8
2	57	1.722	682.0	114.2	129.9	33334.0	183931.1	323.9
2	58	1.723	683.5	101.2	120.5	35576.1	176240.0	302.7
2	59	1.728	685.6	106.8	124.0	35034.3	178660.2	308.7
2	60	1.737	690.3	101.0	120.3	36419.3	171264.8	290.6
2	61	1.746	695.9	103.6	120.7	36520.2	173614.1	293.1
2	62	1.756	701.4	110.0	128.3	36325.7	186031.0	314.6
2	63	1.766	706.7	111.9	130.6	37204.2	190791.2	320.8
2	64	1.775	712.5	119.8	139.5	36505.9	200896.0	339.0

TABLE 3 (Continued)

EXPER NO	DATA NO	V (M/SEC)	TB (C)	TW (C)	TMD (C)	QR (W/M <sup>2</sup> )	QT (W/M <sup>2</sup> )	HT (W/M <sup>2</sup> .K)
2	65	1.782	716.2	115.4	134.5	38334.7	195824.9	325.9
2	66	1.787	719.6	115.5	134.9	38505.3	203091.7	336.2
2	67	1.792	722.7	116.3	136.7	38859.7	200503.3	330.6
2	68	1.799	727.0	112.9	132.1	40825.9	193120.6	314.5
2	69	1.804	730.2	115.3	132.4	41104.7	183243.7	298.0
2	70	1.806	732.5	124.2	142.5	39252.4	208042.1	342.0
2	71	1.811	735.2	120.4	140.1	40675.9	205304.6	333.9
2	72	1.815	737.4	117.2	136.1	41116.2	192960.0	311.1
2	73	1.818	740.0	122.2	141.4	40832.7	205386.1	332.4
2	74	1.819	741.3	125.7	145.1	40816.9	215287.6	349.7
2	75	1.915	741.0	112.1	133.2	42417.2	197543.9	314.1
2	76	1.927	741.7	116.0	134.5	42234.8	192790.1	308.1
2	77	1.948	743.1	117.3	140.2	41586.7	210118.3	335.7
2	78	1.940	744.0	118.5	137.7	42348.1	200118.5	319.9
2	79	1.933	745.6	114.5	137.2	42293.0	212323.0	336.4
2	80	1.486	743.0	125.4	143.5	40877.5	212689.8	344.4
2	81	1.473	734.5	124.1	142.7	39705.4	210329.3	344.6
2	82	1.289	726.9	121.1	143.4	38816.3	210626.7	347.7
2	83	1.279	721.1	124.5	140.5	37929.8	198357.9	332.5
2	84	.950	718.4	131.3	147.8	35446.6	220813.9	376.1
2	85	1.941	730.4	116.5	135.8	40617.3	197841.4	322.3
2	86	1.944	731.9	117.8	135.9	40412.1	200263.8	326.1
2	87	1.930	725.1	113.9	133.5	39671.4	195537.8	319.9
2	88	1.906	717.9	113.8	131.6	38809.7	188039.6	311.3
2	89	1.892	711.3	110.6	126.9	38527.0	180587.4	300.6
2	90	1.879	705.5	99.6	119.9	37625.4	173224.8	285.9
2	91	1.870	700.2	112.7	130.5	35978.0	185991.0	316.6
2	92	1.850	696.0	108.9	123.7	35979.3	180761.8	307.9
2	93	1.841	691.2	109.7	128.5	34683.5	180972.5	311.2
2	94	1.843	687.6	106.1	125.1	34637.1	188155.7	323.6

TABLE 3 (Continued)

EXPER NO	DATA NO	V (M/SEC)	TB (C)	TM (C)	TWO (C)	QR (M/M2)	QT (M/M2)	HT (M/M2.K)
2	95	1.261	688.1	107.8	127.0	34943.9	186398.3	324.7
2	96	1.262	688.2	112.7	129.1	34284.1	186198.2	323.5
2	97	.976	690.0	121.7	138.5	33359.5	206047.3	362.6
2	98	.979	693.8	125.3	140.5	33026.5	201057.6	354.3
2	99	.984	697.4	125.2	140.7	33012.1	206087.8	360.2
2	100	1.861	691.5	107.2	126.9	34608.2	193177.3	330.6
2	101	1.908	706.0	113.9	132.6	36363.2	190859.7	322.3
2	102	1.909	707.1	110.9	129.7	36874.0	197916.0	332.0
2	103	1.908	706.1	111.8	130.0	37125.9	193196.2	325.1
2	104	1.904	704.2	103.1	123.2	36986.1	188061.0	312.9
2	105	1.900	702.4	119.2	134.8	35512.3	198229.5	339.9
2	106	1.904	700.1	115.2	132.5	35143.2	193310.5	330.5
2	107	1.900	697.9	112.7	128.2	35732.0	185838.4	317.6
2	108	1.879	696.4	111.3	127.3	35787.2	188471.8	322.1
2	109	1.885	694.7	110.0	125.7	35133.3	185758.4	317.7
2	110	1.837	693.7	104.9	125.4	35930.6	190735.3	323.9
2	111	1.871	692.7	108.3	123.0	35427.9	185654.3	317.7
2	112	1.858	685.5	110.0	128.4	34344.9	188423.4	327.4
2	113	1.769	639.5	98.3	114.6	29311.7	166591.4	307.8
2	114	1.682	594.3	97.0	107.1	24340.0	147602.2	296.8
2	115	1.620	562.4	85.3	100.3	21608.8	140412.3	294.3
2	116	1.552	527.1	83.4	93.8	18103.4	128549.4	289.7
4	1	1.209	338.9	81.4	107.9	5659.3	76789.6	298.2
4	2	1.477	470.2	97.7	133.2	14013.2	112239.6	301.3
4	3	1.675	569.7	120.2	164.3	22250.2	150578.4	335.0
4	4	1.830	647.8	129.2	182.8	31923.4	161973.4	312.3
4	5	1.871	671.5	132.6	194.2	31480.3	203824.2	378.2
4	6	1.908	685.4	123.9	179.8	36263.6	188595.9	335.9
4	7	1.927	695.0	138.1	195.0	36910.0	191219.0	343.4
4	8	1.945	702.3	126.8	185.5	38248.4	200787.9	348.9

TABLE 3 (Continued)

EXPER NO	DATA NO	V (M/SEC)	TB (C)	TW (C)	TMO (C)	QR (M/M2)	QT (M/M2)	HT (M/M2.K)
4	9	1.926	697.7	132.2	189.4	38050.0	186063.0	329.0
4	10	1.567	696.1	135.1	192.3	36109.3	208380.5	371.4
4	11	1.654	708.0	138.9	197.7	38834.7	203505.0	357.6
4	12	1.570	697.7	133.4	192.6	38145.4	196154.1	347.6
4	13	1.543	692.0	136.6	193.5	36341.5	201126.6	362.1
4	14	1.523	702.1	137.2	197.5	37779.1	203626.4	360.5
4	15	1.232	712.5	139.9	206.9	39976.3	200592.8	364.3
4	16	1.283	715.0	138.7	208.2	39894.3	218421.7	379.0
4	17	1.250	703.7	126.1	188.4	39492.1	208161.5	360.4
4	18	1.227	692.9	144.4	206.7	36193.9	201560.0	367.5
4	19	1.239	702.0	133.8	194.4	40185.4	193630.2	340.8
4	20	2.485	750.7	142.6	204.4	44152.7	220088.8	361.9
4	21	2.502	745.1	133.4	189.7	46426.8	199994.4	326.9
4	22	2.427	723.3	134.5	190.2	42214.9	193191.8	328.1
4	23	2.380	704.5	124.7	174.8	40135.8	188103.1	324.4
4	24	2.348	700.5	130.1	194.1	38276.1	191131.2	335.1
4	25	2.349	700.5	126.5	184.1	39189.6	188454.4	328.3
4	26	2.944	700.7	132.0	186.1	38170.7	195745.1	344.2
4	27	2.958	697.2	124.5	176.7	39032.3	180783.6	315.7
4	28	2.936	696.3	130.4	187.8	37118.6	195886.4	346.2
4	29	2.908	692.6	125.0	172.8	38520.6	183235.2	322.8
4	30	2.969	699.8	123.5	181.3	38875.2	193202.3	335.2
4	31	3.019	712.1	134.7	190.4	40049.8	190827.0	330.5
4	32	3.113	743.2	139.2	198.5	44552.2	205409.4	340.1
4	33	3.088	751.0	133.9	192.8	46848.6	212397.6	344.2
4	34	2.516	751.7	139.9	196.9	47355.7	202513.7	331.0
4	35	2.511	748.8	139.6	199.6	45471.5	215801.7	352.9
4	36	2.034	751.9	138.9	205.7	45730.6	220065.4	359.0
4	37	1.476	742.6	149.2	217.6	42544.2	227834.5	383.9
4	38	1.520	758.1	149.2	214.9	47579.3	215300.8	353.6

TABLE 3 (Continued)

EXPER NO	DATA NO	V (M/SEC)	T8 (C)	TW (C)	TWD (C)	QR (M/M2)	QT (M/M2)	HT (M/M2.K)
4	39	1.529	756.5	148.8	214.8	46979.4	217678.1	358.2
4	40	1.509	743.7	146.4	208.9	45594.0	210273.5	352.0
4	41	1.512	751.4	152.8	216.6	45160.1	222647.2	371.9
4	42	1.516	753.2	146.3	214.1	46038.1	230015.4	379.0
4	43	2.770	608.1	109.8	154.1	28121.7	144628.5	290.2
4	44	2.738	600.7	120.4	167.7	25282.5	152621.1	317.8
4	45	2.298	613.8	117.1	165.0	27531.1	152108.7	306.2
4	46	2.240	597.8	117.2	165.6	25113.0	159861.9	332.6
4	47	2.217	589.0	118.7	168.1	24231.8	147794.1	314.3
4	48	2.237	596.2	106.0	152.4	26425.3	152220.3	310.5
4	49	2.250	600.6	116.4	162.8	25912.4	154941.4	320.0
4	50	1.762	606.2	124.1	178.0	23854.0	179834.0	373.0
4	51	1.780	605.5	122.8	174.1	25328.7	172288.3	356.9
4	52	1.786	600.0	121.2	174.0	24658.3	167526.4	349.9
4	53	1.396	610.8	123.0	168.6	27862.3	157368.0	322.6
4	54	1.415	611.1	125.1	180.0	26292.1	172303.1	354.5
4	55	1.410	602.0	122.6	168.5	26443.8	162601.2	339.2
4	56	2.912	612.5	111.4	155.0	28263.9	154690.5	308.7
4	57	2.743	578.8	109.3	155.6	24049.4	142878.8	304.3
4	58	2.666	547.3	101.5	141.4	20769.8	133148.0	298.7
4	59	2.547	511.5	97.8	131.3	17540.9	116283.9	281.1
4	60	2.473	482.8	90.6	122.0	15107.6	99294.4	253.2
4	61	1.802	500.0	93.3	128.4	16946.3	111528.9	274.2
4	62	1.823	508.9	99.9	136.0	17001.1	121459.2	297.0
4	63	1.796	500.4	98.5	131.6	16285.7	116444.5	289.7
4	64	1.224	492.9	100.2	139.4	15569.4	121772.8	310.1
4	65	1.256	493.8	103.5	144.3	15280.0	124396.4	318.7
4	66	1.533	506.4	105.1	144.2	16019.0	131566.2	327.8
4	67	2.687	529.9	96.8	129.6	19824.5	120940.7	279.2
4	68	2.650	516.1	98.1	133.1	17743.7	121227.9	290.0

TABLE 3 (Continued)

EXPER NO	DATA NO	V (M/SEC)	TB (C)	TM (C)	TWD (C)	QR (M/M2)	QT (M/M2)	HT (M/M2.K)
4	69	2.559	500.4	96.0	128.3	16379.3	111538.7	275.8
4	70	2.539	485.3	92.6	124.8	15287.7	109334.1	278.4
4	71	2.437	459.4	87.5	114.5	13094.0	96954.1	260.7
4	72	2.399	445.2	90.1	120.1	11640.7	99867.8	281.2
4	73	2.350	430.6	82.9	109.2	10906.6	92268.4	265.4
4	74	2.192	382.4	75.9	97.6	7680.9	70629.2	231.2
4	75	2.046	339.8	68.4	86.7	5278.0	68534.8	252.5
4	76	1.923	304.0	64.8	78.7	3170.6	61519.8	257.2
4	77	1.838	275.4	59.1	71.2	2225.6	44502.2	205.7
4	78	1.754	250.3	57.0	68.3	1054.0	44945.3	232.5

TABLE 4: Test Data, SP-2 Particles, Probe with ZnSe Window

EXPER NO	DATA NO	V (M/SEC)	TB (C)	TW (C)	TWD (C)	QR (M/M2)	QT (M/M2)	MT (M/M2.K)
3	1	1.494	251.6	59.5	76.5	2494.5	40261.3	209.6
3	2	1.792	355.7	73.0	100.0	7159.2	61203.6	216.0
3	3	2.013	435.2	80.0	100.7	12317.9	74054.1	211.2
3	4	2.178	494.2	86.4	117.6	17919.2	79175.7	194.2
3	5	2.333	547.3	95.2	131.3	22246.0	90167.3	217.1
3	6	2.437	503.4	97.0	135.0	25900.3	112476.1	231.2
3	7	2.537	610.5	103.7	143.0	30197.0	107202.1	208.4
3	8	2.634	651.3	106.4	149.0	34160.0	126559.7	232.3
3	9	2.700	673.0	112.0	159.0	36830.3	130667.0	247.2
3	10	2.729	683.2	115.6	165.7	37670.4	140500.9	261.6
3	11	2.720	689.5	113.7	164.3	39001.2	143375.0	249.0
3	12	2.766	695.6	110.2	167.0	39325.6	150000.0	261.2
3	13	2.774	701.4	111.7	161.4	40539.2	130290.3	234.5
3	14	2.784	707.0	110.3	166.7	41457.4	143250.5	243.3
3	15	2.819	713.3	116.4	165.0	42450.3	143120.0	239.0
3	16	2.824	717.4	115.7	164.5	43400.2	143071.6	237.0
3	17	2.030	722.7	117.9	169.1	43240.0	157020.9	261.0
3	18	2.055	727.9	110.6	167.5	44690.5	152629.0	250.5
3	19	2.064	732.6	121.9	175.4	44571.6	155420.4	254.5
3	20	2.067	737.3	123.7	172.1	45030.2	150322.5	245.0
3	21	2.900	742.0	116.4	160.0	46251.1	155013.0	247.0
3	22	2.932	746.1	120.5	180.2	46079.0	167470.3	271.2
3	23	2.909	740.0	121.0	174.9	47125.9	162520.9	250.9
3	24	2.933	750.9	120.7	171.1	47610.2	159047.7	253.6
3	25	2.940	755.1	110.4	167.1	40023.5	147407.6	231.5
3	26	3.031	741.3	123.7	173.5	45642.3	159903.5	259.0
3	27	3.755	727.0	112.7	154.5	44320.0	142637.0	231.9
3	28	3.600	686.5	100.4	149.0	37700.3	135062.9	235.0
3	29	3.459	640.5	104.7	147.0	32149.2	129054.4	237.3
3	30	3.346	610.2	100.0	135.9	20402.6	111020.5	216.1

TABLE 4 (Continued)

EXPER NO	DATA NO	V (M/SEC)	TB (C)	TM (C)	TMO (C)	QR (M/M2)	QT (M/M2)	HT (M/M2.K)
3	31	3.259	594.1	99.2	135.5	25516.6	112370.6	227.1
3	32	3.196	577.4	94.7	126.1	23831.7	114769.4	237.6
3	33	3.144	563.3	94.7	127.2	22286.9	105000.5	224.1
3	34	3.092	549.0	92.4	126.5	20387.2	105255.3	230.5
3	35	3.049	536.9	89.5	122.5	19373.0	100497.8	224.6
3	36	3.014	528.3	87.7	117.4	18717.5	105506.9	239.5
3	37	2.997	523.5	86.0	117.1	18489.0	98154.3	224.0
3	38	2.977	518.8	90.2	120.3	17609.2	100756.5	235.1
3	39	2.972	516.2	87.4	117.9	17514.5	98238.7	229.1
3	40	2.839	516.0	86.3	115.6	17514.9	98325.7	228.6
3	41	2.899	514.0	92.1	123.0	16971.0	100924.0	239.2
3	42	2.889	511.0	88.0	118.8	17139.0	96023.1	227.4
3	43	2.868	550.2	98.0	129.1	21080.9	110436.4	244.2
3	44	3.103	572.7	96.7	130.0	23539.4	115089.2	241.8
3	45	3.166	590.1	95.5	127.7	26260.7	104803.0	211.9
3	46	3.264	607.0	102.9	136.2	27421.3	126945.7	251.8
3	47	3.412	616.3	105.5	143.4	27998.9	131873.4	258.2
3	48	3.428	622.7	102.7	140.1	29399.0	124389.4	239.2
3	49	3.864	627.5	98.9	133.8	30309.4	121575.7	230.8
3	50	3.947	632.4	102.9	135.5	30945.6	133807.9	252.7
3	51	3.946	634.8	99.8	135.8	30873.9	131291.1	245.4
3	52	3.907	636.9	103.5	143.2	31192.1	129074.5	242.0
3	53	3.986	639.6	104.2	140.6	31290.1	126585.2	236.4
3	54	4.018	647.3	104.5	140.4	32798.4	126351.9	232.8
3	55	3.983	652.9	105.5	142.2	33465.3	138624.4	253.2
3	56	4.050	657.4	111.5	148.6	33422.7	128851.6	236.0
3	57	4.081	661.1	106.8	142.1	34815.0	128702.8	232.2
3	58	4.113	664.3	106.8	142.6	34876.4	136831.9	244.0
3	59	4.034	665.7	109.2	151.3	35015.0	133688.0	240.2
3	60	4.053	669.2	106.8	145.8	35562.0	138459.7	246.2

TABLE 4 (Continued)

EXPER NO	DATA NO	V (M/SEC)	FB (C)	FM (C)	TWD (C)	QR (M/M2)	QT (M/M2)	HT (M/M2.K)
3	61	4.092	670.7	104.5	141.7	35999.1	138253.2	244.2
3	62	4.066	671.6	112.1	155.6	34928.0	150914.9	269.7
3	63	4.062	673.5	111.0	151.7	35690.9	145800.8	259.2
3	64	4.067	673.5	108.2	144.8	36190.1	135889.6	240.4
3	65	4.092	675.2	108.9	147.8	36660.2	138412.5	244.4
3	66	4.145	677.5	108.9	149.2	36622.3	140664.3	247.4
3	67	3.714	684.5	106.7	147.0	37630.4	140651.1	243.4
3	68	3.804	697.5	112.1	150.5	39858.8	147903.9	252.7
3	69	3.779	708.4	114.5	157.7	41316.6	147897.1	249.0
3	70	3.879	716.7	121.8	165.8	41969.0	155323.7	261.1
3	71	3.936	724.4	118.2	165.0	43551.5	155252.5	256.1
3	72	3.885	731.0	119.0	162.6	45260.2	155016.8	253.3
3	73	3.955	736.4	122.5	166.5	45225.0	155020.7	252.5
3	74	3.897	740.8	123.3	165.6	46264.2	159783.9	258.8
3	75	3.953	743.2	120.1	165.8	46812.0	162113.2	260.2
3	76	4.023	746.4	125.3	176.3	46400.6	172242.3	277.3
3	77	3.930	747.3	122.2	167.5	47475.1	164744.4	263.5
3	78	3.982	750.0	120.9	166.0	48132.4	162202.1	257.8
3	79	3.531	753.3	119.6	160.7	49397.6	157269.6	248.2
3	80	3.519	748.5	119.0	165.9	48023.8	167268.7	265.7
3	81	3.107	751.9	123.0	171.1	48519.7	179627.6	285.6
3	82	3.102	746.6	121.1	169.0	47990.7	172286.2	275.4
3	83	2.526	755.2	122.7	171.4	49645.7	179711.3	284.1
3	84	2.517	751.8	120.9	166.7	50487.4	169739.9	269.0
3	85	2.076	734.3	124.9	169.7	47160.8	167845.8	275.4
3	86	2.075	739.3	127.9	175.6	47857.3	172766.1	282.6
3	87	4.376	755.4	120.9	164.2	49480.9	169647.8	267.4
3	88	4.222	722.5	113.4	153.2	44003.5	157625.0	258.8
3	89	4.761	668.9	107.9	144.5	35658.5	133641.3	238.2
3	90	4.826	656.4	105.9	143.9	33655.9	138781.6	252.1

TABLE 4 (Continued)

EXPER NO	DATA NO	V (M/SEC)	TB (C)	TM (C)	TMD (C)	QR (W/M <sup>2</sup> )	QT (W/M <sup>2</sup> )	HT (W/M <sup>2</sup> .K)
3	91	4.730	645.7	101.8	137.7	32335.3	141286.3	259.8
3	92	4.650	622.3	96.7	126.6	29306.9	119172.1	226.7
3	93	4.495	601.1	92.7	123.2	27040.9	119438.4	234.9
3	94	3.574	597.5	94.2	126.7	26687.2	104873.9	208.4
3	95	3.593	600.8	98.6	129.4	26863.2	122149.5	243.6
3	96	2.650	606.2	97.5	132.1	27515.7	126953.3	249.6
3	97	2.604	593.0	94.1	122.0	26249.2	119576.2	239.7
3	98	2.658	600.6	94.7	129.5	27312.8	119804.8	236.8
3	99	2.081	599.0	98.4	136.4	27311.2	122476.2	244.7
3	100	2.062	598.4	97.1	129.9	27516.8	124714.5	248.8
3	101	2.086	601.1	97.7	131.0	28142.7	112373.5	223.2
3	102	1.658	602.0	100.5	136.1	29114.3	129832.0	258.9

TABLE 5: Test Data, SP-1 Particles, Probe with Solid Copper Face

EXPER NO	DATA NO	V (M/SEC)	TB (C)	TM (C)	TMO (C)	QT (M/M2)	HT (M/M2.K)
5	1	.929	135.5	51.8	49.0	22459.4	268.3
5	2	.992	165.3	61.3	57.2	21891.3	210.5
5	3	1.195	211.5	74.0	69.2	28476.2	207.1
5	4	1.488	328.0	90.9	80.5	61598.2	259.8
5	5	1.686	410.0	100.2	89.1	74967.7	242.0
5	6	1.814	467.8	115.3	100.0	86684.5	245.9
5	7	1.949	516.6	118.3	102.8	100679.7	252.8
5	8	2.050	554.4	120.4	106.2	117496.0	270.7
5	9	2.115	580.8	129.0	111.9	122235.1	270.6
5	10	2.190	611.6	128.0	111.4	119252.4	246.6
5	11	2.259	637.7	135.3	116.9	141063.6	280.8
5	12	2.303	658.4	140.2	120.0	145877.9	281.5
5	13	2.356	676.2	142.9	122.3	155419.9	291.4
5	14	2.391	691.4	146.6	125.7	147929.1	271.5
5	15	2.426	704.5	142.8	122.0	157514.9	280.4
5	16	2.418	701.2	137.8	119.6	154932.4	275.0
5	17	2.425	703.1	147.4	124.7	167427.0	301.3
5	18	2.416	700.0	140.9	121.9	164861.3	294.9
5	19	2.467	724.9	151.1	130.4	179481.7	312.8
5	20	2.540	749.2	154.4	131.4	179196.6	301.3
5	21	2.531	750.2	150.6	128.2	169063.0	282.0
5	22	2.521	741.8	147.1	125.4	176516.7	296.8
5	23	3.044	732.0	144.7	124.5	171812.7	292.5
5	24	3.027	726.6	146.7	125.9	179312.2	309.2
5	25	3.042	734.8	144.6	124.8	169376.0	287.0
5	26	2.989	713.3	141.3	122.5	154759.0	270.6
5	27	2.861	674.0	140.4	121.3	160353.3	300.5
5	28	2.766	640.4	135.2	117.0	145931.5	288.9
5	29	2.686	613.3	132.6	114.5	134192.5	279.2
5	30	2.677	599.1	128.1	111.7	134172.8	284.9

TABLE 5 (Continued)

EXPER NO	DATA NO	V (M/SEC)	TB (C)	TW (C)	TWD (C)	QT (W/M2)	HT (W/M2.K)
5	31	2.702	604.6	132.3	114.6	126831.2	268.5
5	32	2.232	620.7	133.9	115.4	136327.9	280.0
5	33	2.220	612.0	132.9	115.2	141518.4	295.4
5	34	2.181	603.0	135.7	116.3	136682.8	292.5
5	35	2.143	585.2	126.5	110.2	124477.0	271.4
5	36	2.082	566.9	127.4	111.6	124939.4	284.3
5	37	1.980	519.7	115.4	102.5	105649.2	261.3
5	38	1.857	473.6	107.9	95.5	88987.1	243.3
5	39	1.757	433.5	103.7	92.7	79648.7	241.5
5	40	1.668	397.8	98.6	88.6	62960.1	210.4
5	41	1.592	367.4	94.7	85.0	63207.2	231.8
5	42	1.526	340.4	93.8	84.1	53890.2	218.5

TABLE 6: Test Data, SP-2 Particles, Probe with Solid Copper Face

EXPER NO	DATA NO	V (M/SEC)	T8 (C)	TW (C)	TWD (C)	QT (W/M <sup>2</sup> )	HT (W/M <sup>2</sup> .K)
6	1	1.075	264.3	80.6	72.6	3182.3	173.6
6	2	1.280	366.3	97.3	86.7	49809.7	185.2
6	3	1.442	454.6	107.3	95.2	71822.1	206.8
6	4	1.559	513.3	117.2	102.3	87998.4	222.2
6	5	1.628	535.6	119.9	103.1	91735.4	220.7
6	6	1.636	544.0	122.4	105.5	96024.5	227.8
6	7	1.662	560.8	125.2	107.9	100003.2	229.6
6	8	1.700	575.1	123.2	106.2	108232.0	239.5
6	9	1.716	587.4	121.5	106.6	105923.6	227.4
6	10	1.743	600.6	127.7	110.3	112034.0	236.9
6	11	1.736	597.3	128.7	110.8	110109.9	235.0
6	12	1.737	597.8	129.2	111.7	112189.9	239.4
6	13	1.753	605.3	129.4	111.6	118447.6	248.9
6	14	1.743	604.1	129.5	112.2	116417.1	245.3
6	15	2.638	605.8	121.2	106.3	103497.2	213.6
6	16	2.622	600.2	121.4	105.2	107635.9	224.8
6	17	3.196	596.6	122.7	107.5	105669.0	223.0
6	18	3.156	609.4	122.3	106.2	103374.8	212.2
6	19	3.140	604.5	125.7	109.0	107726.1	225.0
6	20	1.850	637.8	131.1	112.7	121958.3	240.7
6	21	1.970	701.8	142.2	119.8	136034.6	243.1
6	22	2.159	770.0	161.5	136.8	177421.7	291.6
6	23	2.110	760.8	156.8	133.0	160763.9	266.2
6	24	2.088	745.3	154.0	130.0	167150.9	242.7
6	25	2.102	751.0	153.9	130.3	158787.4	265.9
6	26	3.047	746.8	140.1	122.2	145941.9	240.6
6	27	3.085	749.4	145.1	125.3	156424.3	258.9
6	28	3.716	748.3	138.7	121.5	152123.8	249.5
6	29	3.527	719.5	139.2	121.4	137872.8	237.6
6	30	3.500	668.2	131.4	113.3	127971.4	238.4

TABLE 6 (Continued)

EXPER NO	DATA NO	V (M/SEC)	TR (C)	TM (C)	TWD (C)	QT (W/M <sup>2</sup> )	HT (W/M <sup>2</sup> .K)
6	31	2.582	631.6	127.4	110.9	119936.0	237.9
6	32	2.578	626.6	123.7	108.9	122017.7	242.6
6	33	2.591	633.9	131.5	114.2	111610.0	222.2
6	34	2.704	663.6	133.7	116.4	130203.8	245.7
6	35	2.778	699.3	144.1	123.5	152976.3	275.5
6	36	2.827	706.5	141.4	120.9	140015.4	247.8
6	37	2.802	701.1	132.8	116.9	138007.4	242.8
6	38	2.014	702.0	144.2	124.2	150853.1	270.4
6	39	1.987	697.7	144.1	124.0	146683.1	265.0
6	40	3.620	706.5	139.5	120.1	139994.7	246.9
6	41	3.493	701.0	137.2	119.3	142220.0	252.3
6	42	3.469	701.9	133.9	116.4	131541.9	231.6
6	43	3.248	642.0	128.2	112.2	126226.1	245.7
6	44	2.294	581.8	119.6	106.4	99628.0	215.6
6	45	2.182	540.6	114.9	101.3	93827.7	220.4
6	46	2.072	500.0	113.5	100.0	85898.2	222.2

## REFERENCES

1. Baskakov, A.P. and J.M. Goldobin. "Radiant Heat Transfer in a Gas-Fluidized Boiling Bed", Heat Transfer-Soviet Research, Vol. 2, No. 6 (1970), pp. 172-179.
2. Baskakov, A.P., B.V. Berg, O.K. Vitt, N.F. Filippovsky, V.A. Kirakosgan, J.M. Goldobin and V.K. Maskaev. "Heat Transfer to Objects Immersed in Fluidized Beds", Powder Technology, Vol. 8 (1973), pp. 273-282.
3. Baskakov, A.P., B.V. Berg, J.M. Goldobin, A.M. Dubinin, A.A. Zharkov, G.Y. Zakharchenko, S.Y. Zyyagin, O.M. Panov, A.V. Sokolov, N.F. Filippovsky, and V.V. Khoroshavtsev. "Heat Transfer to Objects Immersed in Fluidized Beds", Heat Transfer-Soviet Research, Vol. 8, No. 5 (1976), pp. 17-24.
4. Basu, P. "Bed-to-Wall Heat Transfer in a Fluidized Bed Coal Combustor", American Institute of Chemical Engineers Symposium Series (1978), pp. 187-193.
5. Bhattacharya, S.C. and D. Harrison. "Heat Transfer in High Temperature Fluidized Beds", European Congress on Particle Technology, Nuremberg (1977), pp. 1-21.
6. Botterill, J.S.M. and C. T. Sealey. "Radiative Heat Transfer between a Gas-Fluidized Bed and an Exchange Surface", British Chemical Engineering, Vol. 15, No. 9 (1970), pp. 1167-1168.
7. Holman, J.P. Heat Transfer. 4th ed. New York: McGraw-Hill Book Company, 1976.
8. Il'chenko, A.I., V.S. Pikashov, and K.E. Makhorin. "Study of Radiative Heat Transfer in a Fluidized Bed", Journal of Engineering Physics, Vol. 14 (1968), pp. 321-324.
9. Jolley, L.T. "Heat Transfer in Beds of Fluidized Solids", Fuel, Vol. 28 (1949), pp. 114-115.
10. Kharchenko, N.V. and K.E. Makhorin. "The Rate of Heat Transfer between a Fluidized Bed and an Immersed Body at High Temperatures", International Chemical Engineering, Vol. 4, No. 4 (1964), pp. 650-654.
11. Kolar, A.K., N.S. Grewal, and S.C. Saxena. "Investigation of Radiative Contribution in a High Temperature Fluidized

Bed using the Alternate-Slab Model", International Journal of Heat and Mass Transfer, Vol. 22 (1979), pp. 1695-1702.

12. Kunii, D. and O. Levenspiel. Fluidization Engineering. New York: John Wiley and Sons, Inc., 1969.
13. Saxena, S.C., N.S. Grewal, and J.D. Gabor. "Heat Transfer between a Gas Fluidized Bed and Immersed Tubes", Advances in Heat Transfer, Vol. 14 (1978), p. 149.
14. Siegel, R. and J.R. Howell. Thermal Radiation and Heat Transfer. 2nd ed. New York: McGraw-Hill Book Company, 1981.
15. Szekely, J. and R.J. Fisher. "Bed-to-Wall Radiation Heat Transfer in a Gas-Solid Fluidized Bed", Chemical Engineering Science, Vol. 24 (1969), pp. 833-849.
16. Thring, R.H. "Fluidised Bed Combustion for the Stirling Engine", International Journal of Heat and Mass Transfer, Vol. 20 (1977), pp. 911-918.
17. Touloukian, V.S. and D.P. Dewitt. Thermophysical Properties of Matter, Vol. 8 - Thermal Radiative Properties, Non Metallic Solids. New York: IFI/Plenum, 1972, p. 1124.
18. Vedamurthy, V.N. and V.M.K. Sastri. "Analysis of Conductive and Radiative Heat Transfer to the Walls of Fluidized Bed Combustors", International Journal of Heat and Mass Transfer, Vol. 17 (1974), pp. 1-9.
19. Yoshida, K., T. Ueno, and D. Kunii. "Mechanism of Bed-Wall Heat Transfer in a Fluidized Bed at High Temperatures", Chemical Engineering Science, Vol. 29 (1974), pp. 77-82.

#### VITA

Thomas R. Frankenfield was born in Bethlehem, Pennsylvania on May 19, 1949. He is the son of Mr. and Mrs. Robert E. Frankenfield of Bethlehem. He received his Bachelor of Science Degree from the United States Military Academy at West Point, New York on June 9, 1971. He is presently a Captain in the United States Army.

